THE DISSOLUTION OF LIMESTONE, COAL FLY ASH AND BOTTOM ASH IN WET FLUE GAS DESULPHURIZATION

This dissertation is submitted in fulfillment of the requirement for the Magister Technologiae: Engineering: Chemical

LAWRENCE KOECH

213118742

Vaal University of Technology, Main Campus

Private Bag X021, Vanderbijlpark~1900, South Africa

Supervisor: Dr. H. L. Rutto

Co-supervisors: Prof. R. Everson and Prof. H. Neomagus

March, 2015

Declaration

I Lawrence Koech, declare that, to the best of my knowledge, my dissertation is the result of my original work except otherwise stated. It has not been submitted in candidature for any degree in any university or institution. Due references in literature were stated and acknowledged wherever other sources were involved according to the standard referencing practices.

Lawrence Koech 25th March, 2015

Acknowledgements

I would like to express my sincere gratitude to Dr. H.L. Rutto for his guidance and encouragement during my masters research. His kindness and sincerity is greatly appreciated. I would also like to thank my co-supervisors, Prof. R. Everson and Prof. H. Neomagus for their support and discussions which became integral part in my research.

I thank Dr. Lay Shoko for his incredible assistance in the research laboratory. I am grateful for his help, experience and enthusiasm about work. I appreciate the company of my fellow research students from Vaal University of Technology and North-West University, everybody has been helpful and I have learnt so much working together. I would like to thank the Laboratory for Electron Microscopy (NWU) for helping with SEM analysis and also Dr. Sabine for XRD and XRF analysis.

I appreciate the unrelenting support of my parents and friends who stood by me all through my studies.

The financial support from ESKOM and the provision of the samples for this study is greatly acknowledged.

Abstract

Strict environmental regulation on flue gas emission has led to the implementation of FGD technologies in power stations. Wet FGD technology is commonly used because it has high SO_2 removal efficiency, high sorbent utilization and due to availability of the sorbent (limestone) used. SO_2 is removed by passing flue gas through the absorber where it reacts with the slurry containing calcium ions which is obtained by dissolution.

This study presents the findings of the dissolution of a calcium-based material (limestone) for wet FGD process. This was done using a pH stat apparatus and adipic acid as acid titrant. Adipic acid was used because of its buffering effect in wet FGD process. The conditions used for this study are similar to what is encountered in a wet FGD process. The extent of dissolution was determined by analyzing the amount of calcium ions in solution at different dissolution periods. The dissolution kinetics were correlated to the shrinking core model and it was found out that chemical reaction at the surface of the particle is the rate controlling step. This study also investigated the dissolution of coal fly ash and bottom ash. Their dissolution kinetics showed that the diffusion through the product layer was the rate controlling step due to an ash layer formed around the particle. The formation of ash layer was attributed to pozzolanic reaction products which is calcium-alumino-silicate (anorthite) compounds were formed after dissolution.

The effect of fly ash on the dissolution of rate of limestone was also studied using response surface methodology. Limestone reactivity was found to increase with increase in the amount of fly ash added and the pH was found to be strong function of the rate constant compared to other dissolution variables. The presence of silica and alumina in fly ash led to a significant increase in the specific surface area due to hydration products formed after dissolution.

Key words: flue gas desulphurization, dissolution, limestone, fly ash, bottom ash, shrinking core model.

List of publications and conference proceedings

The following is a list of publications, manuscript and conference proceedings in which this dissertation is based on.

Publications

1. Koech L., Everson R., Neomagus H. and Rutto H.L. 2014. A Semi-Empirical Model for Dissolution of Limestone in Adipic Acid for Wet Flue Gas Desulphurization. *Chemical engineering & Technology*. Vol 37 (11) pg. 1919-1928.

2. Koech L., Everson R., Neomagus H. and Rutto H.L. 2014. Dissolution Kinetics of Sorbents and Effect of Additives in Wet Flue Gas Desulfurization. *Reviews in Chemical Engineering*. Vol 30 (6) pg. 553-565.

3. Koech L., Everson R., Neomagus H. and Rutto H.L. 2015. Leaching Kinetics of Bottom Ash Waste as a Source of Calcium Ions. *Air & Waste Management Association*. Vol 65 (2), 126-132.

4. Koech L., Everson R., Neomagus H. and Rutto H.L. 2014. Dissolution Kinetics of South African Coal Fly Ash and Development of a Semi-Empirical Model to Predict Dissolution. *Chemical Industry & Chemical Engineering Quarterly*. DOI:10.2298/CICEQ140423032K

5. Koech L., Everson R., Neomagus H. and Rutto H.L. 2015. The Effect of Fly Ash addition on Limestone Dissolution Rate Constant. *Energy & Fuels* (Accepted for publication).

Conference Proceedings

6. Koech L., Everson R., Neomagus H. and Rutto H.L. 2013. Dissolution Study of a South African Calcium Based Material for Wet Flue Gas Desulphurization. *18th Southern African Coal Science and Technology Indaba*. 13th & 14th November, 2013. Parys, South Africa.

7. Koech L., Everson R., Neomagus H. and Rutto H.L. 2013. Dissolution of Coal Fly Ash for Wet Flue Gas Desulphurization. *International Conference on Chemical, Mining and Metallurgical Engineering (CMME'2013)*. 27th & 28th November, 2013. Johannesburg, South Africa.

8. Koech L., Everson R., Neomagus H. and Rutto H.L. 2013. Dissolution of Bottom Ash for Wet Flue Gas Desulphurization. *International Conference on Chemical, Mining and Metallurgical Engineering (CMME'2013)*. 27th & 28th November, 2013. Johannesburg, South Africa.

Table of Contents

Table of Figures

List of Tables

Symbols and Abbreviations

Symbols

b – Stoichiometric coefficient

K_l – Mass transfer coefficient (m min^{-1})

C_A – Bulk concentration (mol cm^{-3})

ρ_B –molar density (kg mol m^{-3})

R_o – Initial particle radius (m)

t – Reaction time (s)

K_s – Surface reaction rate constant (m min^{-1})

K_o – Pre-exponential factor

K_r – Surface reaction rate constant (m min^{-1})

K_d – Product layer reaction rate constant (min^{-1})

D_e – Product layer effective diffusion coefficient (m^2 min^{-1})

E_a – Activation energy (kJ mol^{-1})

R – Universal gas constant (kJ mol^{-1} K^{-1})

C – Acid concentration (mol dm^{-3})

D – Particle size (µm)

N – Stirring speed (rpm)

P – pH

S/L – Solid to liquid ratio (g ml^{-1})

T – Temperature (K)

D – Particle size (µm)

Abbreviations

FGD – Flue gas desulphurization

CCD – Central composite design

SEM – Scanning electron microscope

XRD – X-ray diffraction

XRF – X-ray fluorescence

BET – Brunauer Emmett and Teller

USEPA – United States Environmental Protection Agency

FTIR – Fourier Transform Infrared

AAS – Atomic absorption spectrophotometer

LOI – Loss on ignition

1. Introduction

Coal is major source of energy in many countries and South Africa depends heavily on it for electricity production. About 77% of its energy needs are from coal (Energy Department, 2014). Continued dependence on coal for electricity production is due to its availability and it is also cheap compared to other energy sources. Coal contains sulphur and it is released to the environment in form of SO_2 during combustion. SO_2 emission is harmful to both human health and environment. It causes acid rains which leads to damage to building and also causes poor atmospheric visibility. Power stations in South Africa have been hard-pressed to meet the international standards on air pollution and also comply with the Air and Quality Act (2005) which monitors emission control in industries. This has led to adoption of the flue gas desulphurization (FGD) technology to remove SO_2 from flue gas.

Most coal fired power plants in South Africa do not have FGD systems in place and therefore great amount of SO_2 is released to the atmosphere during combustion. There are three categories of FGD processes: wet, semi-dry and dry processes. Wet FGD process is the most commonly used in power stations because it has high desulphurization efficiency of about 93 - 97% and also because of the availability of the sorbent (Miszczyk and Darowicki, 2002). In this process, flue enters the absorber and comes in contact with a slurry containing either slaked lime ($Ca(OH)_2$) or limestone ($CaCO_3$) as a sorbent. SO_2 in flue gas is removed by chemical absorption where it reacts with the slurry at a temperature of around 50°C to form gypsum; a product which can be utilized.

The slurry sprayed in the absorber is prepared by dissolution which takes place before the absorber. Dissolution plays a significant role because it affects the overall performance of the wet FGD process. It is also essential for operation, absorber performance modeling and during design stage of the system. The dissolution kinetics of the sorbent can be affected by factors like the slurry pH, reaction temperature and the amount of sorbent introduced (added) into the slurry. The shrinking core model best describes the dissolution kinetics of the sorbent in the slurry because it considers a particle reacting with the fluid reactant while its size reduces as the reaction proceeds.

Production of electricity from coal leads to production of solid wastes such as coal fly ash and bottom ash. Currently South Africa coal power stations produce approximately 17000 tons of ash per day (General Communication - ESKOM, 2014). This is being placed in landfills and part of it is sold to cement industries for use as cement extender. Placing ash in landfills is an environmental concern because it contains heavy compounds like arsenic, antimony, boron, chromium and vanadium which may contaminate soil and water sources through leaching (Sushil and Batra, 2006; Goodarzi, 2006). It is therefore necessary to do safe disposal of the ash or re-use the ash in FGD processes to act as additives or partial substitutes for sorbents.

The performance of a wet FGD system using $CaCO_3$ as a sorbent can be optimized by use of additives which can improve the buffer capacity of the slurry and also improve the dissolution of the sorbent (Rochelle and King, 1977; Stergarsek et al., 1999). These additives include organic acids like adipic acid, glutaric acid and succinic acid. Additives can act as structural modifiers that eventually improve the sulphur retaining capacity of the sorbents. Siliceous materials such as coal fly ash and bottom ash contain Al_2O_3, SiO_2 and CaO which can improve SO_2 removal capacity if used as additives. Due to their pozzolanic properties, it leads to increase in the specific surface area of sorbents prepared from it thus improving desulphurization efficiency (Lee et al., 2005; Ogenga et al., 2009).

This study focuses on the dissolution kinetics of limestone, coal fly ash and bottom ash for wet flue gas desulphurization. Dissolution experiments were carried out using a pH stat apparatus and adipic acid was used as an acid titrant. Dissolution kinetics was studied with focus on the reaction variables such pH, temperature, solid to liquid ratio and acid concentration. The shrinking core model was used to analyze the experimental data and study the kinetics. Semi-empirical models describing the effect of reaction variables on the sorbent dissolution were developed. The sorbent physical properties of at different dissolution periods were analyzed using X-ray diffraction (XRD), X-ray flourescence (XRF), Fourier Transform Infrared (FTIR), Brannauer-Emmet-Teller (BET) and scanning electron microscope analysis methods.

1.1. Problem statement

Most power stations have adopted wet FGD system for removal of SO_2 from flue gas because of its efficiency and also due to the availability of the sorbent (limestone) used in the process. The technology has also been adopted in South Africa by some power stations and is currently being installed. It was required to generate experimental data and develop dissolution kinetics from a calcium based material that will be used as a sorbent in the FGD process. The experimental data was to be used in the absorber performance modeling during the design stage of the system and also for process operation. For efficient operation of the process it is important to understand the dissolution kinetics of the sorbent to be used and the effects of the reaction variables as well. This can be effectively studied in a laboratory scale set up using a pH stat apparatus.

There are other solid wastes associated with the use of coal for electricity generation; they include coal fly ash and bottom ash. They are regarded as harmful to the environment if not safely disposed. Most of it is currently being placed in landfills and the rest sold to cement industries. Because they are mostly siliceous materials, they can be beneficially used as additives or partial substitute for sorbent in FGD process. This will in turn reduce the risk of environmental pollution. To see the possibility of using the ash as additives for FGD, their dissolution kinetics was studied using a pH stat apparatus. The influence of addition of coal fly ash on the dissolution rate constant of limestone was also studied using central composite design (CCD).

1.2. Main Objective

To determine the dissolution kinetics of a calcium based material (limestone), fly ash and bottom for wet flue gas desulphurization system.

1.2.1. Specific objectives

1. To determine the dissolution kinetics of limestone in wet FGD system and fit the experimental data using the shrinking core model
2. To determine the dissolution properties and kinetics of coal fly ash for wet FGD system

3. To establish the leaching kinetics of calcium ions from bottom ash for wet FGD system
4. To determine the effect of coal fly ash on the dissolution rate of limestone using response surface methodology

References

Energy Department, Republic of South Africa 2014, *Coal resources*. Available: www.energy.gov.za [2014, February].

General Communication - ESKOM 2014, *About Electricity - Facts and Figures*. Available: www.eskom.co.za [2014, Februrary].

Goodarzi, F. 2006. Characteristics and composition of fly ash from Canadian coal-fired power plants. *Fuel,* vol. 85, no. 10, pp. 1418-1427.

Lee, K.T., Bhatia, S. and Mohamed, A.R. 2005. Preparation and characterization of sorbents prepared from ash (waste material) for sulfur dioxide (SO_2) removal. *Journal of material cycles and waste management,* vol. 7, no. 1, pp. 16-23.

Miszczyk, A. and Darowicki, K. 2002. Reliability of Flue Gas Desulphurization Installations-the Essential Condition of Efficient Air Pollution Control. *Polish Journal of Environmental Studies,* vol. 11, no. 3.

National Environmental Management, South Africa 2005. Air and Quality Act, Act No. 30 of 2004, Cape Town.

Ogenga, D., Siagi, Z., Onyango, M. and Mbarawa, M. 2009. Influence of hydration variables on the properties of South African calcium/siliceous-based material. *Frontiers of Chemical Engineering in China,* vol. 3, no. 1, pp. 46-51.

Rochelle, G.T. and King, C.J. 1977. The effect of additives on mass transfer in $CaCO_3$ or CaO slurry scrubbing of SO_2 from waste gases. *Industrial & Engineering Chemistry Fundamentals,* vol. 16, no. 1, pp. 67-75.

Stergarsek, A., Gerbec, M., Kocjancic, R. and Frkal, P. 1999. Modeling and experimental measurements of limestone dissolution under enhanced wet limestone FGD process conditions. *Acta Chimica Slovenska,* vol. 46, no. 3, pp. 323-333.

Sushil, S. and Batra, V.S. 2006. Analysis of fly ash heavy metal content and disposal in three thermal power plants in India. *Fuel,* vol. 85, no. 17, pp. 2676-2679.

2. Literature Review

2.1. Flue Gas Desulphurization

Flue gas desulphurization (FGD) technology is a scrubbing process that is used for SO_2 removal from coal fired power plants utility boilers. FGD systems uses calcium, magnesium or sodium based alkaline reagents to remove SO_2 from flue gas. The reagent is injected directly into the duct or into the spray tower where flue gas passes. The absorbed SO_2 is neutralized or oxidized by the reagent to form calcium sulphate or sodium sulphate.

Basing on how the solid wastes are generated, scrubbers are divided as once through or regenerable. Once through scrubber system is where the spent sorbent is disposed as waste or used as a by-product while regenerable systems is where the sorbent is recycled back into the system (Cooper and Alley, 1994). Regenerable processes have higher costs compared to once through processes. However they can still be a better choice if space and disposal options are limited and markets for the by-products (gypsum) are available. Both once through and regenerable systems can further be categorized as dry, semi-dry and wet FGD systems (Srivastava, 2000).

2.1.1. Wet FGD system

Wet FGD system uses either limestone or lime as a sorbent. Limestone is cheap but it has sulphur dioxide removal efficiencies of approximately 90% while on the other hand, lime is easier to manage on-site and sulphur dioxide removal efficiency of up to 95% but it is more costly (Cooper and Alley, 1994). Wet FGD system is most commonly used in thermal power plants and dominates the commercial market. Wet FGD unit is normally installed after removal of particulate matter from flue gas using electrostatic precipitator or a baghouse.

Limestone slurry is prepared in two consecutive steps: crushing or milling often to fine powder with desired particle size using ball mill and mixing limestone with water in a slurry preparation tank (dissolution). The sorbent is then pumped to the absorber for SO_2 removal. The absorber is a vertically oriented spray tower with a counter-current flow of flue gas and the slurry. Flue gas is treated by spraying lime or limestone slurry

downwards using spray nozzles so as to atomize the slurry into fine droplets and contact the gas uniformly. The flue gas moves upwards counter-currently to the spray slurry moving downwards through the absorber (Sargent and Lundy, 2003).

SO_2 in flue gas is removed both by sorption and reaction with the slurry. The reactions take place even at the reaction tank, where fine particles of limestone dissolve and react with SO_2. The overall reactions inside the absorber and at the reaction tank are represented by:

$$SO_{2(g)} + CaCO_{3(s)} + {}^{1}/_{2}\, H_2O_{(l)} \rightarrow CaSO_3 \cdot {}^{1}/_{2}\, H_2O_{(s)} + CO_{2(g)} \quad (2.1)$$

$$SO_{2(g)} + CaCO_{3(s)} + {}^{1}/_{2}\, O_{2(g)} + 2H_2O_{(l)} \rightarrow CaSO_4.2H_2O_{(s)} + CO_{2(g)} \quad (2.2)$$

Entrained droplets in the desulphurized gas are removed by passing the gas through a mist eliminator before being sent to the stack.

After contacting with gas, the slurry collects at the reaction tank where dissolution and crystallization reactions take place. This is majorly controlled by the pH of the liquid which is a function of the number of moles of Ca^{2+} ions added per SO_2 removed (Srivastava, 2000). The slurry is agitated to prevent settling as more limestone or lime is added to the reaction tank in order to replenish what has been used.

For limestone forced oxidation (LSFO) process, the slurry is aerated in the reaction tank to oxidize calcium sulphite ($CaSO_3 \cdot \frac{1}{2} H_2O$) to calcium sulphate ($CaSO_4 \cdot 2H_2O$) (gypsum), which precipitates. Precipitated gypsum is removed from the reaction tank and dewatered to produce gypsum cake for disposal or sale. The water removed from gypsum is returned to the process (Sargent and Lundy, 2007). A typical wet flue gas desulphurization system is illustrated in Figure 2.1.

Wet FGD process has high capital and operating expenses due to the handling of the liquid reagent and waste. It is however the most preferred process for coal-fired power plants due to the low cost of limestone and high SO_2 removal efficiencies between 90% and 98% (USEPA, 2003).

Dissolution which takes place in the slurry/reaction tank plays an important role in the operation of a wet FGD system. The presence of water layer around the sorbent particle

is important for absorption of SO_2 to occur. Therefore attention is necessary on the dissolution kinetics of sorbent as regards to factors which influence dissolution and additives which can be used to enhance the performance of wet FGD systems.

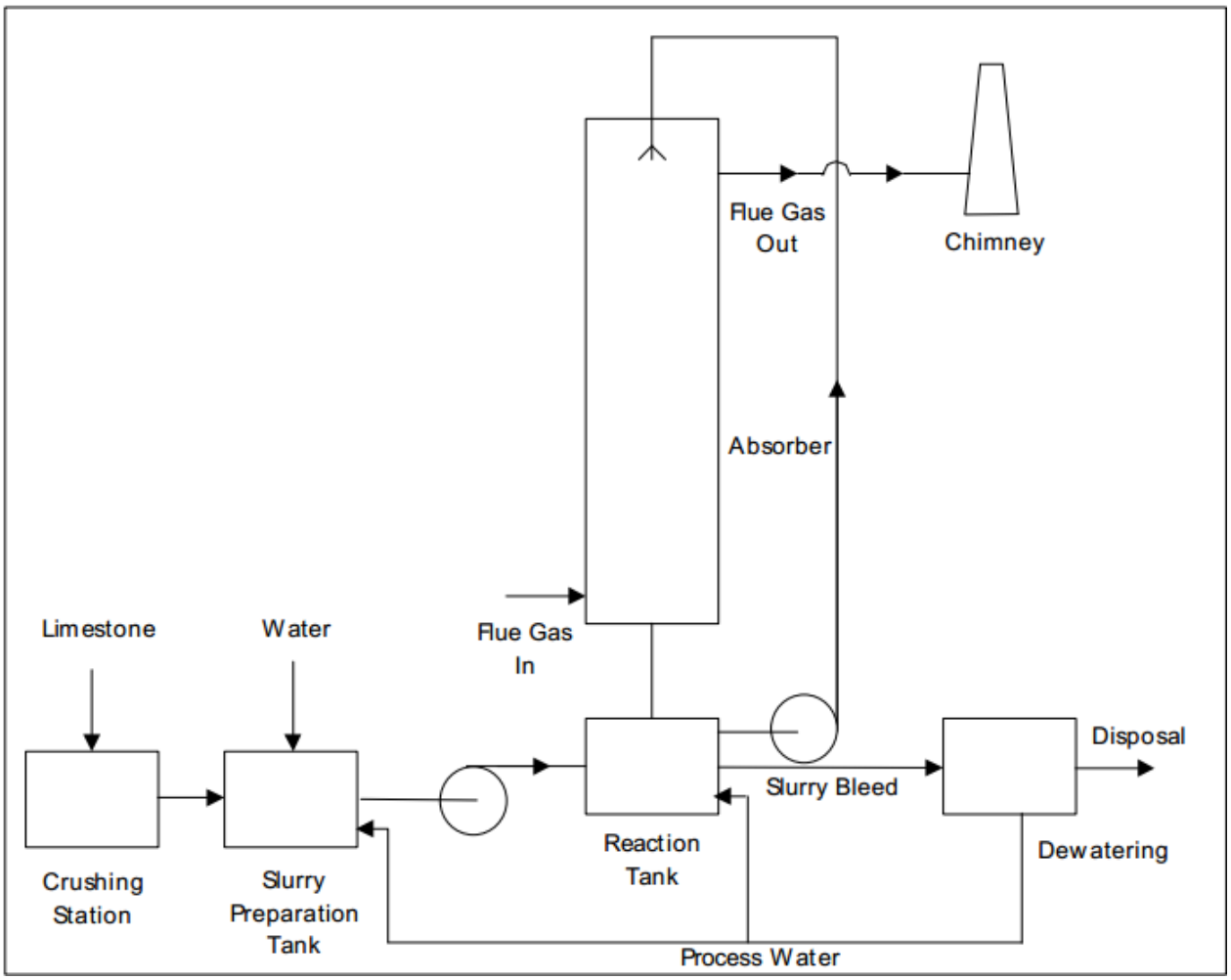

Figure 2. 1: Wet FGD system (Srivastava, 2000).

2.1.2. Dry FGD system

Dry FGD uses dry sorbent which is mostly alkaline. Finely dispersed powdered sorbent is brought into contact with flue gas inside the spray dryer to remove SO_2 by chemical reaction. The dry sorbent powder is injected directly into the furnace, the economizer or downstream ductwork and water is injected upstream or downstream of the absorber of the dry sorbent to humidify the flue gas. This enhances the removal of SO_2 from flue

gas (Srivastava, 2000). As SO_2 is removed, water evaporates from the sorbent leaving a dry waste product which is removed using a baghouse or an electrostatic precipitator. A representation of a dry FGD system is illustrated in Figure 2.2.

Dry FGD system has a lower operating cost that the wet FGD system because of its simplicity, less water usage and less waste disposal. It needs less space hence they are good for retrofit applications. However, It has lower SO_2 removal efficiency than wet FGD systems (between 50% and 60% for calcium based sorbents and over 80% for sodium based sorbents) (USEPA, 2003).

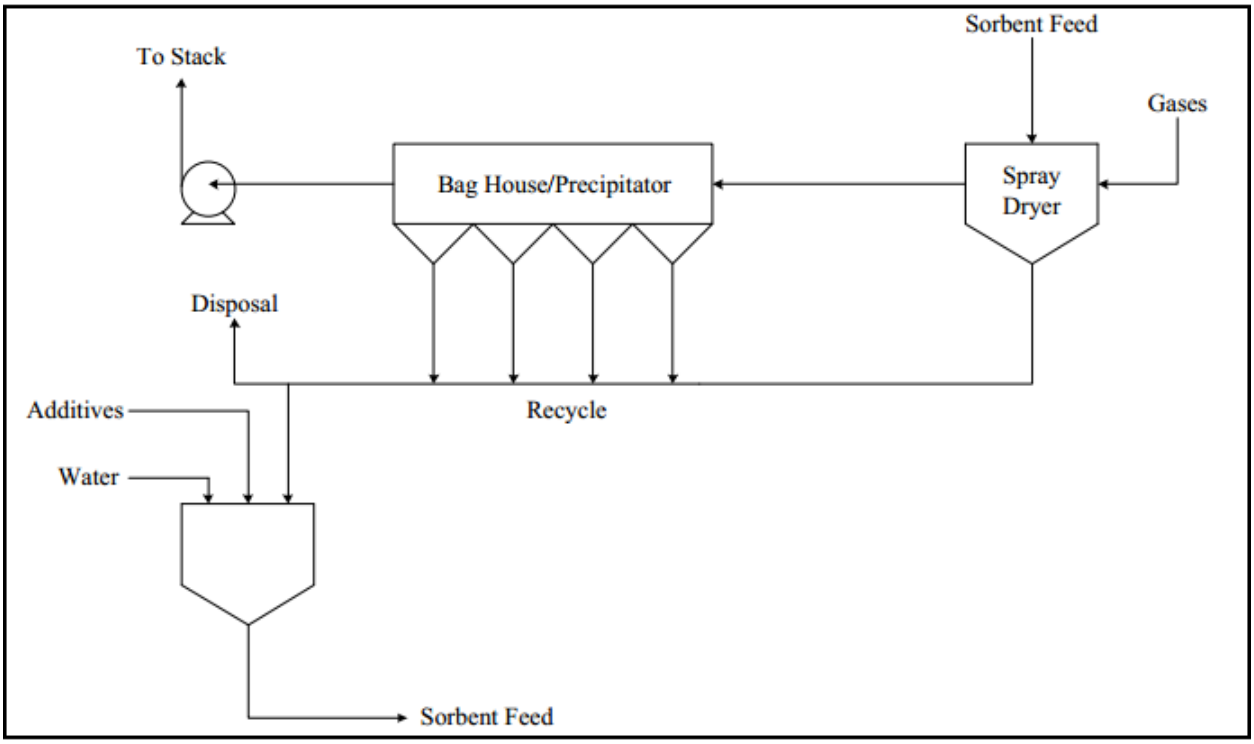

Figure 2. 2: Dry FGD system (Mandlall, 1993)

2.1.3. Semi-dry FGD system

Semi-dry FGD system uses sodium and calcium based reagents as sorbents. Lime is most commonly used because it is cheaper compared to sodium based sorbents. Fresh lime slurry is prepared in a slaker to form slurry with a high sorbent concentration. The lime slurry is dispersed using rotary atomizers or dual-fluid nozzles into the flue gas (USEPA, 2003). The hot flue gases mixes with the slurry leading to evaporation of water

in the slurry and drying the reaction product in the process. The reactions that take place in the spray dryer are represented as:

$$SO_{2(g)} + Ca(OH)_{2(s)} \rightarrow CaSO_3 \cdot {}^1/_2\, H_2O_{(s)} + {}^1/_2\, H_2O_{(l)} \quad (2.3)$$

$$SO_{3(g)} + Ca(OH)_{2(s)} + H_2O_{(l)} \rightarrow CaSO_4 \cdot 2H_2O_{(s)} \quad (2.4)$$

$${}^1/_2\, O_{2(g)} + CaSO_{3(s)} \rightarrow CaSO_{4(s)} \quad (2.5)$$

The reaction product is collected at a downstream precipitator for disposal, and can be used as a by-product or recycled to the slurry.

Sorbent usage in semi-dry systems is limited by its available residence time for gas-solid reaction. This leads to lower SO_2 removal efficiencies between 80% and 90% in comparison to wet FGD system. The capital and operating cost for semi-dry scrubbers is lower than wet FGD system because equipment for handling waste is not required (USEPA, 2003).

2.2. Sorbents for FGD

There is a wide range of sorbents used for flue gas desulphurization process and they play an integral role in the process. The choice of these sorbents is dependent on the design of the of the FGD plant. The choice of sorbent used also vary according to the final required product from the desulphurization process. Sorbents can be calcium, sodium or magnesium based.

Calcium based sorbents is mostly commonly used in non-regenerable processes because they produce safe and stable end-products (Fellner and Khandl, 1999) Calcium based sorbents include limestone, lime, hydrated lime and dolomite. Limestone is mostly used in wet FGD processes because it is cheap and abundantly available. Limestone composition may vary depending on its source but it has high $CaCO_3$ content. For non-regenerable processes using limestone or lime, the sorbent is first prepared by crushing using a ball mill and then mixed with water in a slurry tank to form slurry. The slurry is then pumped to the absorber where it reacts with SO_2 to form an insoluble calcium sulphite or calcium sulphate (Ahlbeck et al., 1995). Wet FGD

processes using limestone as a sorbent have high SO_2 removal efficiency of about 95% (Song and Park, 2001) making it a suitable sorbent for large scale FGD systems. Dolomite and limestone are also used for alkali injection process where the sorbent is calcined (to 800-1100K) to producing calcines to reacts with SO_2 to produce calcium sulphate and magnesium sulphate. This process has low sorbent utilization efficiency of about 20-30% (Karatepe, 2000). The use of dolomite has been found to exhibit better sorbent utilization because it is more porous when compared to limestone (Elert et al., 2002).

Sodium based sorbents are used in dual alkali processes where the alkali is a mixture of sodium hydroxide (NaOH), sodium carbonate (Na_2CO_3) and sodium sulphite (Na_2SO_3) solution. SO_2 reacts with the sodium alkali mixture and the spent liquor is regenerated using a second alkali (either lime or limestone). Calcium sulphite and calcium sulphate generated from regeneration is removed and the regenerated sodium sorbent solution is returned to the process again. This process is has about 95% SO_2 removal efficiency (Karatepe, 2000) but it is expensive and produces hazardous wastes which are harmful to the environment. The reaction between SO_2 and alkaline components (NaOH, Na_2CO_3 and Na_2SO_3) takes place as follows:

$$2NaOH_{(aq)} + SO_{2(g)} \rightarrow Na_2SO_{3(s)} + H_2O_{(l)} \quad (2.6)$$

$$NaOH_{(aq)} + SO_{2(g)} \rightarrow NaHSO_{3(s)} \quad (2.7)$$

$$Na_2CO_{3(s)} + 2SO_{2(g)} + H_2O_{(l)} \rightarrow 2NaHSO_{3(s)} + CO_{2(g)} \quad (2.8)$$

$$Na_2CO_{3(s)} + SO_{2(g)} \rightarrow Na_2SO_{3(s)} + CO_{2(g)} \quad (2.9)$$

$$Na_2SO_{3(s)} + SO_{2(g)} + H_2O_{(l)} \rightarrow 2NaHSO_{3(s)} \quad (2.10)$$

The presence of oxygen in the system oxidizes sodium sulphite to sulphate

$$2Na_2SO_{3(s)} + O_{2(g)} \rightarrow 2Na_2SO_{4(s)} \quad (2.11)$$

Sodium bisulphite, sulphite and sulphate react with second alkali (lime or limestone) to generate sodium alkali solution and produce calcium sulphite and sulphate.

$$2NaHSO_{3(s)} + Ca(OH)_{2(aq)} \rightarrow Na_2SO_{3(s)} + CaSO_3.{}^1/_2\,H_2O_{(s)} + {}^3/_2\,H_2O_{(l)} \quad (2.12)$$

$$Na_2SO_{3(s)} + Ca(OH)_{2(aq)} + {}^1/_2\, H_2O_{(l)} \rightarrow 2NaOH_{(aq)} + CaSO_3.{}^1/_2\, H_2O_{(s)} \quad (2.13)$$

$$Na_2SO_{4(s)} + Ca(OH)_{2(aq)} \rightarrow 2NaOH_{(aq)} + CaSO_{4(s)} \quad (2.14)$$

Magnesium enhanced lime process uses magnesium and lime to form a more reactive slurry at a pH 7.5 – 8.5. Magnesium salts are more soluble and therefore allows the scrubbing process to take place in alkaline medium. This leads to high SO_2 removal capacity (Lani and Babu, 1997). Ammonium based sorbents are also used in SO_2 removal. Ammonia slurry reacts with SO_2 to form ammonium sulphate ($(NH_4)_2SO_4$) which is a fertilizer (Alix et al., 2003). Because of the cost of ammonia sorbent, this process is not commonly used. Table 2.1 shows different types of FGD scrubbing processes and their respective sorbents with SO_2 removal efficiency.

Table 2. 1: Process types and sorbents used with their efficiencies

Category	Process type	Sorbent type	SO_2 removal efficiency	
Wet scrubbing				
	Limestone/lime inhibited oxidation	Lime or limestone	90 – 98%	(Moser, 1993)
	Lime/limestone forced oxidation (LSFO)	Lime or limestone	90 – 98%	(Srivastava, 2000)
	Magnesium enhance process	Magnesium oxide	90%	(Srivastava and Jozewicz, 2001)
	Dual alkali	Sodium hydroxide or carbonate	90 – 95%	(Wu et al., 2001)
	Ammonia based	Ammonia	90%	(Gao et al., 2010)
	Seawater	Seawater	96%	(Jia-Twu and Ming-Chu, 2011)
	Aluminium sulphate process	$Al_2(SO_4)_3$, $Al(OH)_2$	95%	(Jamil et al., 2013)
	Urea process	Urea		(Jamil et al., 2013)

Dry scrubbing				
	Spray dry	Lime/limestone/soda ash	80 – 90%	(Karatepe, 2000)
	Calcium-based alkali injection	Limestone	50 – 60%	(Bortz et al., 1989)
	Sodium-based alkali injection	Trona/nahcolite	>80%	(Giovanni and Smith, 1990)
	Humidified sorbent injection (continuous fluidized bed)	Calcium hydroxide, fly ash	50 – 70%	(Karatepe, 2000)
	Adsorption	Activated carbon	90%	(Mochida et al., 2000)
	Catalytic oxidation	Oxidation catalyst	95%	(Liu et al., 2003)

2.3. Factors affecting dissolution process in wet FGD system

The overall performance of a wet FGD system and the removal of SO_2 are strongly dependent on the quality and type of the sorbent used and also the rate of it dissolving in solution. It also affects the potential of scaling caused by calcium sulphite ($CaSO_3$) and calcium sulphate ($CaSO_4$) in the scrubber (Rochelle et al., 1983). Dissolution rate of a sorbent in the slurry tank is dependent on variety of factors like the slurry temperature, pH, impurities, sorbent particle size and sorbent additives. Therefore it is necessary to optimize these variables in order to achieve maximum sorbent utilization as well as achieve improved SO_2 removal capacity in wet FGD systems.

2.3.1. Slurry pH

Many studies have been done extensively to determine the effects of pH on dissolution especially in limestone. Berner and Morse (1974) performed an experiment on dissolution of limestone from different sources and it was observed that at low pH (less than 4), the dissolution rate is approximately proportional to the hydrogen ion concentration and therefore maximum dissolution occurs. Similar results were observed in a study done by Plummer et al. (1979) and Uchida et al. (1978). A study on the kinetics of calcite dissolution was done by Fred and Foglar (1998) and it was found out that when the pH is lower than 2.9, dissolution is influenced by the rate of transport of reactants to the surface and the rate of products away from the surface.

Limestone dissolution rate varies according to the partial pressure of CO_2 at the middle pH ranges. Above the pH of 5, dissolution rate is controlled by diffusion of OH^-, HCO_3^- and other species (Chan and Rochelle, 1982). At higher pH values, limestone dissolution rate decreases.

2.3.2. Temperature

Dissolution rate of sorbents varies greatly with temperature. The slurry temperature influences the equilibrium constants between the chemical species in solution. Conversion decreases at low temperature. The dissolution of $CaCO_3$ in limestone is considered an endothermic reaction because when the temperature rises, entropy increases resulting in more products (Meserole et al., 1982). Also a study by Sjoberg

and Rickard (1984) showed that surface chemical reaction and mass transfer are the main controlling steps in calcite dissolution. Thus the dissolution rate is a function temperature and this can be expressed for a heterogeneous reaction using the Arrhenius equation:

$$Ln\ K_r = \frac{E_a}{RT} + Ln\ K_o \quad (2.15)$$

Where E_a is the apparent activation energy, R is the gas rate constant (8.314 J/kmol), K_o is a constant, T is the temperature and K_r is the dissolution rate constant.

For heterogeneous reaction systems, the apparent activation energy is used to distinguish between transport controlled reactions, surface chemical reaction controlled reactions or mixed reactions. The surface chemical reaction controlled processes have higher values of E_a than the transport controlled reactions (mass transfer) (Letterman, 1995).

At the temperature of 25°C calcite dissolution is dependent on mass transfer (Sjoberg and Rickard, 1984). This is because of the diffusion of H^+ from the liquid bulk region through the mass transfer boundary layer to the surface of the particle. Lund et al. (Lund et al., 1975) studied the dissolution of calcite using HCl. They found out that calcite dissolution at 25°C is limited by mass transfer while at 15.6°C both mass transfer and surface chemical reaction control were important.

2.3.3. Particle size distribution and surface area

The sorbent particle size has a great effect on the dissolution rate which is directly proportional to sorbent utilization in wet FGD system. Sorbent with finer particle sizes have been found to have greater SO_2 removal efficiency in wet FGD system (Chang et al., 1982). This is due to increased surface area, leading to more calcium ions being exposed for chemo-sorption reaction. Fine limestone could either be natural occurring or obtained by grinding of larger particles. The reactivity of limestone can be measured by evaluating the effect of particle size distribution (PSD). The experimental data and the models developed by Johnsson and Kiil (2000) showed that PSD has a great influence on limestone reactivity. This was in agreement with research conducted by Frandsen et al. (2001) who found out that lowering the particle size from 20 to 4µm

reduced residual limestone from 4.3 to 1.3 wt.% and also increased the overall degree of desulphurization from 83 to 87% in wet FGD system. Sjoberg (1976) did an experiment using pure analytical Calcium carbonate with different particle sizes and it was observed that the dissolution rate mass transfer increased proportionately with the calcite surface area. An experiment by Sun et al. (2010) also indicated that limestone dissolution rate of limestone particle increases with a decrease in particle size. A mass transfer model developed by Ukawa et al. (1993) to study the effect of PSD and different compositions on limestone dissolution showed that the dissolution rate constant is proportional to the hydrogen ion activity.

2.3.4. Additives and impurities

The rate of sorbent dissolution and reaction with SO_2 in wet FGD system can be enhanced by addition of organic or inorganic additives. Many studies have been conducted on the effects of additives on wet FGD systems (Rochelle et al., 1982; Zheng et al., 1997; Heidel et al., 2014; Ru-shan et al., 2011).

Organic compounds when added to sorbent slurry will effectively improve the mass transfer coefficient of the liquid phase (Ru-shan et al., 2011). This leads to strengthening of the buffer capacity of the pH value between gas-liquid phase and the liquid bulk as well which improves SO_2 removal efficiency. Additives can also reduce the dissolution resistance of the sorbent or diffusion resistance of SO_2, therefore raising the utilization of sorbent. Additives are used to stabilize the slurry pH and allow desulfurization to take place at controlled pH and reduce the scale formation in the system.

Sorbent dissolution rate is also influenced by the presence of impurities in solution with calcium carbonate. The most common impurities present in limestone sorbent include silica, iron, magnesium, dissolved sulfites and aluminium complexes. The impurities present in sorbents depend on their sources. These impurities are mostly contained in low quality limestone and could adversely affect the scrubber performance. A study was conducted by Jarvis et al. (1991) on selection of limestone reagents for wet FGD system with magnesium and dolomite as impurities. Dolomite was found to be inert while the presence of magnesium leads to improved FGD system performance. Also

Letterman (1995) found out that calcite with high insoluble impurities has low dissolution rate because the impurities reduce the calcite area being exposed to solution.

2.4. Additives for wet flue gas desulphurization

In an effort to improve the overall desulphurization efficiency of a wet FGD system, additives can be used to improve sorbent utilization and also accelerate SO_2 – sorbent reaction. Additives can improve the ionic diffusivity and SO_2 dioxide diffusion through the product layer which in turn leads to maximum utilization of the sorbent (Adanez et al., 1997). Additives can also accelerate dissolution rate of sorbents such as limestone which has low solubility in wet FGD process. These additives can be organic acids, inorganic salts or compound additives.

During limestone dissolution, additives can have the following effects on the system (Ru-shan et al., 2011):

- Improve the sorbent reactivity
- Improve SO_2 removal rate
- Prevent scale formation in the scrubber system
- Cause buffer effect on the slurry solution
- Increase sorbent utilization

A good additive is regarded as one that can reduce the dissolution resistance of the sorbent, improve desulfurization by reducing the diffusion resistance of SO_2, stabilize the slurry pH and minimize scale formation in the scrubber system. Additives in wet FGD systems can also change the dewatering properties of the waste product making the process more economical (Maldei, 1993). Additives can be categorized as:

2.4.1. Organic acids and buffer additives

A theoretical study by Rochelle and King (1977) indicated that an organic acid with buffering capacity between interfaces provides optimum enhancement. Adipic acid and other organic buffers enhance the transport of H^+ ions in the liquid film between liquid/gas and liquid/solid (Frandsen et al., 2001). The presence of an additive in the slurry serves as transport mechanism for H^+ therefore improves limestone dissolution

because it is greatly dependent of H^+ diffusion to the surface of the particle when the pH is less than 5.

Studied conducted by Rochelle et al. (1982) showed that adipic acid provides good buffering effect in wet FGD processes with forced oxidation. Other organic acids that can be used to provide good buffering in wet FGD processes include in dibasic acid – DBA (a liquid mixture of dicarboxylic acids), glycolic acid, maleic acid, glutaric acid, citric acid and succinic acid (Chang and Mobley, 1983). A study by Frandsen et al., (2001) reported that adipic acid increases limestone dissolution rate by providing additional transport of H^+ from the bulk liquid region to the liquid film surrounding the surface of the particle. Limestone dissolves when the hadipate-ion (AH^-) releases H^+ on the limestone particle surface where it reacts with CO_3^{2-}. Adipic acid also increases SO_2 removal rate by acting as a medium of transport for H^+ from the bulk phase thereby promoting the dissociation of SO_2.

Liu and Xiao (2006b) used acetic acid as an additive and they observed similar effects as adipic acid on limestone dissolution enhancement and buffer action on the slurry. It was found that the buffer capacity of acetic acid increased when its concentration was increased and it can buffer the pH of the gas/liquid interface and the pH of the bulk liquid phase. Liu and Xiao (2006a) studied the absorption of SO_2 into limestone slurry with the addition of organic additives such as acetic acid. The presence of acetic acid in the slurry was found to cause a shift in the reaction towards the gas-liquid interface therefore improving SO_2 removal capacity.

Liu et al. (2008) studied limestone dissolution with different organic additives (acetic acid and benzoic acid). It was reported that the mixture of the two additives exhibited a higher buffering capacity compared to the individual acids. This was attributed to an increase in surface area due to foaming. Benzoic acid was observed to have a weaker buffering capacity compared to acetic acid.

2.4.2. Inorganic salt additives

Inorganic salts have been found to be effective in improving sorbent utilization and system desulphurization capacity. These are salts of sodium, magnesium and calcium. Rochelle and King (1977) used sodium and magnesium salts as additives and they

found that they are soluble when added to the slurry and they accumulate as soluble sulphates. They further indicated that the bicarbonate formed due to this does not react with SO_2 fast enough and hence enhances mass transfer on the system. Sodium salt additive was used by Wang et al, (2002) when Na_2CO_3 was used. A high calcium conversion was observed in limestone, which led to better sorbent utilization.

Davini et al. (1992) studied the effect of using NaCl as an additive on desulphurization properties of limestone. They found out that it improved the desulphurization efficiency of the sorbent by formation of a suitable porous structure and better size distribution in the limestone. A study by Ehrlich (1975) indicated that sodium chloride inhibits the formation of calcium sulphate shell which can stop absorption of more SO_2. This leads to high desulfurization efficiency in the sorbent used. The use of Sodium chloride as an additive can improve sulphur retention capacity of a sorbent used. Adanez et al., (1997) used NaCl to enhance the desulphurization capacity of $Ca(OH)_2$ and it was found to improve its sulphur retention capacity.

The use of $MgSO_4$ and Na_2SO_4 was studied by Wenshou et al. (2002) and they found out that there was an improved rate of desulphurization when used as an additive. $MgSO_4$ and Na_2SO_4 promoted limestone dissolution rate in the slurry with its mass transfer characteristics also being improved. The use of $CaCl_2$ as an additive was studied by Dong et al. (2004) for wet limestone FGD process. They observed an increase in the conversion of calcium ions which was attributed to low pH caused by the presence of $CaCl_2$.

2.4.3. Ammonium salts additives

Ammonium compound additives have been found to have an effect on the chemistry of the dissolution process. It affects the slurry buffer capacity and also the dissolution rate of the sorbent. Stergarsek et al. (1999) found that the presence of ammonium in during dissolution increases the buffer capacity and consequently improve the dissolution of limestone. Their results also indicated a corresponding decrease in liquid to gas ratio required for the same absorber performance. The use of ammonium salts was found to have a similar effect as adipic acid in wet FGD process.

The presence of ammonium salt has also been found to enhance the absorption of SO_2 from flue gas by acting as a means of transport for SO_2 from the gas phase to the liquid phase. Ammonium salts provide additional transport of H^+ which reacts with limestone therefore leading to an increase in the dissolution of limestone (Rutto et al., 2009; Wang et al., 2012). A study by Takashina et al. (2002) on the effect of ammonium concentration on the SO_2 absorption in limestone slurry showed an increase in the rate of SO_2 removal with ammonium concentration on the slurry concentration.

2.5. Dissolution rate determination methods

Dissolution studies were first investigated on calcite and aragonite to determine their solubilities and dissolution rates. Peterson (1966) and Berner (1966) investigated the dissolution of calcite in sea water under laboratory conditions. Dissolution studies have commonly been determined using two methods: the free drift method and the pH stat apparatus. The free drift method allows the dissolution to start at a lower pH value of 4 and then left to drift to equilibrium as limestone particles dissolve. The dissolution rate is determined from the change in the value of the pH with time. The pH stat allows dissolution to take place at constant pH throughout the process. This is achieved by adding the necessary amount of acid to the solution as the dissolution takes place. The dissolution rate is evaluated from the amount of acid added with time (Maldei, 1993). A representation of pH stat apparatus is shown in Figure 2.3.

The pH stat method was developed by Morse in 1974 and it has been used by Morse and Berner (1972), Morse (1974) and Chan and Rochelle (1982) among others. The free drift method has been used by Sjoberg (1976), and Plummer et al. (1978). Many other studies have been conducted using the pH stat technique to study the kinetic behaviors of different sorbents during dissolution. Chang et al. (1982) studied the effect of particle size distribution on the rate of limestone dissolution by developing a mass transfer model. The model was able to predict dissolution rates and it was observed that limestone dissolution was mostly affected by the particle size distribution (PSD). Ukawa et al. (1993) studied the effects of PSD on the rate of limestone dissolution using a

mass transfer model that was developed. It was observed that the dissolution rate constant of limestone is proportional to the hydrogen ion activity.

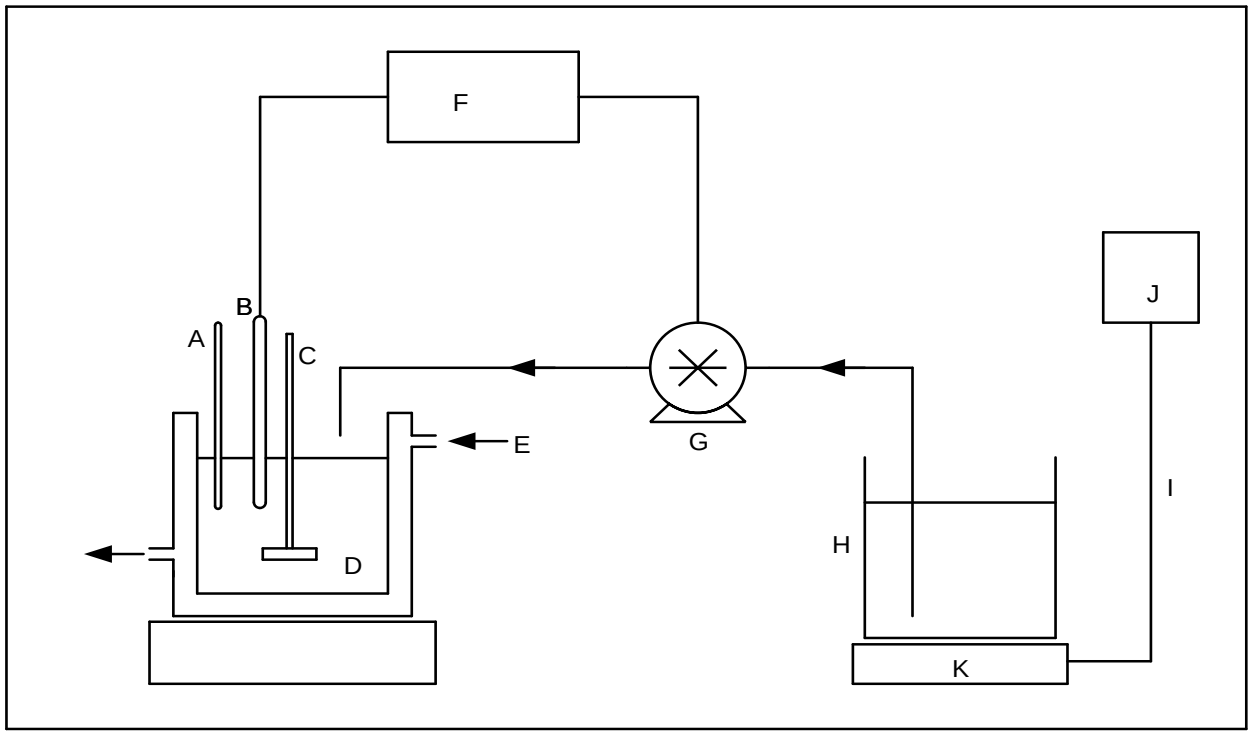

Figure 2. 3: Figure 2.3: A pH stat apparatus used in dissolution studies (A-thermometer, B-pH electrode, C-stirrer, D-reaction vessel, E-Heating medium, F-pH controller, G-acid pump, I-cable, J-computer and K-weighing balance).

2.6. Kinetics of dissolution

Dissolution kinetics has been used in different research areas such as to study karst formation in limestone, water chemistry in calcite deposits and deep sea water sedimentation (Morse and Mackenzie, 1990; Plan, 2005; Eisenlohr et al., 1999). Dissolution kinetic data is important in industrial processes for design of wet FGD plants. In wet FGD process dissolution kinetics can be used to describe how particles react with the fluid reactant and the dissolution chemistry of the process.

The dissolution process in a wet FGD process is a heterogeneous reaction system involving a liquid reactant and solid particles which react to for solid and liquid products. This is represented as:

$$aA(Fluid) + bB(Solid) \rightarrow cC(Fluid) + dD(Solid) \quad (2.16)$$

There are two models that can be used to describe non-catalytic heterogeneous reaction systems; the shrinking core model and the progressive conversion model (Levenspiel, 1972). The progressive conversion model considers that the solid reactant gets continuously converted throughout the particle while the shrinking core model considers a reaction first occurring at the surface of the particle before proceeding to the unreacted core of the particle. The shrinking core model best describes a wide range of reactions systems and reasonable represents the reality.

Plummer et al. (1978) studied the kinetics of calcite dissolution in aqueous media proposed three reactions that occur simultaneously:

$$H^{+}_{(aq)} + CaCO_{3(s)} \leftrightarrow Ca^{2+}_{(aq)} + HCO^{-}_{3(s)} \quad (2.17)$$

$$H_2CO_{3(aq)} + CaCO_{3(s)} \leftrightarrow Ca^{2+}_{(aq)} + 2HCO^{-}_{3(s)} \quad (2.18)$$

$$H_2O_{(l)} + CaCO_{3(s)} \leftrightarrow Ca^{2+}_{(aq)} + HCO^{-}_{3(aq)} + OH^{-}_{(aq)} \quad (2.19)$$

The pH was observed to have a significant effect on dissolution. H^{+} ions dominate the dissolution reaction at low pH (eqn. 2.17) and at high pH (eqn. 2.19). Studies conducted by Fredd and Foglar (1998) demonstrated that dissolution of calcite in acidic media is mostly influenced by the rate of transport of reactants and products to the surface of the particle and also away from the particle surface.

The kinetics of limestone dissolution has mostly been studied using the unreacted shrinking core model. The kinetic analysis of the dissolution of a South African limestone by Siagi and Mbarawa (2009) showed that limestone dissolution in acidic media transpired according to the shrinking core model with rate controlling step being the surface chemical reaction. Xiang et al. (2009) also studied the kinetics of limestone using the shrinking core model and their experimental results indicated that dissolution of limestone is controlled by mass transfer and surface chemical reactions. A study of limestone dissolution from different sources by Shih et al. (2000) showed that dissolution is controlled by mass transfer of hydrogen ions with chemical reactions in the liquid film surrounding the particle.

2.6.1. The shrinking core model

Sorbent dissolution in a wet FGD process is a heterogeneous reaction in which the fluid reactant comes in contact with the solid particles, reacts with it and results in the formation of a product. This can be described by two processes, the transportation of fluid reactants from the liquid bulk region and transportation of the products from the surface of the particle to the liquid bulk region. The solid particles may shrink or remain unchanged in size depending on the amount of impurities present and the product that is formed. The shrinking core model has largely been used to study the dissolution kinetics of different sorbent materials for wet FGD system (Teir et al., 2007; Demirkıran, 2008; Siagi et al., 2007; Marabi et al., 2008; Bharadwaj et al., 2013).

The shrinking core model considers reactant reaction on the surface of the solid particle to produce products in aqueous and in solid state which may remain on the surface of the particle. As the reaction proceeds, more products are formed and the fluid reactants from the bulk liquid phase encounter diffusion resistance from undissolved particles. This is shown in Figure 2.4. As this occurs, the size of the unreacted core also reduces (Levenspiel, 1972). In a fluid-solid reaction system, the following three steps are considered to occur in series:

- Diffusion of the liquid reactants from the liquid bulk phase through the liquid film to the surface of the particle
- Reaction of the fluid reactants with the solid at the surface of the solid particle
- Diffusion of the reaction products from the surface of the solid back to the liquid bulk phase.

For a non-catalytic heterogeneous reaction system, it is controlled by one of the following steps: diffusion through the product layer, diffusion through the film layer or chemical reaction at the surface of the unreacted core. The slowest of these steps is considered rate controlling step.

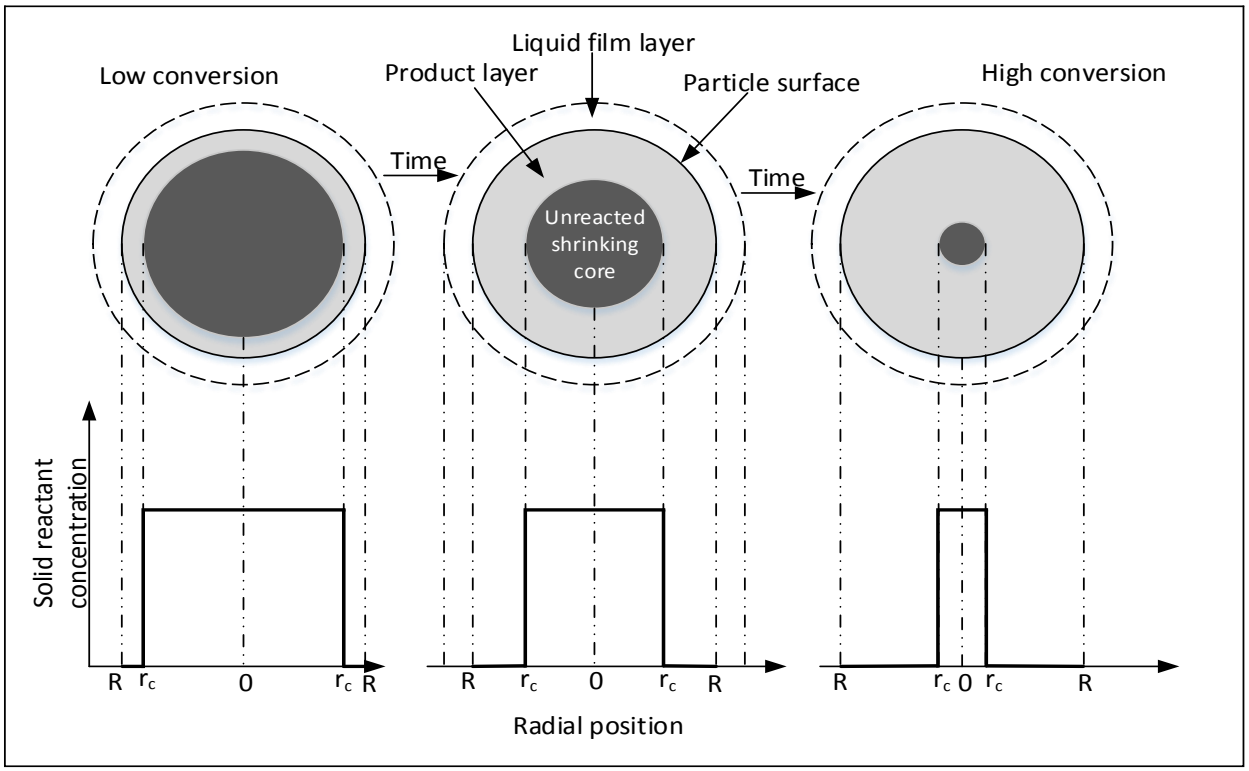

Figure 2. 4: Graphical representation of the shrinking core model (Levenspiel, 1972)

2.6.1.1. Diffusion through the film layer

For diffusion through the film layer, the fluid reactants diffuse through the film and product layer is formed before reacting. The layer of products formed as well as the film layer provides resistance to the diffusion of the fluid reactants to the unreacted core. The reaction profile is shown in Figure 2.5.

A liquid-solid heterogeneous reaction system is represented by the following:

$$A_{(l)} + bB_{(s)} \rightarrow cC_{(l)} + dD_{(s)} \tag{2.20}$$

The time taken in film layer diffusion control for a particle to react completely is represented by:

$$t = \frac{\rho_B R}{3bK_i C_A} X \tag{2.21}$$

$$X = 1 - \left(\frac{r_c}{R_i}\right)^3 \tag{2.22}$$

where, r_c is final particle radius

R_i - Initial particle radius

K_i - Mass transfer coefficient

ρ_B - Molar density of B in the solid

R - Universal gas constant

X - Fractional conversion of a sphere

b - Stoichiometric coefficient

C_A - Bulk concentration

Equation (21) represents the relationship between the reaction time and the conversion for a film layer diffusion controlled process.

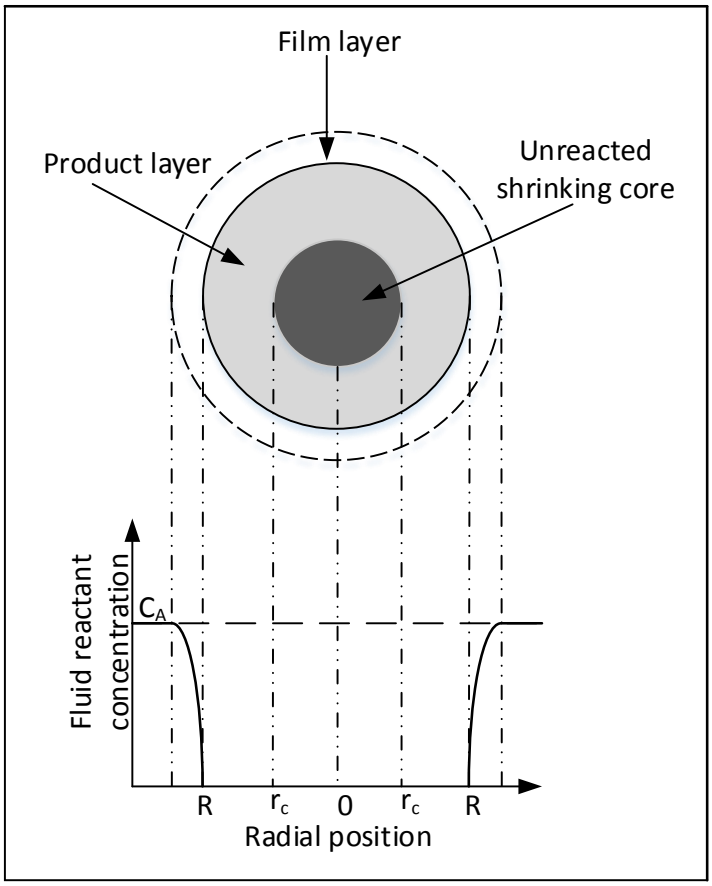

Figure 2. 5: Fluid film diffusion graphical representation (Levenspiel, 1972)

2.6.1.2. Diffusion through the Product Layer

As dissolution proceeds, products are formed which may remain on the surface of the particle. This is what provides resistance to the movement of fluid reactants into the unreacted core and this can be the controlling step in dissolution. This is represented in Figure 2.6.

For this kind of reaction mechanism, the relationship between the conversion and the reaction time can be represented as:

$$t = \frac{\rho_B R}{3bK_g(C_{AB}-C_{Ae})}\left(1 + 2(1-X) - 3(1-X)^{2/3}\right) \quad (2.23)$$

The diffusion rate of the process can be obtained from the slope of a linear relationship between $1 + 2(1-X) - 3(1-X)^{2/3}$ and the reaction time. This will determine of diffusion through the product layer can be rate controlling.

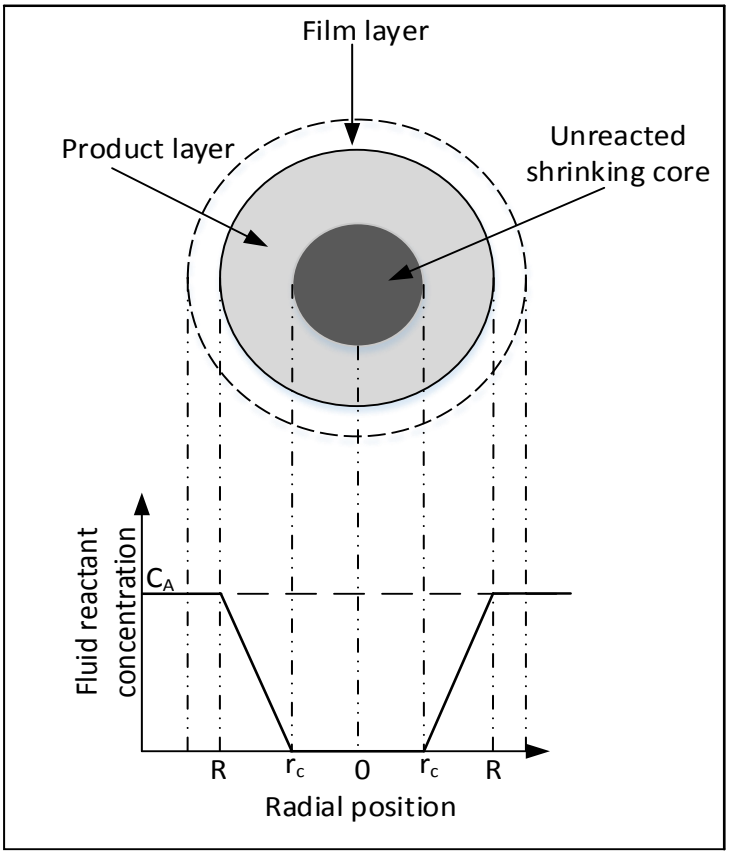

Figure 2. 6: Diffusion through the product layer graphical representation (Levenspiel, 1972)

2.6.1.3. Chemical Reaction

The reaction between the fluid reactants and the solid on the surface of the particle may be the slowest step making it rate controlling (shown in Figure 2.7). When a process is controlled by chemical reaction, the time required for the particle to react completely is given by:

$$t = \frac{\rho_B R}{3bK_g(C_{AB}-C_{Ae})}\left(1-(1-X)^{1/3}\right) \quad (2.24)$$

The reaction rate constant is obtained from the linear relationship between $1-(1-X)^{1/3}$ and the reaction time. With this relationship, it can be interpreted if the dissolution process is controlled by chemical reaction at the surface of the particle.

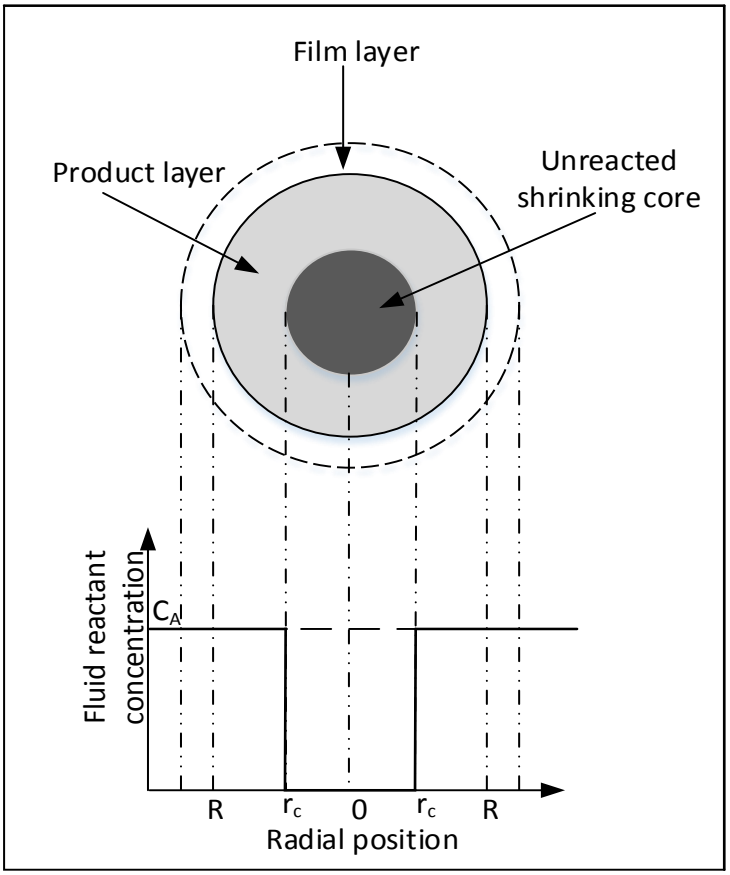

Figure 2. 7: Surface chemical reaction control graphical representation (Levenspiel, 1972)

Table 2.2 shows activation energies for different sorbent and their respective rate determining steps obtained by different authors in their dissolution studies.

Table 2. 2: Activation energies of different sorbents obtained by different authors

Author	Sorbent	Temperature Range (°C)	Activation energy	Controlling step	Technique used
(Siagi and Mbarawa, 2009)	Calcium based material	30 - 70°C	26.1 kJ/mol	Chemical reaction	pH stat
(Abali et al., 2007)	Calcined manganese ore	20 - 70°C	25.51 kJ/mol	Pseudo – first order reaction	N/A
(Bharadwaj et al., 2013)	Magnesium Hydroxide	22 - 52°C	42±6 kJ/mol	Diffusion control	pH stat
(Barton and Vatanatham, 1976)	Limestone	1 - 75°C	15 kJ/mol	Hydrogen diffusion	N/A
(Lacin et al., 2005)	Natural magnesite	40 - 70°C	78.4 kJ/mol	Chemical reaction	N/A
(Xiang et al., 2009)	Limestone in presence of sulfite	25 - 55°C	29.82 kJ/mol	Chemical reaction	pH stat
(Guo et al., 2011)	Magnesium hydrate	25 - 55°C	14.18 kJ/mol	Mass transfer	pH stat
(Zhao et al., 2013)	Calcium based alkaline industrial wastes	30 - 50°C	14.51±1 kJ/mol 7.89±1 kJ/mol	Surface reaction Film diffusion	pH stat
(Rutto and Enweremadu, 2011a)	Magnesium based material	30.15 - 70.15°C	45.685 kJ/mol	Chemical reaction	pH stat
(Alkattan et al., 1998)	Calcite and limestone	25 - 80°C	19±4 kJ/mol		Free-drift rotating disk

(Gledhill and Morse, 2006)	Calcite	25 - 82.5°C	21±1 kJ/mol	Diffusion control	N/A
(Rutto and Enweremadu, 2011b)	Calcium based material	75 - 105°C	20.62 kJ/mol	Chemical reaction	pH stat

N/A – Not available

2.7. Sorbent Characterization

2.7.1. X-ray fluorescence (XRF)

XRF spectroscopy technique uses X-ray to determine the major and trace elements in a solid sample. The X-ray is generated when charged particles are accelerated at a high potential difference to collide with matter (Nuffield, 1966). The energy generated is enough to excite the inner shell electrons in the sample thereby emitting secondary X-ray fluorescence radiation energy of the ionized electrons in the atoms. The element abundance is a measure of the intensity of the secondary X-ray fluorescence spectra which is measured using X-ray spectrometer. XRF technique is capable of detecting (determining) all the elements in the period table even at low concentration (Nuffield, 1966).

2.7.2. X-ray diffraction (XRD)

XRD uses X-rays produced when high speed electrons meet a solid object in an X-ray tube. A heated tungsten filament is used to produce electrons by applying a high potential difference and directed towards a target. The X-ray tube operates in a vacuum so as to allow free flow of electrons. When high speed electrons hit the atoms of the target, X-ray is released which is allowed to leave the tube in a window. The tungsten filament gets heated and water is used to cool it down. The pattern of this X-ray on the lattices of atoms in a crystal is generated and analyzed. The interpretation of this pattern gives a better understanding and information on the nature of the material and its structure (Cesareo, 1999; Nuffield, 1966; West, 1988).

2.7.3. Brannauer-Emmet-Teller (BET) surface area and porosity measurement

The property of a material in terms of the specific surface area and the porosity is important in many process applications such as catalysis, pharmaceuticals, sintered materials as well as sorbents for FGD. As dissolution takes place, it is expected that there is an increase in the specific surface which has been proven to improve SO_2 removal capacity. The extent of the formation of the specific surface area is determined using the BET method.

Specific surface area is determined by the amount of gas molecules that are adsorbed on the surface of the adsorbate. Nitrogen, krypton or Argon gases are normally used. Gas molecules may be adsorbed on the surface of the adsorbate either through chemical (chemisorption) or physical (physisorption) process (Mikhail and Robens, 1983). The physical process is a reversible process while the chemical process may not be reversible. The BET surface area method uses the physical process and the monolayer capacity is evaluated from the adsorption isotherm. Monolayer capacity is the quantity of adsorbate which can fill a monolayer on the solid surface. The monolayer capacity is proportional to the specific surface area, S (m^2/g) according the following relationship:

$$S = \frac{X_m N A_m}{M \times 10^4} \times 10^{-16} = \frac{X_m N A_m}{M} \times 10^{-20} \quad (2.25)$$

X_m is the monolayer capacity

M is the adsorbate molecular weight

A_m is the area in Angstrom units

Adsorption isotherms are used to determine the pore size by gas adsorption method. There are six classes of isotherms used to distinguish the pore sizes (Sing et al., 1982). This is represented in Figure 2.8.

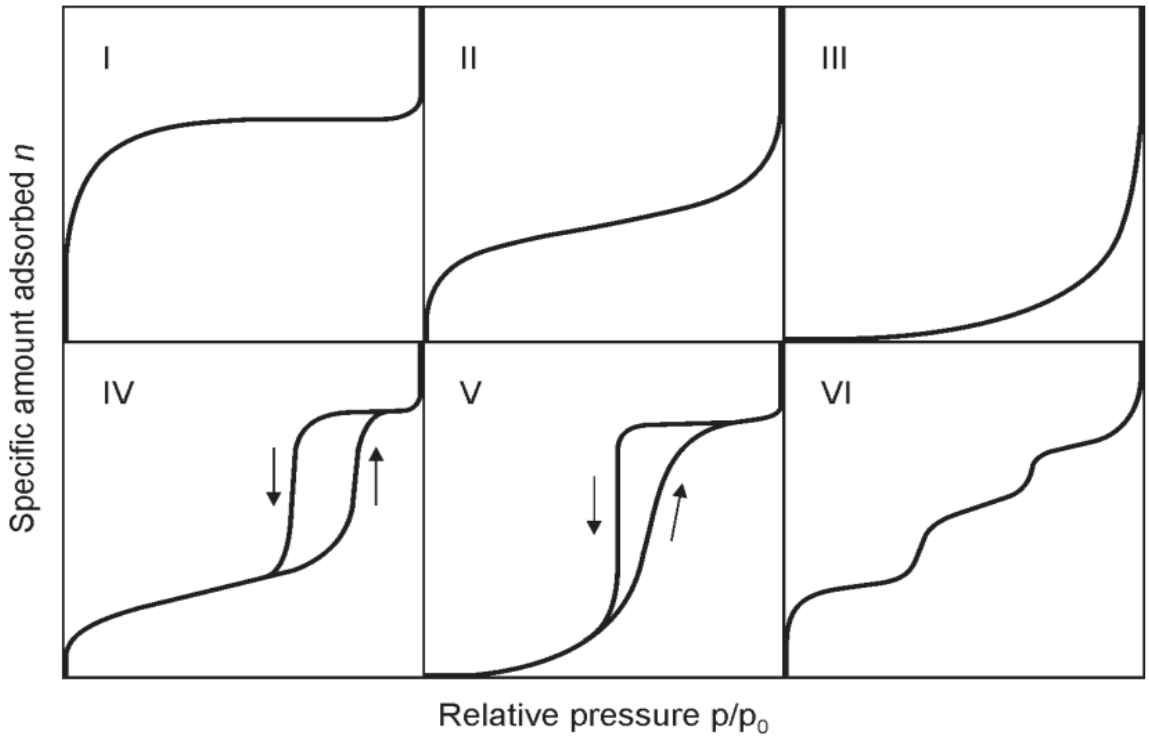

Figure 2. 8: Classification of adsorption isotherms (Sing et al., 1982)

Type I isotherm: These are solids having microporous pores

Type II isotherm: This is powder having pore diameter greater the micropores and less than macropores. It has unrestricted monolayer-multilayer adsorption.

Type III isotherm: This is depicted when the interaction of the adsorbate is larger than the adsorbent surface area.

Type IV isotherm: This is exhibited by porous solids with mesopore range pores.

Type V isotherm: This is due to adsorbate-adsorbent interactions. This is also for solids having pores in the mesopore range.

Type VI isotherm: This is exhibited on a stepwise adsorption on a porous surface.

2.7.4. Scanning electron microscopy (SEM)

It is necessary to observe how dissolution affects the surface morphology of a sorbent. This is done using a scanning electron microscope to produce high magnification images. SEM images help in interpreting the composition, surface structure and crystallinity of sample. SEM uses a beam of electrons directed on the sample which

comes in contact with atoms present on the sample surface. When electrons meet the atoms, a signal is generated which describes the surface morphology of the sample and its composition. SEM also uses secondary electrons to achieve images because the electrons are highly reliable in presenting the topographical features (Hatch, 1984). SEM technique is mostly used because it has a greater focal point and high spatial resolution (Devaney and Chidlaw, 1978).

2.7.5. Fourier Transform Infrared Spectroscopy (FTIR)

FTIR is a technique used to derive information from a sample regarding its composition and structural changes upon chemical modification (Madejova, 2002). FTIR determines the structural bonding, functional groups and the chemical properties of a sample. Therefore it can be used to monitor the structural changes and process changes for physiological conditions (Braiman and Rothschild, 1988).

Old FTIR techniques uses mull techniques or KBr pellets which requires sample preparation. Technology has led to introduction of new techniques such as Attenuated Total Reflectance (ATR), diffuse reflectance (DRIFT) or specular reflectance. The DRIFT and the ATR techniques require no sample preparation and it is increasingly being used worldwide.

2.8. Design of experiments (DoE)

A lot of experiments are done in research as well as in optimization and system development. This necessitates the use of design of experiments. Design of experiments is a systematic approach that is used to obtain an estimate of the number of experiments which can satisfy minimum number of experimental runs with large sample size and still provide relevant results (Mason et al., 1989; Thompson, 1982). It is the operation of gathering of information where two or multiple variables are involved. It involves the stages in which experiments are chosen to test a hypothesis. These stages include experimental subjects, what to be carried out and the choice to instruments to be used (Jacquez, 1998). Design of experiment is used in research in order to obtain optimum conditions for experiments by varying the different variables involved. It helps to optimize relevant information collected with minimum waste of resources and time.

DoE influences the parameter estimation and the results to be obtained because it determines the process in which relevant dynamics become visible from the measured data (Hametner et al., 2013).

2.8.1. Types of DoE

2.8.1.1. One factor at a time

This type of DoE allows one variable to be investigated while all other independent variables are held constant. It is one of the most commonly used type of DoE. One factor at a time allows one to find out whether a factor has an effect on the experiment easily because information is received after every run rather than waiting for the whole experiment to be completed (Qu and Jeff Wu, 2005). It is most preferred because it allows the investigator to react quickly to the data found and also allows the investigator to focus on the optimum regions of the experiment (Friedman and Savage, 1947; Daniel, 1973). However one factor at a time method has been discouraged mainly because it is susceptible to bias and required more runs to obtain an estimate of some interactions and also the results obtained are not general (Wu and Hamada, 2000; Logothetis and Wynn, 1989).

2.8.1.2. Central composite design

Central composite design is one of the most commonly used second order design because of its usefulness for systems with potential interaction effects between variables. It can be used either in a single experiment or in a sequential experiment (Thompson, 1982; Lazic, 2004; Cox and Reid, 2000). CCD contains factorial or fractional factorial 2^k design with central points as C_o augmented with 2k axial points which allow curvature evaluation. The number of experimental runs needed to develop a CCD model is given as $N = 2^k+2k+C_o$ (Box and Wilson, 1992). The axial points, central points and factorial points are used to evaluate the quadratic terms, magnitude of the experimental error and the interaction terms respectively (Myer and Montgomery, 2002).

2.9. References

Abali, Y., LU, S.K.O. and Kaymak, J. 2007. Dissolution kinetics of calcinated manganese ore in acetic acid solutions. C. B. U. Journal of Science, , pp. 81-88.

Adanez, J., Fierro, V., Garcia-Labiano, F. and Palacios, J. 1997. Study of modified calcium hydroxides for enhancing SO_2 removal during sorbent injection in pulverized coal boilers. Fuel, vol. 76, no. 3, pp. 257-265.

Ahlbeck, J., Engman, T., Fältén, S. and Vihma, M. 1995. Measuring the reactivity of limestone for wet flue-gas desulfurization. Chemical engineering science, vol. 50, no. 7, pp. 1081-1089.

Alix,F. R., Dancan,J. L. and McLarnon,C. R. 2003. Sulphur dioxide removal using ammonia, 6,605,263. Washington, DC: U.S. Patent and Trademark Office.

Alkattan, M., Oelkers, E.H., Dandurand, J. and Schott, J. 1998. An experimental study of calcite and limestone dissolution rates as a function of pH from− 1 to 3 and temperature from 25 to 80 C. Chemical Geology, vol. 151, no. 1, pp. 199-214.

Barton, P. and Vatanatham, T. 1976. Kinetics of limestone neutralization of acid waters. Environmental science & technology, vol. 10, no. 3, pp. 262-266.

Berner, R.A. and Morse, J.W. 1974. Dissolution kinetics of calcium carbonate in sea water; IV, Theory of calcite dissolution. American Journal of Science, vol. 274, no. 2, pp. 108-134.

Berner, R.A. 1966. Diagenesis of carbonate sediments: interaction of magnesium in sea water with mineral grains. Science (New York, N.Y.), vol. 153, no. 3732, pp. 188-191.

Bharadwaj, H.K., Lee, J., Li, X., Liu, Z. and Keener, T.C. 2013. Dissolution kinetics of magnesium hydroxide for CO_2 separation from coal-fired power plants. Journal of hazardous materials, vol. 250, pp. 292-297.

Bortz, S., Roman, V. and Offen, G. 1989. Hydrate and process parameters controlling SO2 removal during hydroxide injection near 1000 F, Proceedings of First Combined FGD and Dry SO2 Control Symposium , pp. 8.

Box, G.E. and Behnken, D.W. 1960. Some new three level designs for the study of quantitative variables. Technometrics, vol. 2, no. 4, pp. 455-475.

Box, G. and Wilson, K. 1992, On the Experimental Attainment of Optimum Conditions in Breakthroughs in Statistics Springer, , pp. 270-310.

Braiman, M.S. and Rothschild, K.J. 1988. Fourier transform infrared techniques for probing membrane protein structure. Annual Review of Biophysics and Biophysical Chemistry, vol. 17, no. 1, pp. 541-570.

Cesareo, R. 1999, X-Ray Fluorescence Spectrometry, Wiley Online Library.

Chan, P. and Rochelle, G.T. 1982. Limestone dissolution. Flue Gas Desulfurization, vol. 188.

Chang, C., Dempsey, J.H., Borgwardt, R.H., Toprac, A.J. and Rochelle, G.T. 1982. Effect of limestone type and grind on SO_2 scrubber performance. The cost-reduction effect of finer limestone grinding on SO_2 scrubber efficiency can be very considerable. Environmental Progress, vol. 1, no. 1, pp. 59-65.

Chang, J.C. and Mobley, J.D. 1983. Testing and Commercialization of Byproduct Dibasic acids as Buffer Additives for Limestone Flue Gas desulfurization Systems. Journal of the Air Pollution Control Association, vol. 33, no. 10, pp. 955-962.

Cooper, C.D. and Alley, F. 1994, Air pollution control: A design approach, Waveland Press Prospect Heights, IL.

Cox, D.R. and Reid, N. 2000, The theory of the design of experiments, CRC Press.

Daniel, C. 1973. One-at-a-time plans. Journal of the American statistical association, vol. 68, no. 342, pp. 353-360.

Davini, P., DeMichele, G. and Ghetti, P. 1992. An investigation of the influence of sodium chloride on the desulphurization properties of limestone. Fuel, vol. 71, no. 7, pp. 831-834.

Demirkıran, N. 2008. A study on dissolution of ulexite in ammonium acetate solutions. Chemical Engineering Journal, vol. 141, no. 1, pp. 180-186.

Devaney, A. and Chidlaw, R. 1978. On the uniqueness question in the problem of phase retrieval from intensity measurements. JOSA, vol. 68, no. 10, pp. 1352-1354.

Dong, P., Cao, H., Bie, R. and Yu, H. 2004. Experimental study on effect of inorganic salts as additives on wet flue gas desulphurization. Journal of Harbin Institute of Technology, vol. 5, pp. 016.

Ehrlich, S. 1975. Conf. on fluidized combustion, Institute of Fuel, Symp Ser London, 1975, pp. 1 - 10.

Eisenlohr, L., Meteva, K., Gabrovsek, F. and Dreybrodt, W. 1999. The inhibiting action of intrinsic impurities in natural calcium carbonate minerals to their dissolution kinetics in aqueous $H_2O–CO_2$ solutions. Geochimica et Cosmochimica Acta, vol. 63, no. 7, pp. 989-1001.

Elert, K., Rodriguez-Navarro, C., Pardo, E.S., Hansen, E. and Cazalla, O. 2002. Lime mortars for the conservation of historic buildings. Studies in Conservation, vol. 47, no. 1, pp. 62-75.

Fellner, P. and Khandl, V. 1999. Characterization of Limestone Reactivity for Absorption of SO_2 from Fume Gases. Chemical papars, vol. 53, no. 4, pp. 238-241.

Ferreira, S.C., Bruns, R., Ferreira, H., Matos, G., David, J., Brandao, G., da Silva, E.P., Portugal, L., Dos Reis, P. and Souza, A. 2007. Box-Behnken design: An alternative for the optimization of analytical methods. Analytica Chimica Acta, vol. 597, no. 2, pp. 179-186.

Frandsen, J.B., Kiil, S. and Johnsson, J.E. 2001. Optimisation of a wet FGD pilot plant using fine limestone and organic acids. Chemical Engineering Science, vol. 56, no. 10, pp. 3275-3287.

Fredd, C.N. and Fogler, H.S. 1998. The kinetics of calcite dissolution in acetic acid solutions. Chemical engineering science, vol. 53, no. 22, pp. 3863-3874.

Friedman, M. and Savage, L.J. 1947. Planning experiments seeking maxima. Techniques of statistical analysis, , pp. 365-372.

Gao, X., Ding, H., Du, Z., Wu, Z., Fang, M., Luo, Z. and Cen, K. 2010. Gas–liquid absorption reaction between $(NH_4)_2SO3$ solution and SO2 for ammonia-based wet flue gas desulfurization. Applied Energy, vol. 87, no. 8, pp. 2647.

Giovanni,D. V. and Smith,W. B. 1990. Process for removal of particulates and SO_2 from combustion gases, 4,956,162. Washington, DC: U.S. Patent and Trademark Office.

Gledhill, D.K. and Morse, J.W. 2006. Calcite dissolution kinetics in Na–Ca–Mg–Cl brines. Geochimica et Cosmochimica Acta, vol. 70, no. 23, pp. 5802-5813.

Guo, R., Pan, W., Zhang, X., Xu, H. and Ren, J. 2011. Dissolution rate of magnesium hydrate for wet flue gas desulfurization. Fuel, vol. 90, no. 1, pp. 7-10.

Hametner, C., Stadlbauer, M., Deregnaucourt, M., Jakubek, S. and Winsel, T. 2013. Optimal experiment design based on local model networks and multilayer perceptron networks. Engineering Applications of Artificial Intelligence, vol. 26, no. 1, pp. 251-261.

Hatch, J.E. 1984, Aluminum: properties and physical metallurgy, ASM International.

Heidel, B., Hilber, M. and Scheffknecht, G. 2014. Impact of additives for enhanced sulfur dioxide removal on re-emissions of mercury in wet flue gas desulfurization. Applied Energy, vol. 114, pp. 485-491.

Jacquez, J.A. 1998. Design of experiments. Journal of the Franklin Institute, vol. 335, no. 2, pp. 259-279.

Jamil, R., Ming, L., Jamil, I. and Jamil, R. 2013. Application and Development Trend of Flue Gas Desulfurization (FGD) Process: A Review.

Jarvis, J., Meserole, F., Owens, D. and Roothaan, E. 1991. Factors Involved in the Selection of Limestone Reagents for Use in Wet FGD Systems, Proceedings: 1991 EPRI/EPA/DOE SO 2 Control Symposium .

Jia-Twu, l. and Ming-Chu, C. 2011, Using seawater to remove SO_2 in a FGD system in Waste water treatment and reutilization.

Johnsson, J.E. and Kiil, S. 2000, Sulphur Chemistry in Combustion II in Pollutants from Combustion Springer, , pp. 283-301.

Kaladhar, M., Subbaiah, K., Rao, C.S. and Rao, K.N. 2011. Application of Taguchi approach and utility concept in solving the multi-objective problem when turning AISI 202 austenitic stainless steel. Journal of Engineering Science and Technology Review, vol. 4, no. 1, pp. 55-61.

Karatepe, N. 2000. A comparison of flue gas desulfurization processes. Energy Sources, vol. 22, no. 3, pp. 197-206.

Khuri, A.I. and Mukhopadhyay, S. 2010. Response surface methodology. Wiley Interdisciplinary Reviews: Computational Statistics, vol. 2, no. 2, pp. 128-149.

Lacin, O., Dönmez, B. and Demir, F. 2005. Dissolution kinetics of natural magnesite in acetic acid solutions. International Journal of Mineral Processing, vol. 75, no. 1, pp. 91-99.

Lani, B. and Babu, M. 1997. Phase II: the age of high velocity scrubbing, Fuel and Energy Abstracts Elsevier Science, .

Lazic, Z.R. 2004, Design and Analysis of Experiments: Section 2.3, Wiley Online Library.

Letterman, R.D. 1995, Calcium carbonate dissolution rate in limestone contactors, US Environmental Protection Agency, Risk Reduction Engineering Laboratory.

Levenspiel, O. 1972, Chemical Reaction Engineering, 2nd edn, John Wiley and Sons., New York.

Liu, Q., Li, C. and Li, Y. 2003. SO_2 removal from flue gas by activated semi-cokes: 1. The preparation of catalysts and determination of operating conditions. Carbon, vol. 41, no. 12, pp. 2217-2223.

Liu, S. and Xiao, W. 2006a. Modeling and simulation of a bubbling SO_2 absorber with granular limestone slurry and an organic acid additive. Chemical Engineering & Technology, vol. 29, no. 10, pp. 1167-1173.

Liu, S., Liu, P., Gao, J., Liu, J., Ye, Z. and Xu, C. 2008. Simulation studies on limestone dissolution with organic acid additives in limestone-based flue gas desulfurization, Bioinformatics and Biomedical Engineering, 2008. ICBBE 2008. The 2nd International Conference on IEEE, , pp. 3899.

Liu, S. and Xiao, W. 2006b. New wet flue gas desulfurization process using granular limestone and organic acid additives. International Journal of Chemical Reactor Engineering, vol. 4, no. 1.

Logothetis, N. and Wynn, H.P. 1989, Quality through design: experimental design, off-line quality control, and Taguchi's contributions, Clarendon Press Oxford.

Lund, K., Fogler, H.S., McCune, C. and Ault, J. 1975. Acidization II. The dissolution of calcite in hydrochloric acid. Chemical Engineering Science, vol. 30, no. 8, pp. 825-835.

Lundstedt, T., Seifert, E., Abramo, L., Thelin, B., Nyström, Å, Pettersen, J. and Bergman, R. 1998. Experimental design and optimization. Chemometrics and Intelligent Laboratory Systems, vol. 42, no. 1, pp. 3-40.

Maldei, M. 1993, Low Temperature Dry Scrubbing Reaction Kinetics and Mechanisms: Limestone Dissolution and Solubility, Ohio University.

Mandlall, D.K. 1993, Production of improved calcium-based sorbents for sulphur dioxide capture.

Marabi, A., Mayor, G., Burbidge, A., Wallach, R. and Saguy, I. 2008. Assessing dissolution kinetics of powders by a single particle approach. Chemical Engineering Journal, vol. 139, no. 1, pp. 118-127.

Mason, R.L., Gunst, R.F. and Hess, J.L. 1989. Statistical design and analysis of experiments: With applications to engineering and science.

Meserole, F.B., Glover, R.L. and Stewart, D.A. 1982. Studies of the major factors affecting magnesium limestone dissolution. Flue Gas Desulfurization, , pp. 99-111.

Mikhail, R.S. and Robens, E. 1983, Microstructure and thermal analysis of solid surface s, Wiley.

Mochida, I., Korai, Y., Shirahama, M., Kawano, S., Hada, T., Seo, Y., Yoshikawa, M. and Yasutake, A. 2000. Removal of SO_x and NO_x over activated carbon fibers. Carbon, vol. 38, no. 2, pp. 227-239.

Morse, J.W. 1974. Dissolution kinetics of calcium carbonate in sea water; III, A new method for the study of carbonate reaction kinetics. American Journal of Science, vol. 274, no. 2, pp. 97-107.

Morse, J.W. and Berner, R.A. 1972. Dissolution kinetics of calcium carbonate in sea water; I, A kinetic origin for the lysocline. American Journal of Science, vol. 272, no. 9, pp. 840-851.

Morse, J.W. and Mackenzie, F.T. 1990, Geochemistry of sedimentary carbonates, Elsevier.

Moser, R. 1993. Prospects for Inhibited Oxidation FGD Systems, Proceedings of 1993 SO_2 Control Symposium Research Triangle Park, NC, February, 1995, pp. 53 -1 - 53 - 21.

Myer, R. and Montgomery, D.C. 2002. Response Surface Methodology: process and product optimization using designed experiment. John Wiley and Sons, New York, , pp. 343-350.

Nuffield, E.W. 1966. X-ray diffraction methods.

Palanikumar, K. 2008. Application of Taguchi and response surface methodologies for surface roughness in machining glass fiber reinforced plastics by PCD tooling. The

International Journal of Advanced Manufacturing Technology, vol. 36, no. 1-2, pp. 19-27.

Peterson, M.N. 1966. Calcite: rates of dissolution in a vertical profile in the central pacific. Science (New York, N.Y.), vol. 154, no. 3756, pp. 1542-1544.

Plan, L. 2005. Factors controlling carbonate dissolution rates quantified in a field test in the Austrian alps. Geomorphology, vol. 68, no. 3, pp. 201-212.

Plummer, L., Parkhurst, D. and Wigley, T. 1979, Critical review of the kinetics of calcite dissolution and precipitation in .

Plummer, L., Wigley, T. and Parkhurst, D. 1978. The kinetics of calcite dissolution in CO_2-water systems at 5 degrees to 60 degrees C and 0.0 to 1.0 atm CO_2. American Journal of Science, vol. 278, no. 2, pp. 179-216.

Qu, X. and Jeff Wu, C. 2005. One-factor-at-a-time designs of resolution V. Journal of statistical planning and inference, vol. 131, no. 2, pp. 407-416.

Rochelle, G.T., Chan, P.K. and Toprac, A.J. 1983, Limestone Dissolution in Flue Gas Desulfurization Processes, US Environmental Protection Agency, Industrial Environmental Research Laboratory.

Rochelle, G.T. and King, C.J. 1977. The effect of additives on mass transfer in $CaCO_3$ or CaO slurry scrubbing of SO_2 from waste gases. Industrial & Engineering Chemistry Fundamentals, vol. 16, no. 1, pp. 67-75.

Rochelle, G.T., Weems, W.T., Smith, R.J. and Hsiang, M.W. 1982. Buffer additives for lime/limestone slurry scrubbing. ACS symposium series, vol. 188, pp. 243-265.

Ross, P.J. 1988. Taguchi techniques for quality engineering: loss function, orthogonal experiments, parameter and tolerance design.

Ru-shan, R., Xue-min, H., Fa-en, S. and Da-hua, J. 2011. Application of additives to the wet flue gas desulfurization, Electric Technology and Civil Engineering (ICETCE), 2011 International Conference on IEEE, , pp. 1037.

Rutto, H. and Enweremadu, C. 2011a. The dissolution study of a South African magnesium-based material from different sources using a pH-stat. Chemical Industry and Chemical Engineering Quarterly, vol. 17, no. 4, pp. 459-468.

Rutto, H. and Enweremadu, C. 2011b. A study on dissolution of a South African calcium based material in acetic acid solution for flue gas desulphurization, Electrical and

Control Engineering (ICECE), 2011 International Conference on IEEE, , pp. 5701 - 5705.

Rutto, H., Siagi, Z. and Mbarawa, M. 2009. Effect of ammonium compounds on dissolution rate of South African calcium-based material. Journal of hazardous materials, vol. 168, no. 2, pp. 1532-1536.

Sargent and Lundy 2007, Flue gas desulphurization technology evaluation - Dry lime vs wet limestone FGD, National Lime Association, Chicago, USA.

Sargent and Lundy 2003, New wet flue gas desulphurization evaluation, National Lime Association, Chicago, USA.

Shih, S., Lin, J. and Shiau, G. 2000. Dissolution rates of limestones of different sources. Journal of hazardous materials, vol. 79, no. 1, pp. 159-171.

Siagi, Z. and Mbarawa, M. 2009. Dissolution rate of South African calcium-based materials at constant pH. Journal of hazardous materials, vol. 163, no. 2, pp. 678-682.

Siagi, Z., Mbarawa, M., Mohamed, A., Lee, K. and Dahlan, I. 2007. The effects of limestone type on the sulphur capture of slaked lime. Fuel, vol. 86, no. 17, pp. 2660-2666.

Sing, K., Sing, K., Everett, D., Haul, R., Moscou, L., Pierotti, R., Rouquerol, J. and Siemieniewska, T. 1982. Reporting physisorption data for gas/solid systems. Pure Appl.Chem, vol. 54, no. 11, pp. 2201.

Sjoberg, E.L. and Rickard, D.T. 1984. Temperature dependence of calcite dissolution kinetics between 1 and 62 C at pH 2.7 to 8.4 in aqueous solutions. Geochimica et Cosmochimica Acta, vol. 48, no. 3, pp. 485-493.

Sjoberg, E. 1976. A fundamental equation for calcite dissolution kinetics. Geochimica et Cosmochimica Acta, vol. 40, no. 4, pp. 441-447.

Song, H. and Park, J. 2001. Improvement of SO_2 removal by the solubility change of $Ca(OH)_2$ in the spray dryer system. Environmental technology, vol. 22, no. 9, pp. 1001-1006.

Srivastava, R.K. 2000. Controlling SO_2 Emissions--a Review of Technologies.

Srivastava, R.K. and Jozewicz, W. 2001. Flue gas desulfurization: The state of the art. Journal of the Air & Waste Management Association, vol. 51, no. 12, pp. 1676-1688.

Stergarsek, A., Gerbec, M., Kocjancic, R. and Frkal, P. 1999. Modelling and experimental measurements of limestone dissolution under enhanced wet limestone FGD process conditions. Acta Chimica Slovenska, vol. 46, no. 3, pp. 323-333.

Sun, B., Zhou, Q., Chen, X., Xu, T. and Hui, S. 2010. Effect of particle size in a limestone–hydrochloric acid reaction system. Journal of hazardous materials, vol. 179, no. 1, pp. 400-408.

Takashina, T., Honjo, S., Ukawa, N. and Iwashita, K. 2002. Effect of ammonium concentration on SO_2 absorption in a wet limestone gypsum FGD process. Journal of Chemical Engineering of Japan, vol. 35, no. 2, pp. 197-204.

Teir, S., Revitzer, H., Eloneva, S., Fogelholm, C. and Zevenhoven, R. 2007. Dissolution of natural serpentinite in mineral and organic acids. International Journal of Mineral Processing, vol. 83, no. 1, pp. 36-46.

Thompson, D. 1982. Response surface experimentation1. Journal of Food Processing and Preservation, vol. 6, no. 3, pp. 155-188.

Uchida, S., Moriguchi, H., Maejima, H., Koide, K. and Kageyama, S. 1978. Absorption of sulfur dioxide into limestone slurry in a stirred tank reactor. The Canadian Journal of Chemical Engineering, vol. 56, no. 6, pp. 690-697.

Ukawa, N., Takashina, T., Shinoda, N. and Shimizu, T. 1993. Effects of particle size distribution on limestone dissolution in wet FGD process applications. Environmental Progress, vol. 12, no. 3, pp. 238-242.

USEPA 2003, Air pollution control factsheet: flue gas desulphurization - wet, spray dry and dry scrubbers, United States Environmental Protection Agency.

Wang, C., Shen, X. and Xu, Y. 2002. Investigation on sulfation of modified Ca-based sorbent. Fuel Processing Technology, vol. 79, no. 2, pp. 121-133.

Wang, Z., Zhang, X., Zhou, Z., Chen, W., Zhou, J. and Cen, K. 2012. Effect of Additive Agents on the Simultaneous Absorption of NO_2 and SO_2 in the Calcium Sulfite Slurry. Energy & Fuels, vol. 26, no. 9, pp. 5583-5589.

Wenshou, S., Zhongbiao, W. and Tianen, T. 2002. Promoting effects of additives on limestone dissolution in flue gas desulfurization process. China Environmental Science, vol. 22, pp. 305-308.

West, A.R. 1988, Basic solid state chemistry, Wiley New York.

Wu, C. and Hamada, M. 2000. Experiments: Planning, analysis, and parameter design optimization.

Wu, Z., Liu, Y. and Tan, T. 2001. Study of dual-alkali FGD process. Acta Scientiae Circumstantiae, vol. 21, no. 5, pp. 534-537.

Xiang, G., Rui-tang, G., Hong-lei, D., Zhong-yang, L. and Ke-fa, C. 2009. Dissolution rate of limestone for wet flue gas desulfurization in the presence of sulfite. Journal of hazardous materials, vol. 168, no. 2, pp. 1059-1064.

Zhao, J., Li, Y., Han, K., Niu, S. and Lu, C. 2013. Dissolution Characteristics of Calcium-Based Alkaline Industrial Wastes. Journal of Chemical Engineering of Japan, vol. 46, no. 12, pp. 827-832.

Zheng, J., Harris, C.C. and Somasundaran, P. 1997. The effect of additives on stirred media milling of limestone. Powder Technology, vol. 91, no. 3, pp. 173-179.

3. A semi-empirical model for limestone dissolution in adipic acid for wet flue gas desulphurization

3.1. Abstract

Wet Flue gas desulphurization (FGD) systems are commonly used to remove sulphur dioxide by contacting it with limestone in aqueous phase in which is obtained by dissolution. This study investigates the effects of pH (5.5 - 7.0), stirring speed (100 - 400 rpm), solid to liquid ratio (5 - 15 wt. %), acid concentration (0.05 - 0.1M) and temperature (303 – 348K) on the dissolution rate of limestone in adipic acid were investigated using a pH stat apparatus. The reaction dissolution kinetics was investigated by fitting the experimental data into the shrinking core model. Sorbent characterization at different dissolution periods was done using: X-ray fluorescence (XRF), X-ray diffraction (XRD), Brunauer-Emmett-Teller (BET) surface area and scanning electron microscope (SEM). An increase in the specific surface area of the sorbent was observed which was attributed to formation of portlandite which was depicted in XRD analysis. The experimental data were found to fit the shrinking core model with the chemical reaction control. A semi-empirical model was developed from the experimental data to describe the dissolution kinetics:

$$1-(1-X)^{\frac{1}{3}} = 126.5326C^{1.4982}N^{0.7019}\left(\frac{S}{L}\right)^{-0.8056}P^{-1.4539}e^{\left(-29240/RT\right)}t$$

Where C is acid concentration, S/L is solid to liquid ratio, N is stirring speed and P is pH. The activation energy for the process was found to be 29.24kJ/mol.

Key words: Limestone, dissolution, characterization and semi-empirical model.

3.2. Introduction

Sulphur dioxide and nitrogen oxide emissions are as a result of combustion of fossil fuel such as coal. It is known to have detrimental effects on environment and human health; it can cause poor atmospheric visibility, increase the occurrence of respiratory diseases and damage to buildings (Klimont et al., 2013; Kunkel et al., 2013). This has resulted in stringent regulations imposed on coal-fired power plants by many countries. The implementation of flue gas desulphurization (FGD) in power stations has largely been as a result of strict environmental and air quality legislations. Legislations have been passed in South Africa that govern and set standards for emission control, air quality checks and planning (National Environmental Management, South Africa, 2005).

There are several technologies that have been designed to remove sulphur dioxide from flue gas. Flue gas desulphurization (FGD) is largely used to curb sulphur dioxide emission from large electric utilities such as boilers in coal combustion. FGD systems are mostly used because of high sulphur dioxide removal efficiency. FGD systems are categorized as wet, dry and semi dry FGD (You and Li, 2013). Wet FGD systems are largely used because of high SO_2 removal efficiency and also high sorbent utilization (Song and Park, 2001). SO_2 in flue gas is removed by contacting it with limestone in aqueous phase in which it reacts with limestone to form calcium sulphate and calcium sulphite.

The aqueous phase of limestone is obtained by dissolution which is an important step in wet FGD process. The pH-Stat and the free drift methods are the two commonly used methods for determining dissolution rates (Berner and Morse, 1974). The pH stat has been used most commonly in limestone dissolution. Shih et al. (2000) studied the dissolution of limestone from different sources and it was found that dissolution is controlled by mass transfer of hydrogen ions accompanied by surface chemical reaction. It is accelerated by the reaction of H^+ with OH^- ions within the liquid film. A study by Fred and Fogler (1998) showed that dissolution of calcite is also controlled by rate of transport of fluid reactants to the particle surface, the kinetics of reversible surface reaction and the diffusion of reaction products away from the particle surface.

A shrinking core model was used for the study of dissolution kinetics of magnesite from different sources in South Africa and the controlling step was found to be surface chemical reaction (Limo and Enweremadu, 2011). A predictive model for dissolution of limestone was developed by Ukawa et al., (1993), based in mass transfer mechanism of limestone dissolution at different particles sizes.

Sulphur dioxide removal efficiency of wet FGD plants using limestone as sorbent can be improved by use of fine limestone and addition of various organic acids. Any organic acid with buffering capacity in the interval between pH of the gas/liquid interface and pH of bulk liquid phase would enhance dissolution (Liu et al., 2010; Rutto and Enweremadu, 2011; Potgieter and Gregory, 2012). This led to use adipic acid because it provides good buffer mechanism in wet FGD processes. Glutaric acid, succinic acid and dibasic acid (liquid solution of adipic acid) have also been found to have good buffering effect during dissolution (Qin et al., 2013). The concentration of organic acid, the acidity of limestone slurry and the kind of organic acid used are the main factors that affect limestone dissolution rate (Liu et al., 2010).

This study investigates the dissolution kinetics of limestone in wet flue gas desulphurization process by varying the stirring speed, acid concentration, pH, solid to liquid ratio and temperature. Characterization is also done at different dissolution periods to determine the effects of dissolution on the sorbent. The raw and the used sorbents were characterized using XRD, XRF, FTIR and SEM analysis methods.

3.3. Method

3.3.1. Materials

Limestone samples were obtained from a local mine and the XRF analysis showed the chemical composition of limestone as 83.66% $CaCO_3$, 1.4% MgO, 0.94% SiO_2, 0.36% Fe_2O_3 and 0.04% H_2O with Loss on ignition of 9.84%. The raw material was crushed using a ball mill and sieved to different particle sizes using shaking screen sieves. The chemicals used were adipic acid and calcium standards for AAS were obtained from Sigma Aldrich.

3.3.2. Method

A predetermined amount of limestone was added to the reactor vessel containing distilled water. The temperature, solid to liquid ratio, acid concentration, stirring speed and pH were varied according to the experimental design. This was done using temperature controlled magnetic stirrer. The pH of the reaction mixture was determined using pH electrode dipped into the solution and connected to a pH controller having a specific pH range of pH 0.01. When the pH goes beyond the set value, the pump gets activated automatically and adds the acid to the reaction vessel and lower the pH value to the set point. The experimental setup for the experiment is illustrated in Figure 3.1. A sample was then be removed, filtered and analyzed for calcium ions using Atomic Absorption Spectrophotometer (AAS) using a hollow cathode lamp for Calcium element analysis. The dissolution fraction was evaluated as follows:

$$X = (Calcium\ ions\ in\ solution)/(Total\ amount\ of\ calcium\ ions\ in\ original\ sample)$$

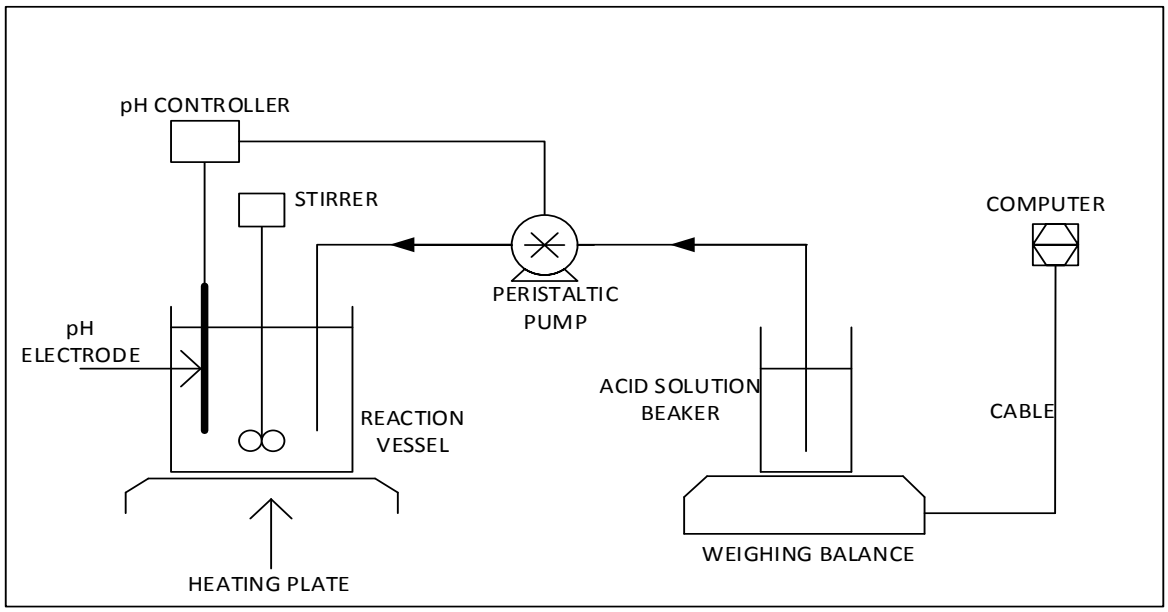

Figure 3 1: Schematic diagram showing the experimental set up for dissolution of limestone in adipic acid.

3.3.3. Sorbent characterization techniques

Qualitative analysis of raw limestone and the sorbents after dissolution was done using XRD to determine the phases present. The material was prepared using a back loading preparation method. Two samples were scanned after addition of 20% Si for qualitative

determination of amorphous content. The sorbent was milled using a McCrone micronizing mill. It was analyzed with a PANalytical Empyrean diffractometer with PIXcel detector and fixed with Fe filtered Co-Kα radiation. The phases were identified using X'pert Highscore Plus software.

FTIR analysis was done using Perkin Elmer spectrum (400 FT-IR/FT-NIR) machine to determine the functional groups present in the samples. The machine is equipped with a universal attenuated total reflectance (ATR) accessory. The detector on the FT-IR/FT-NIR instrument was made from diamond and there was no sample preparation required. The samples were scanned at a range of 4000 to 650 cm^{-1}.

The morphological structure of the samples at different dissolution periods was examined using a scanning electron microscope (SEM). Before the analysis, the samples were sprinkled on an adhesive carbon tape and were metallized using gold. The images of the samples were recorded at various magnifications.

The BET standard method was used to determine the specific surface area of raw limestone and sorbents after dissolution. The pore size distribution was determined from nitrogen adsorption-desorption isotherm by the BJH method in a surface area and porosity analyzer.

3.4. Shrinking core model theory

The dissolution of solid particles in liquid system can be described by the dissociation of solute particles from the solid surface and diffusion of these particles towards the liquid bulk phase (Yuan et al., 2012; Bhaskarwar, 1988). The shrinking core model considers that the reaction first occurs at the surface of the particle then moves towards the centre. As the reaction proceeds, the unreacted core of the particle is reduced in size while more solid and aqueous products are formed. For a reaction of this kind the following three steps are considered to occur in series during the reaction (Szubert et al., 2006):

- Movement of the fluid reactant through the bulk liquid layer to the solid surface
- Reaction of the fluid reactant with the solid on the surface of the solid
- Movement of the reaction products through the film layer back to the bulk of the fluid

For a heterogeneous reaction system it can be controlled by: product layer diffusion, diffusion through the fluid film diffusion or the chemical reaction at the surface of the core of the unreacted particle. The slowest of above steps is considered as the rate controlling step in the system. Since the analyzed sample for this experiment is high purity limestone and has no ash layer during reaction, it is regarded that dissolution can either be controlled by diffusion through the fluid film or chemical reaction at the surface of the particle. The rate equations can therefore be integrated and written as follows:

$$X = \frac{3bk_l C_A}{\rho_B R_0} t = k_r t \qquad \text{Fluid film diffusion} \qquad (3.1)$$

$$1 - (1 - X)^{\frac{1}{3}} = \frac{bk_s C_A}{\rho_B R_0} t = k_r t \qquad \text{Chemical reaction control} \qquad (3.2)$$

The experimental data were tested into the integral rate equations for the shrinking size. The apparent rate constants and the corresponding regression coefficients were obtained graphically from the slope of the linear relationship between $1 - (1 - X)^{\frac{1}{3}}$ and the reaction time.

The temperature dependence on the reaction rate constant is expressed using the Arrhenius law:

$$K = K_o e^{\left(-E_a/RT\right)} \qquad (3.3)$$

Where K_o is the pre-exponential factor, E_a is the apparent activation energy, *R* is the universal gas constant and *T* is the temperature.

The values of the activation energy E_a and K_o are obtained from a linear relationship between -ln K and 1/T. The activation energy for product layer diffusion controlled reaction is usually below 20kJ/mol while chemically controlled reaction is 40-80 kJ/mol (Zhang et al., 2011; Siagi and Mbarawa, 2009). This therefore needs a precise evaluation of the activation energy in order to determine the reaction mechanism.

3.5. Results and Discussion

3.5.1. Mechanism for dissolution of limestone

The rate at which Ca^{2+} ions are leached out from limestone ($CaCO_3$ dissolution) plays an important role in the sulphation process. Sulphur dioxide removal depends on the amount of Ca^{2+} ions in solution. The mechanism for dissolution of $CaCO_3$ in limestone in the presence of adipic acid is as follows:

Adipic acid first undergoes dissociation to form adipate and hydrogen ions in solution, this occurs according to eqn. (3.4) below:

$$C_6H_{10}O_{4(aq)} \rightarrow C_6H_8O_{4(aq)}^{2-} + 2H_{(aq)}^{+} \quad (3.4)$$

The $CaCO_3$ in limestone then undergoes dissolution by adipate complexation. It reacts as follows:

$$CaCO_{3(s)} + C_6H_8O_{4(aq)}^{2-} + H_2O \rightarrow CaC_6H_8O_{4(aq)} + 2OH_{(aq)}^{-} + CO_{2(g)} \quad (3.5)$$

Dissolution of $CaCO_3$ by hydrogen complexation can also occur leading to more calcium ions in solution as shown in eqn. (3.6):

$$CaCO_{3(s)} + H^{+}{}_{(aq)} \rightarrow Ca^{2+}{}_{(aq)} + OH_{(aq)}^{-} + CO_{2(g)} \quad (3.6)$$

Adipic acid can also be formed in the bulk (eqn. 3.7) and can further dissolute $CaCO_3$ to form calcium adipate complex in solution (eqn. 3.8).

$$C_6H_8O_{4(aq)}^{2-} + 2H_{(aq)}^{+} \rightarrow C_6H_{10}O_{4(aq)} \quad (3.7)$$

$$CaCO_{3(s)} + C_6H_{10}O_{4(aq)} \rightarrow CaC_6H_8O_{4(aq)} + 2OH_{(aq)}^{-} + CO_{2(g)} \quad (3.8)$$

Dissociation of calcium complexes (formed from eqn. 3.8) and precipitation of calcium hydroxide in the bulk of the solution is due to super saturation (Rocha et al., 2004; Birchal et al., 2000); this is shown is eqn. 3.9 and 3.10. Hydration of calcium results in the formation of large hydroxide aggregates with large surface area. This leads to improved surface area in sorbents for flue gas desulphurization (van der Merwe and Strydom, 2006).

$$CaC_6H_8O_{4(aq)} \rightarrow C_6H_8O_{4(aq)}^{2-} + Ca_{(aq)}^{2+} \quad (3.9)$$

$$Ca_{(aq)}^{2+} + 2OH_{(aq)}^{-} \rightarrow Ca(OH)_{2(s)} \quad (3.10)$$

3.5.2. XRD analysis

Figure 3.2 shows the experimental results of XRD analysis. The main mineralogical constituents of raw limestone and the sorbents after dissolution are portlandite $(Ca(OH)_2)$ and calcite $(CaCO_3)$. The presence of portlandite $(Ca(OH)_2)$ peaks in raw limestone could have been due to contamination or exposure to moisture during preparation for XRD analysis (Monnin et al., 2006).

Figure 2 also shows portlandite peaks increases with dissolution period while calcite peaks reduces with prolonged dissolution period. The reduction of calcite peaks shows that dissolution occurred as calcium ions are leached out of calcium carbonate. The increase in portlandite peak is due to hydration process which occurs with time. The formation of portlandite contributes to the increase in specific surface area which can improve the rate of SO_2 absorption in flue gas desulphurization.

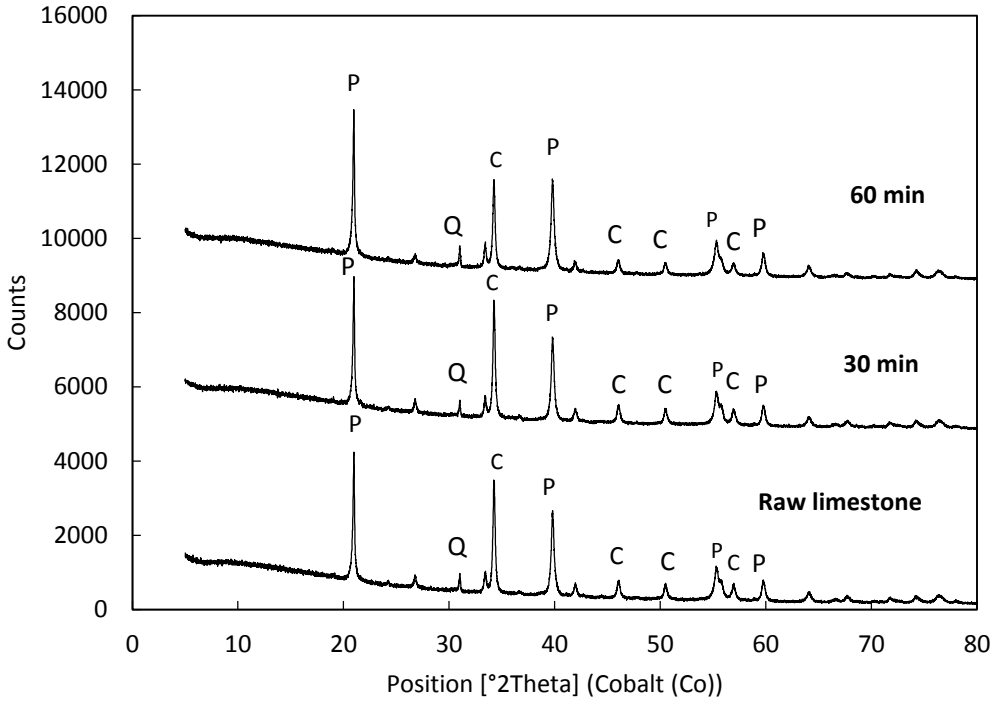

Figure 3 2: X-ray diffraction patterns representing limestone fresh sample and the sorbents at different dissolution periods (P - portlandite, C – calcite, Q - quartz).

3.5.3. BET surface area.

Figure 3.3 shows the adsorption/desorption isotherm plot together with the specific surface area for raw limestone and sorbents after dissolution. It is observed that the specific surface area of the samples increased after dissolution. The maximum surface area is observed at 60 minutes (18.56m^2/g). The increase in surface area could be attributed to the products of hydration (formation of portlandite). This is found to be in good agreement with the results obtained by the XRD analysis. It could also be attributed to pores created due to the removal of $CaCO_3$ from the solid particles into solution.

The adsorption/desorption isotherm plot shows that the raw limestone and the sorbents after dissolution belong to a typical type II isotherm according to IUPAC (International Union of Pure and Applied Chemistry) classification, characterizing multilayer adsorption that shows macroporous material (Hadjar et al., 2008). This indicates that the particles are mesopores having their pore diameters larger that than micropores. Pore sizes between 2 and 100 µm have been identified as the effective zone for the sulphation reaction between SO_2 and sorbent (Garea et al., 1997; Lee et al., 2005).

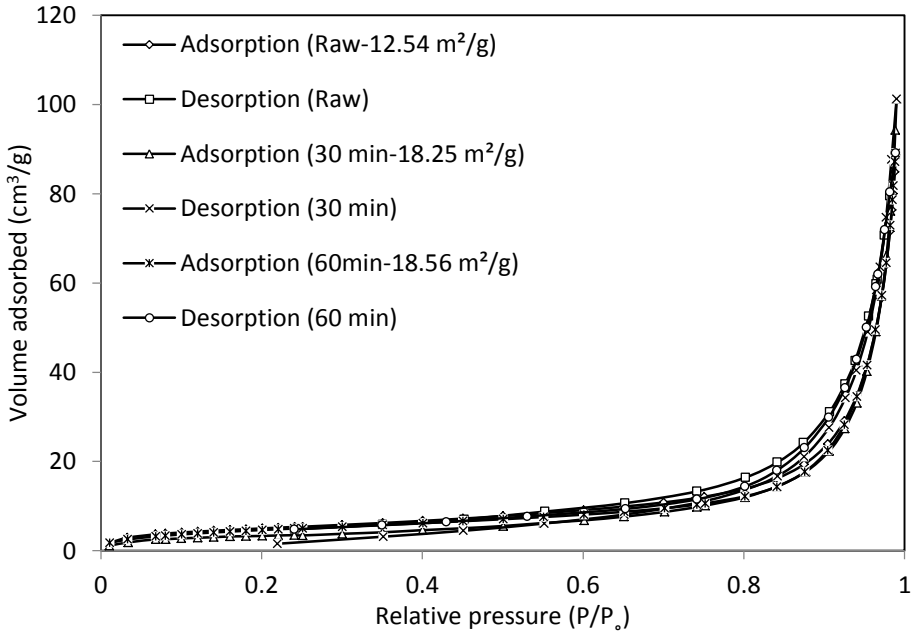

Figure 3 3: Adsorption/desorption isotherms and specific surface areas for raw limestone and the sorbents after dissolution

3.5.4. FTIR analysis

Figure 3.4 represents the FTIR spectra of the samples before and after dissolution. The characteristic bands appearing at 2512, 1793, 1420, 875 and 712 cm^{-1} indicates the presence of calcite (Sdiri et al., 2010). This shows that the main constituent of raw limestone and the sorbents after dissolution is calcium in form of calcite as it can be seen in the characteristic bands. A strong band at low frequency range (1200-900 cm^{-1}) suggests the presence of quartz together with calcite (Sdiri et al., 2010). From Figure 5, the peak appearing at 1087 cm^{-1} represents quartz and it also occurs at 798 cm^{-1} and 799 cm^{-1}. The infrared peak at 3643 cm^{-1} is due to hydroxyl stretching region with Si-O-Si in the samples. This results from the outer hydroxyl ions in the sample (Maravelaki-Kalaitzaki and Kallithrakas-Kontos, 2003).

The removal of carbonate minerals due to dissolution lead to reduced infrared peaks of calcite in the sorbents after dissolution. The effect of this can be seen in the Figure 5 at 2512, 1793, 873 and 712 cm^{-1} infrared peaks. Dissolution also had an effect on silicate material in the samples with the characteristic bands at 1087 and 799 cm^{-1} being reduced in the sorbents after dissolution.

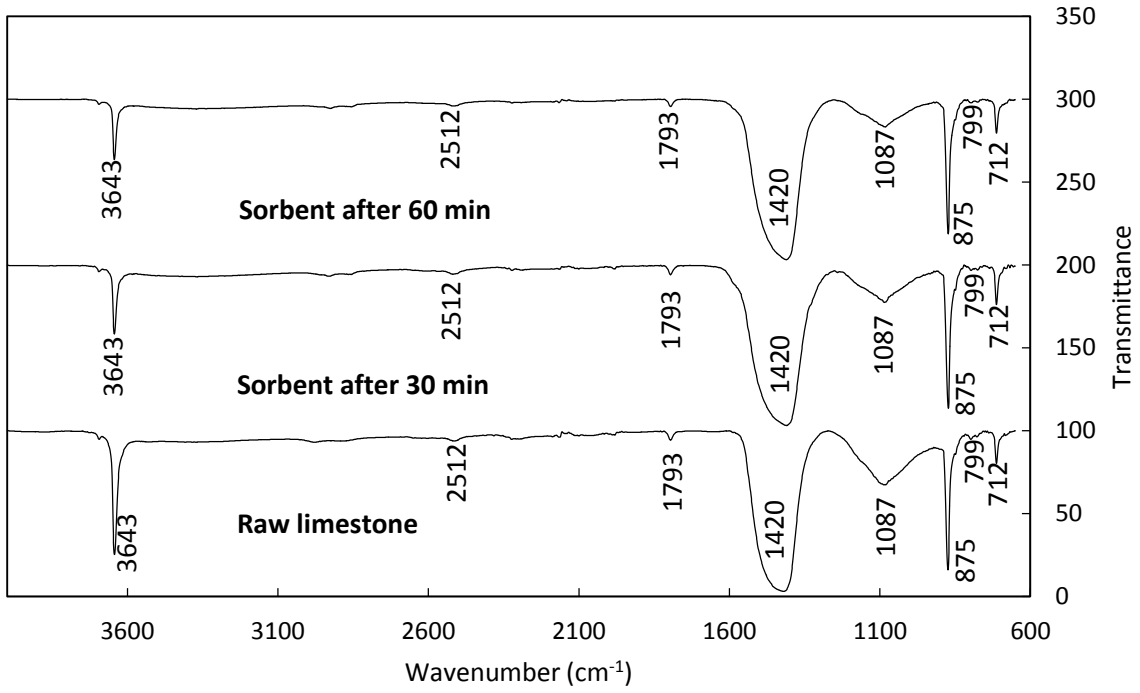

Figure 3 4: FTIR spectra for raw limestone and the synthesized sorbents after 30 and 60 minutes.

3.5.5. Effects of reaction variables on dissolution rate of limestone

3.5.5.1. Effect of solid to liquid ratio

This experiment was done in the range of 5-15 wt. %. The temperature, stirring speed, acid concentration and pH were kept constant at 333K, 200rpm, 0.1M and 5.5 respectively. The results are represented in Figure 3.5(a). A high conversion of calcium ions was noticed from the lowest solid to liquid ratio. This is because there is decrease in the fluid reactant per unit weight of the solid as solid to liquid ratio increases.

3.5.5.2. Effect of acid concentration

To investigate the effect of acid concentration on dissolution of limestone, different experiments were performed at 0.05M, 0.075M, 0.1M and 0.15M adipic acid. The solid to liquid ratio, temperature stirring speed and pH were kept constant at 7.5 wt. %, 333K 200 rpm and 5.5 respectively. Figure 3.5(b) shows the experimental results and it is observed that conversion of calcium ions increases as acid concentration increases. An

increase in acid concentration leads to improved transport of the fluid reactant from the liquid bulk to the surface of the solid particle and dissolution is enhanced because more carbonate ions react with H^+ ion therefore dissociating $CaCO_3$.

3.5.5.3. Effect of stirring speed

The effect of stirring speed on limestone dissolution was performed using 0.1M adipic acid at a temperature of 333K, solid to liquid ratio of 7.5 wt. % and pH 5.5. The stirring speed was varied from 100 rpm, 200 rpm, 300 rpm and 400 rpm. The experimental results are shown in Figure 3.5(c) which indicates that the dissolution of limestone increases with increase in stirring speed. Increase in stirring speed causes a decrease in film layer resistance, therefore causing an increase in dissolution rate.

3.5.5.4. Effect of pH

To investigate the effect of pH on limestone dissolution rate, four experiments were carried out by varying the pH from 5.5-7.0. The experiments were carried out at a temperature of 333K, 7.5 wt. % solid to liquid ratio, 0.1M acid concentration and 200 rpm stirring speed. Figure 3.5(d) shows the experimental results which indicate that the conversion of limestone in adipic acid increases with decrease in pH. The decrease in pH leads to an increase in the apparent mass transfer coefficient therefore leading to a increase in dissolution.

3.5.5.5. Effect of temperature

This was analyzed by varying the temperatures from 303K-348K. This was investigated using 0.1M acid concentration, 7.5 wt. % solid to liquid ratio, 200 rpm stirring speed and pH of 5.5. The experimental results are represented in Figure 3.5(e) and it can be seen that there is an increase in the dissolution rate with increase in temperature. High temperatures increase the reaction rate because there is high energy collision between molecules which result in more reactions between the solid particle and the fluid reactant.

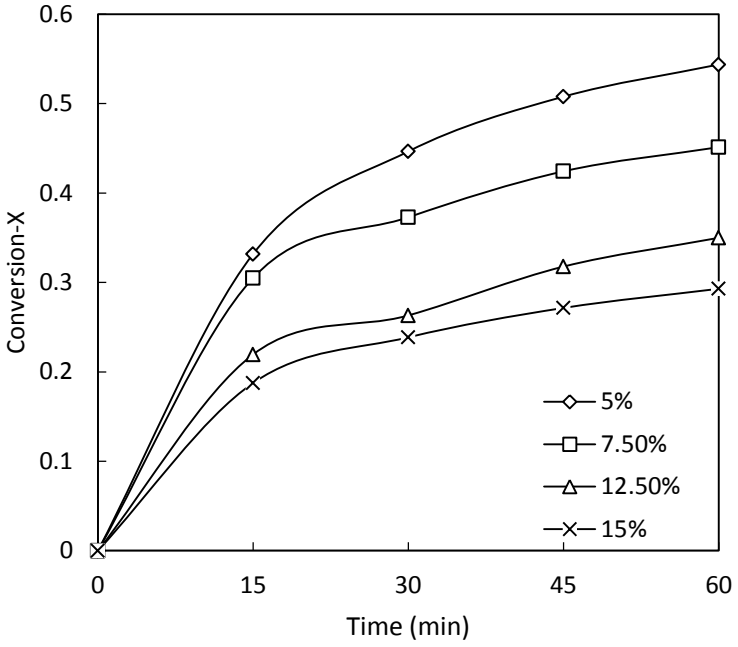
0.6
0.5
0.4
0.3
0.2
0.1
0
Conversion-X
0
15
30
45
60
Time (min)
5%
7.50%
12.50%
15%

(a)

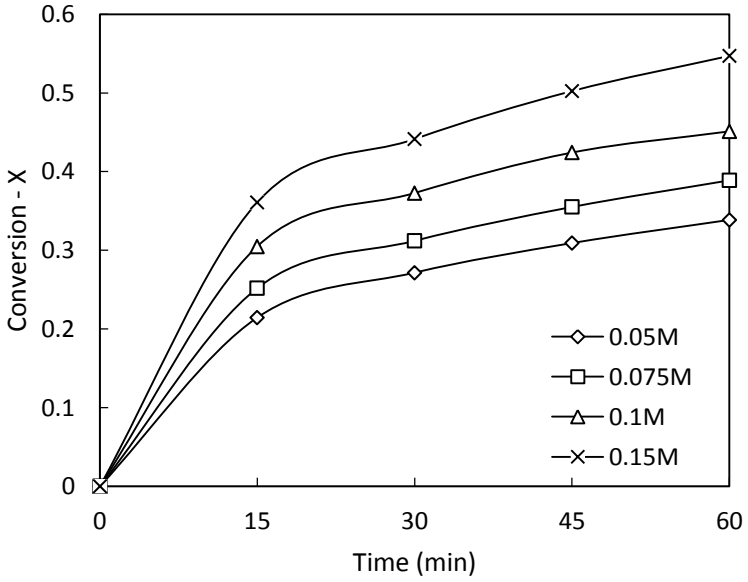
0.6
0.5
0.4
0.3
0.2
0.1
0
Conversion - X
0
15
30
45
60
Time (min)
0.05M
0.075M
0.1M
0.15M

(b)

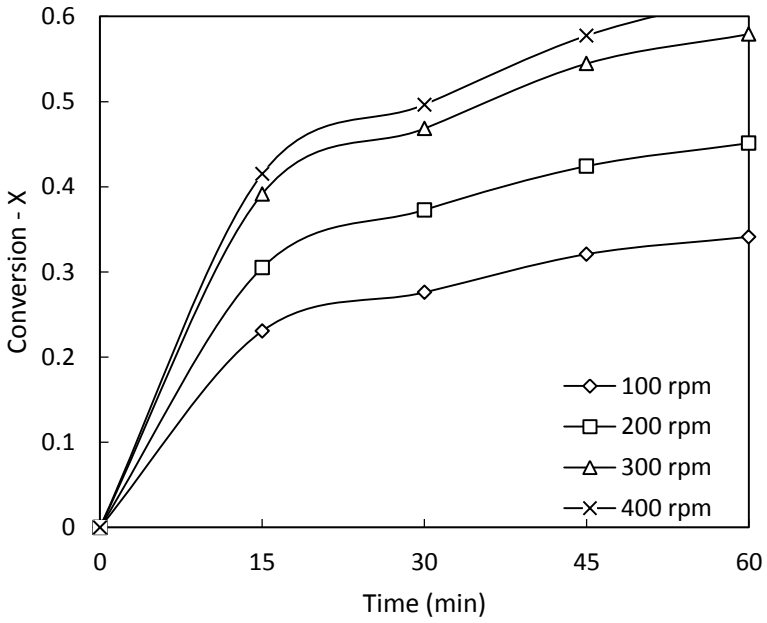
0.6
0.5
0.4
0.3
0.2
0.1
0
Conversion - X
0
15
30
45
60
Time (min)
100 rpm
200 rpm
300 rpm
400 rpm

(c)

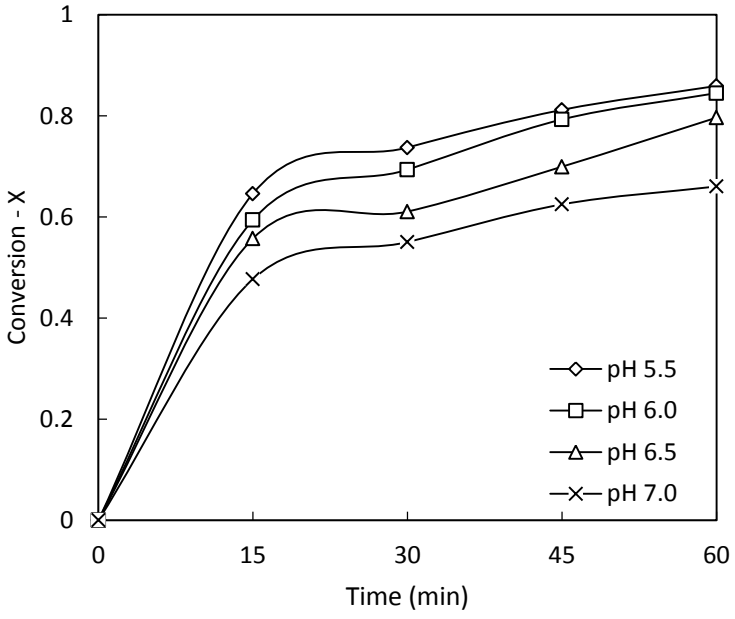
1
0.8
0.6
0.4
0.2
0
Conversion - X
0
15
30
45
60
Time (min)
pH 5.5
pH 6.0
pH 6.5
pH 7.0

(d)

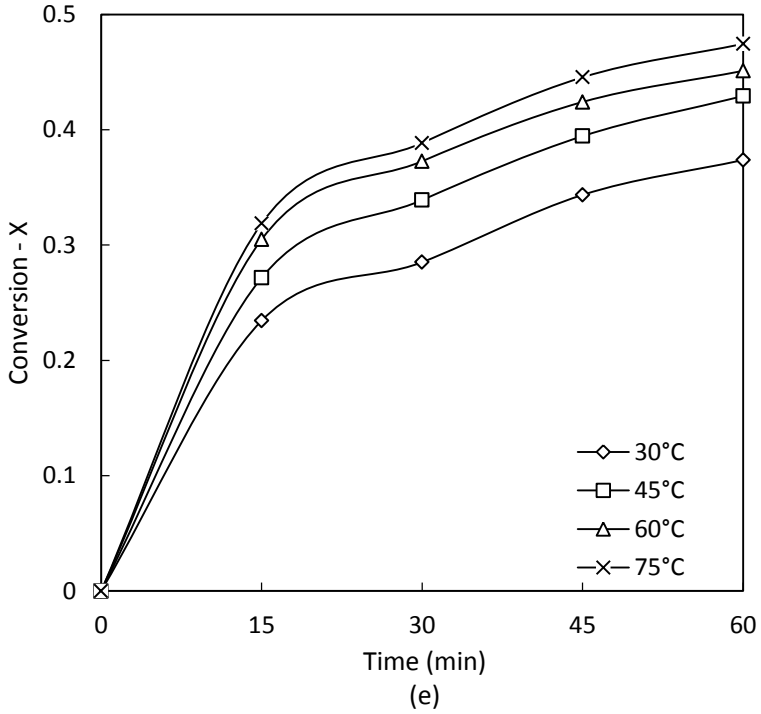

Figure 3 5: Effect of different solid to liquid ratio (a), acid concentration (b), stirring speed (c), pH (d) and temperature (e) on the dissolution of limestone in adipic acid.

3.5.6. Kinetic analysis

The Figures 3.6(a) - (e) show the linear relationship between $1-(1-X)^{\frac{1}{3}}$ and the reaction time for different solid to liquid ratio (a), acid concentration (b), stirring speed (c), pH (d) and temperature (e) respectively. The apparent rate constants and the corresponding regression coefficients obtained from these plots are represented in Table 3.1.

Table 3. 1: Dissolution rate constants and their regression coefficients

Process Variables		Surface chemical reaction: $1-(1-X)^{\frac{1}{3}}=K_r t$	
		$K_r(min)^{-1}$	R^2
Temperature (K)			
	303	0.0012	0.9843
	318	0.0019	0.9821
	333	0.0028	0.9583
	348	0.0059	0.9635

Stirring speed (rpm)			
	100	0.0017	0.9605
	200	0.0028	0.9583
	300	0.0037	0.9669
	400	0.0044	0.9789
Solid to liquid ratio (wt. %)			
	5	0.0039	0.9775
	7.5	0.0028	0.9583
	12.5	0.0018	0.9872
	15	0.0016	0.9712
concentration (M)			
	0.05	0.0011	0.9769
	0.075	0.0017	0.9749
	0.1	0.0028	0.9583
	0.15	0.0057	0.9753
pH			
	5.5	0.0028	0.9767
	6	0.0023	0.9554
	6.5	0.0022	0.9612
	7	0.0019	0.9514

A semi–empirical model including all the process variables can then be written as follows:

$$K_r = K_o C^a N^b \left(\frac{S}{L}\right)^C P^d e^{\left(-E_a/RT\right)} \quad (3.11)$$

Combining equation (3.2) and (3.11), the following equation is obtained.

$$1 - (1 - X)^{\frac{1}{3}} = K_o C^a N^b \left(\frac{S}{L}\right)^C P^d e^{\left(-E_a/RT\right)} t \quad (3.12)$$

The constants *a, b, c,* and *d* are the reaction orders evaluated from the rate constants.

The order of the reaction for concentration was obtained from the slope of a plot of $\ln K_r$ versus $\ln C$ which is represented in Figure 3.7(a). The reaction order was obtained to be 1.4982 with the correlation coefficient of 0.978. The reaction orders for solid to liquid ratio, stirring speed and pH were found to be -0.8056, 0.7019 and -1.4539 respectively;

this was obtained from Figures 3.7(b) – 3.7(d). Their correlation coefficients are 0.9988, 0.9981 and 0.9733 respectively.

Using the apparent rate constants for temperature, the Arrhenius plot was generated and is shown in Figure 3.8. From the slope in the diagram, the activation energy was determined to be 29.24kJ/mol and the Y-intercept was determined to be 126.5326. The value of the activation energy shows that dissolution of limestone in adipic acid is controlled by chemical reaction diffusion control mechanism.

Equation (3.12) with all the dissolution variables can therefore be written as:

$$1-(1-X)^{\frac{1}{3}} = 126.5326C^{1.4982}N^{0.7019}\left(\frac{S}{L}\right)^{-0.8056}P^{-1.4539}e^{\left(-29240/RT\right)}t \qquad (3.13)$$

Where, C is concentration, N is the stirring speed, (S/L) is the solid to liquid ratio and P is the pH.

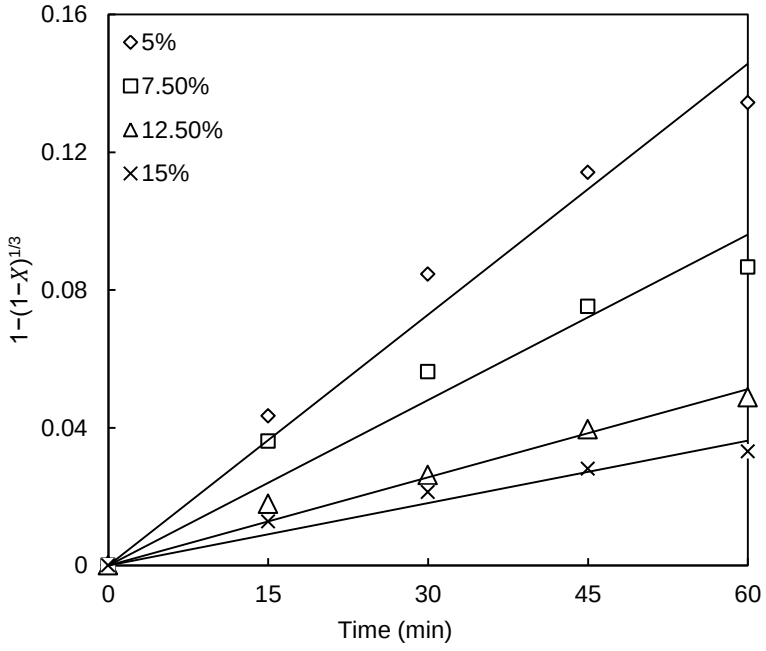

(a)

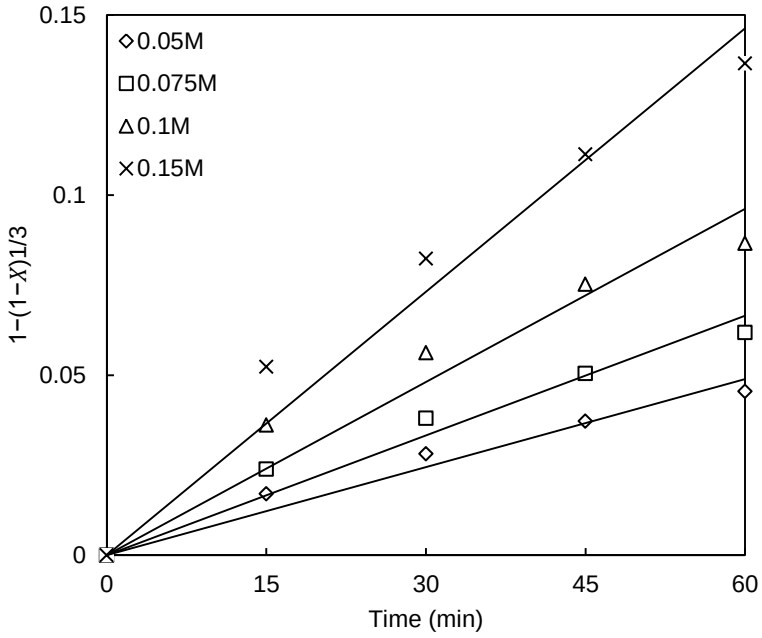
0.15
0.1
0.05
0
0.05M
0.075M
0.1M
0.15M
1−(1−X)1/3
0
15
30
45
60
Time (min)

(b)

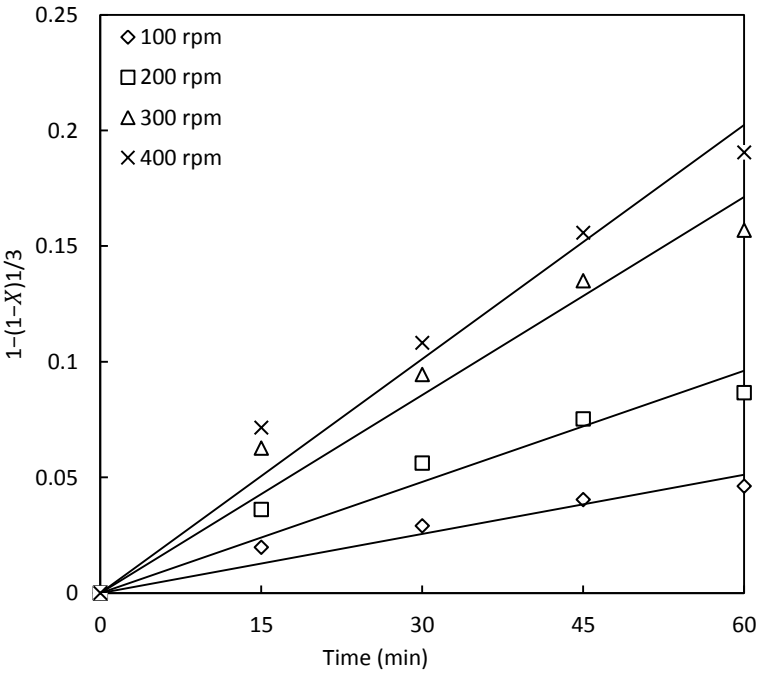
0.25
0.2
0.15
0.1
0.05
0
100 rpm
200 rpm
300 rpm
400 rpm
1−(1−X)1/3
0
15
30
45
60
Time (min)

(c)

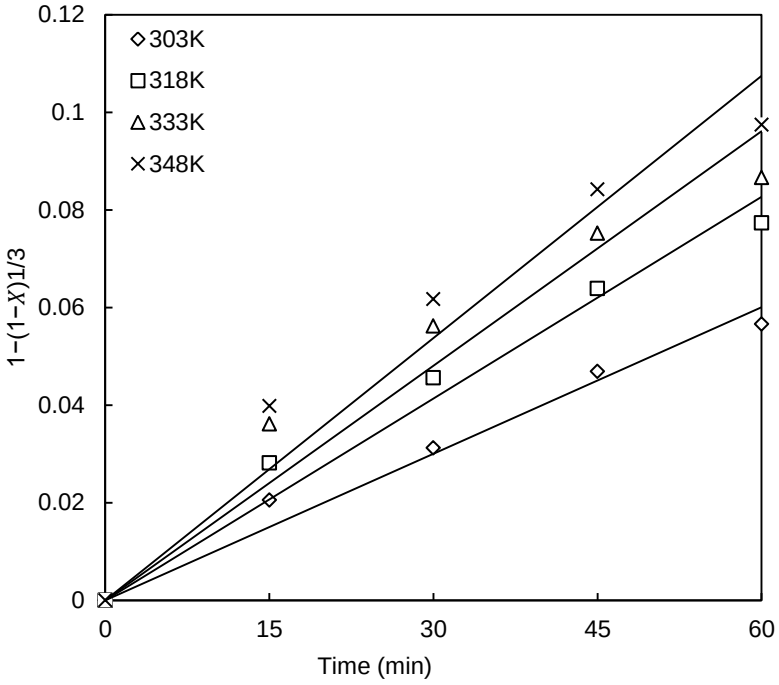

(d)

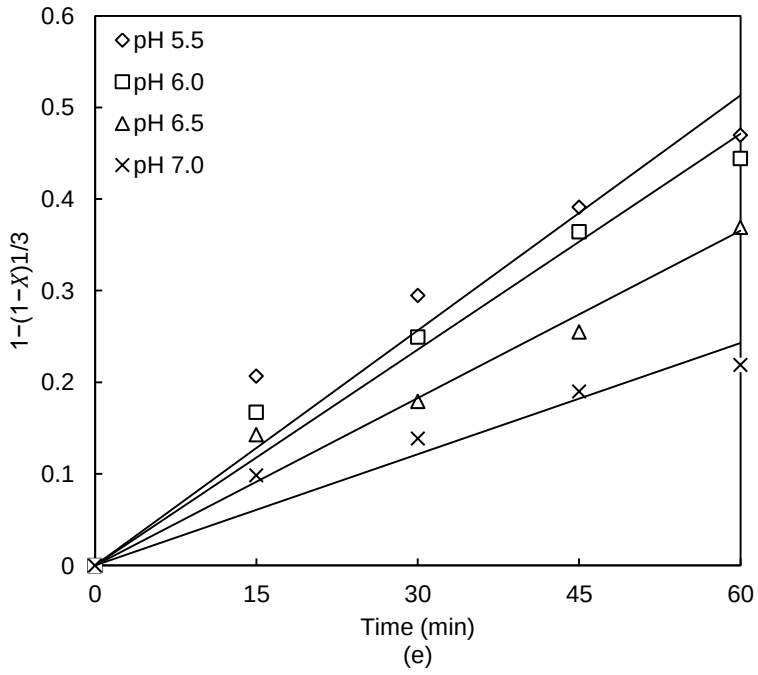

(e)

Figure 3 6: Variation of $\mathbf{1}-(\mathbf{1}-\boldsymbol{X})^{\frac{\mathbf{1}}{\mathbf{3}}}$ with different with time for different solid to liquid ratio (a), acid concentration (b), stirring speed (c), temperature (d) and pH (e).

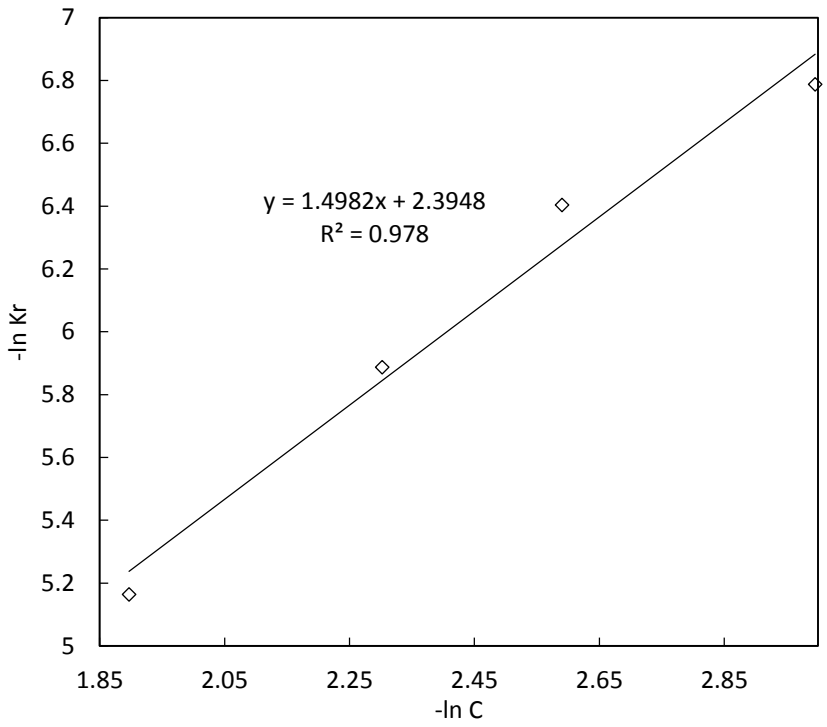
y = 1.4982x + 2.3948
R² = 0.978
-ln Kr
-ln C
7
6.8
6.6
6.4
6.2
6
5.8
5.6
5.4
5.2
5
1.85
2.05
2.25
2.45
2.65
2.85

(a)

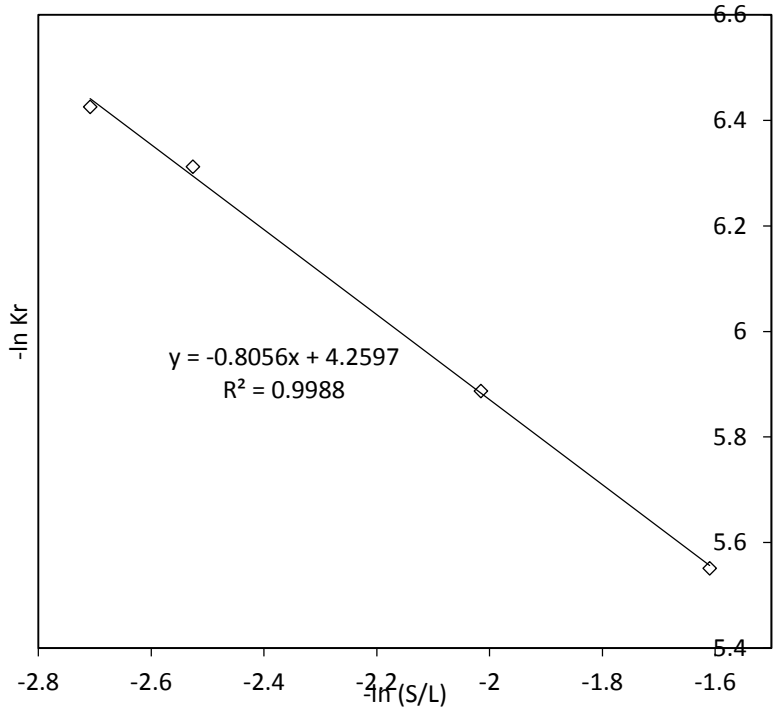
y = -0.8056x + 4.2597
R² = 0.9988
-ln Kr
-ln (S/L)
6.6
6.4
6.2
6
5.8
5.6
5.4
-2.8
-2.6
-2.4
-2.2
-2
-1.8
-1.6

(b)

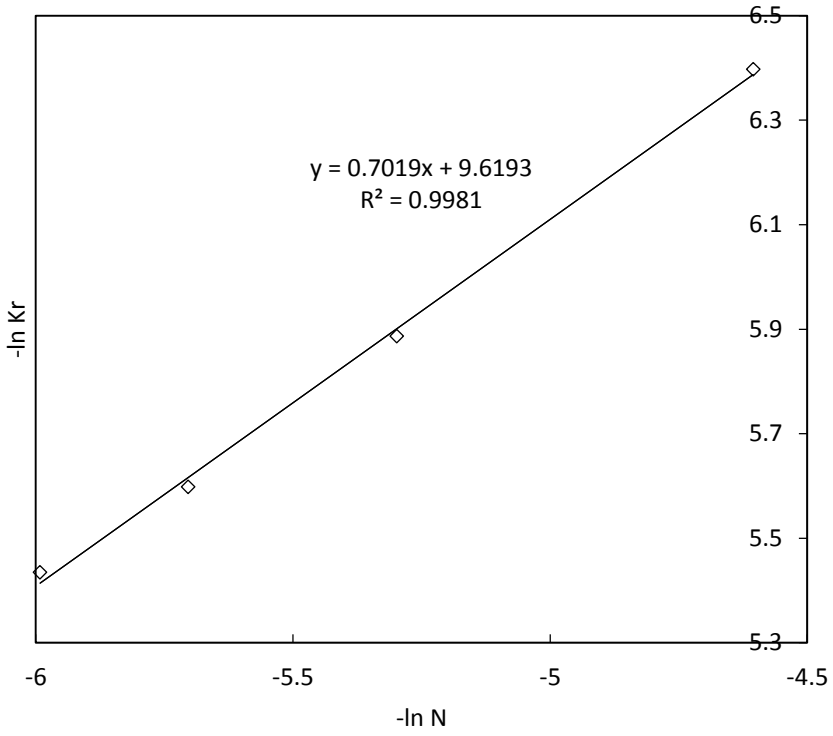

(c)

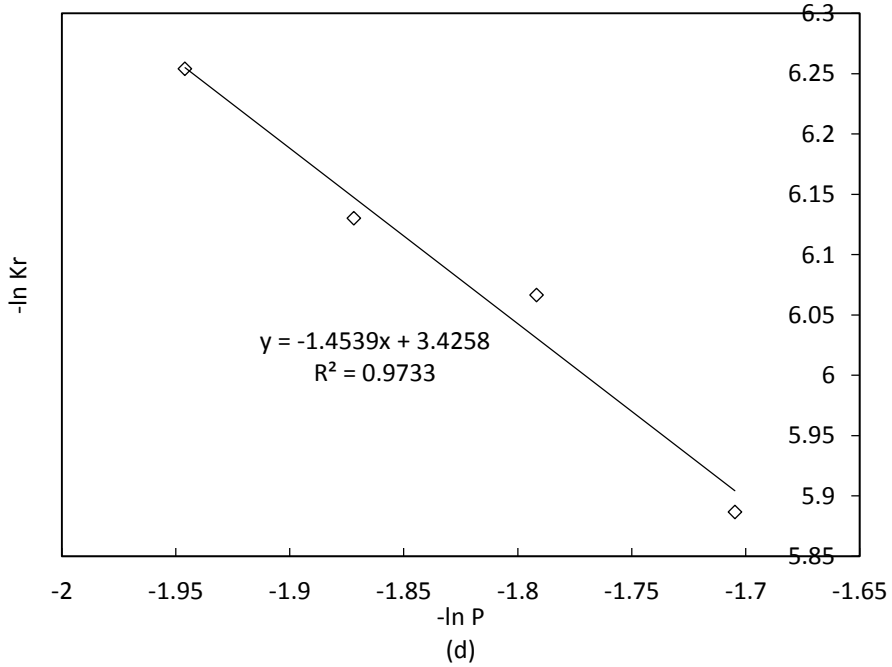

(d)

Figure 3 7: Variation of $-\ln K_r$ with –ln C (a), -ln (S/L) (b), –ln N (c) and –ln P (d).

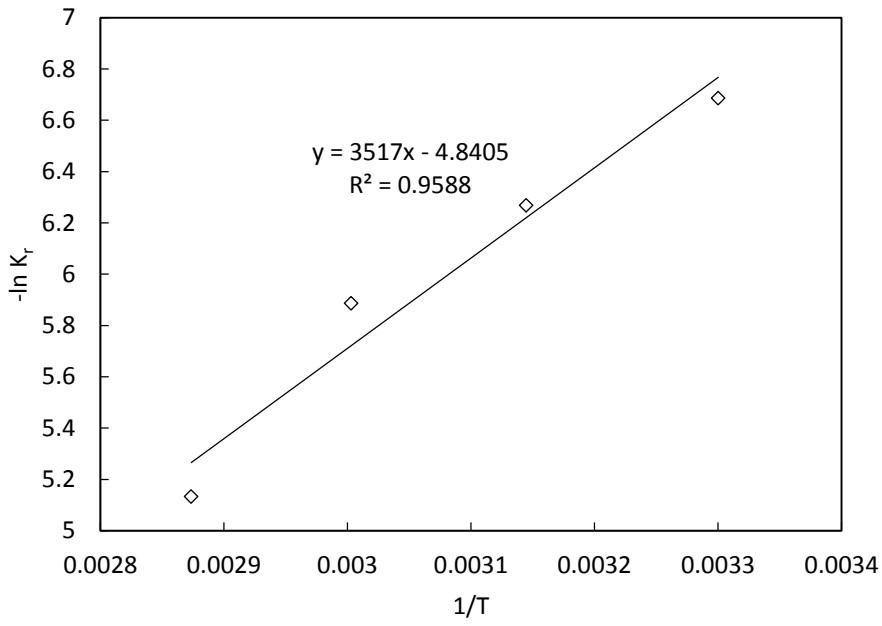

Figure 3 8: Arrhenius plot for dissolution of limestone in adipic acid

3.5.7. Scanning electron microscope

Figure 3.9 shows SEM micrographs for raw limestone and sorbents after dissolution. It is evident that raw limestone has particles ranging from small to large particles which are distributed throughout the surface and have smooth surfaces (Figure 2.9(a)).

The synthesized sorbents after dissolution are composed of porous irregular particles (Figure 2.9(b)) with relatively rough surfaces than raw limestone. This is attributed to the removal of carbonate minerals due to dissolution. It is also observed that fine particles are agglomerated together to form large particles.

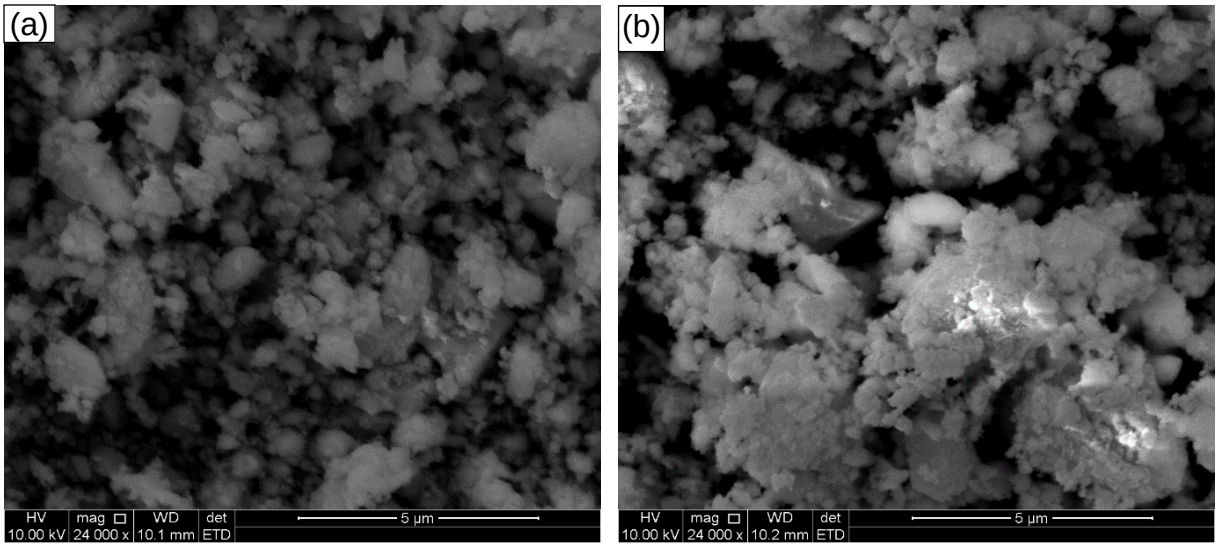

Figure 3 9: SEM micrographs for (a) raw limestone, and (b) sorbent after 60 minutes.

Conclusion

This study focuses on the dissolution kinetics of limestone in adipic acid. The effects of the process variables; solid to liquid ratio, stirring speed, acid concentration, temperature and pH were investigated. It was found out that the dissolution rate of limestone increases with increase in acid concentration, stirring speed and temperature but it decreased with increase in solid to liquid ratio and pH. XRD analysis showed an increase in portlandite peaks after dissolution which resulted in increase of specific surface area which is in excellent agreement with the results obtained from the BET surface area. The dissolution of limestone follows a shrinking core model with the chemical reaction control and the activation energy for the process being 29.24kJ/mol. The semi empirical model developed for the process was evaluated to be

$$1-(1-X)^{\frac{1}{3}} = 126.5326C^{1.4982}N^{0.7019}\left(\frac{S}{L}\right)^{-0.8056}P^{-1.4539}e^{\left(-29240/RT\right)}t$$

The SEM micrographs showed a more porous structure with relatively rough surface in the sorbent after dissolution and also fine agglomerated particles attached to big particles.

3.6. References

Berner, R.A. and Morse, J.W. 1974. Dissolution kinetics of calcium carbonate in sea water; IV, Theory of calcite dissolution. American Journal of Science, vol. 274, no. 2, pp. 108-134.

Bhaskarwar, A.N. 1988. On application of the method of kinetic invariants to the description of dissolution accompanied by a chemical reaction. Chemical Engineering Communications, vol. 72, no. 1, pp. 25-34.

Birchal, V., Rocha, S. and Ciminelli, V. 2000. The effect of magnesite calcination conditions on magnesia hydration. Minerals Engineering, vol. 13, no. 14, pp. 1629-1633.

Fredd, C.N. and Fogler, H.S. 1998. The kinetics of calcite dissolution in acetic acid solutions. Chemical engineering science, vol. 53, no. 22, pp. 3863-3874.

Garea, A., Fernandez, I., Viguri, J., Ortiz, M., Fernandez, J., Renedo, M. and Irabien, J. 1997. Fly-ash/calcium hydroxide mixtures for SO_2 removal: structural properties and maximum yield. Chemical Engineering Journal, vol. 66, no. 3, pp. 171-179.

Hadjar, H., Hamdi, B., Jaber, M., Brendlé, J., Kessaissia, Z., Balard, H. and Donnet, J. 2008. Elaboration and characterisation of new mesoporous materials from diatomite and charcoal. Microporous and Mesoporous Materials, vol. 107, no. 3, pp. 219-226.

Klimont, Z., Smith, S.J. and Cofala, J. 2013. The last decade of global anthropogenic sulfur dioxide: 2000–2011 emissions. Environmental Research Letters, vol. 8, no. 1, pp. 014003.

Kunkel, D., Tost, H. and Lawrence, M. 2013. Impact of anthropogenic emissions from major population centers on global and regional aerosol budgets, EGU General Assembly Conference Abstracts, pp. 7083.

Lee, K.T., Bhatia, S. and Mohamed, A.R. 2005. Preparation and characterization of sorbents prepared from ash (waste material) for sulfur dioxide (SO_2) removal. Journal of material cycles and waste management, vol. 7, no. 1, pp. 16-23.

Limo, R.H. and Enweremadu, C. 2011. The dissolution study of a South African magnesium-based material from different sources using a pH-stat. Chemical Industry and Chemical Engineering Quarterly, vol. 17, no. 4, pp. 459-468.

Liu, S., Qiu, W., Qu, B. and Xu, Y. 2010. Dissolution Characteristics of Limestone with Organic Acid, Bioinformatics and Biomedical Engineering (iCBBE), 2010 4th International Conference on IEEE, pp. 1.

Maravelaki-Kalaitzaki, P. and Kallithrakas-Kontos, N. 2003. Pigment and terracotta analysis of Hellenistic figurines in Crete. Analytica Chimica Acta, vol. 497, no. 1, pp. 209-225.

Monnin, Y., Dégrugilliers, P., Bulteel, D. and Garcia-Diaz, E. 2006. Petrography study of two siliceous limestones submitted to alkali-silica reaction. Cement and Concrete Research, vol. 36, no. 8, pp. 1460-1466.

National Environmental Management, South Africa 2005. Air and Quality Act, Act No. 30 of 2004, Cape Town.

Potgieter, J. and Gregory, H. 2012. Dissolution kinetics of quicklime in various organic solvents and solutions. Environmental technology, vol. 33, no. 10, pp. 1191-1195.

Qin, S., Hansen, B.B. and Kiil, S. 2013. Foaming in wet flue gas desulfurization plants: Laboratory-scale investigation of long-term performance of antifoaming agents. AIChE Journal, vol. 59, no. 10, pp. 3741-3747.

Rocha, S.D., Mansur, M.B. and Ciminelli, V.S. 2004. Kinetics and mechanistic analysis of caustic magnesia hydration. Journal of Chemical Technology and Biotechnology, vol. 79, no. 8, pp. 816-821.

Rutto, H. and Enweremadu, C. 2011. A study on dissolution of a South African calcium based material in acetic acid solution for flue gas desulphurisation, Electrical and Control Engineering (ICECE), 2011 International Conference on IEEE, , pp. 5701 - 5705.

Sdiri, A., Higashi, T., Hatta, T., Jamoussi, F. and Tase, N. 2010. Mineralogical and spectroscopic characterization, and potential environmental use of limestone from the Abiod formation, Tunisia. Environmental Earth Sciences, vol. 61, no. 6, pp. 1275-1287.

Shih, S., Lin, J. and Shiau, G. 2000. Dissolution rates of limestone from different sources. Journal of hazardous materials, vol. 79, no. 1, pp. 159-171.

Siagi, Z. and Mbarawa, M. 2009. Dissolution rate of South African calcium-based materials at constant pH. Journal of hazardous materials, vol. 163, no. 2, pp. 678-682.

Song, H. and Park, J. 2001. Improvement of SO_2 removal by the solubility change of $Ca(OH)_2$ in the spray dryer system. Environmental technology, vol. 22, no. 9, pp. 1001-1006.

Szubert, A., Lupiński, M. and Sadowski, Z. 2006. Application of shrinking core model to bioleaching of black shale particles. Physicochemical Problems of Mineral Processing, vol. 40, pp. 211-225.

Ukawa, N., Takashina, T., Shinoda, N. and Shimizu, T. 1993. Effects of particle size distribution on limestone dissolution in wet FGD process applications. Environmental Progress, vol. 12, no. 3, pp. 238-242.

Van der Merwe, E. and Strydom, C. 2006. Hydration of medium reactive magnesium oxide using hydration agents. Journal of Thermal Analysis and Calorimetry, vol. 84, no. 2, pp. 467-471.

You, C. and Li, Y. 2013. Desulfurization Characteristics of Rapidly Hydrated Sorbents with Various Adhesive Carrier Particles for a Semidry CFB-FGD System. Environmental science & technology, vol. 47, no. 6, pp. 2754-2759.

Yuan, Q., Jia, X. and Williams, R.A. 2012. Validation of a Multi-Component Digital Dissolution Model for Irregular Particles. Powder Technology, vol. 240, pp. 25-30.

Zhang, R., Hu, S. and Zhang, X. 2011. Dissolution rates of silicate minerals in water from a subcritical to a supercritical state: effect of solvent properties. Research on Chemical Intermediates, vol. 37, no. 2-5, pp. 243-258.

4. Dissolution Kinetics of South African Coal Fly Ash and the Development of a Semi-empirical Model to Predict Dissolution

4.1. Abstract

Wet flue gas desulphurization (FGD) is a crucial technology which can be used to abate the emission of sulphur dioxide in coal power plants. The dissolution of coal fly ash in adipic acid is investigated by varying acid concentration (0.05–0.15M), particle size (45–150μm), pH (5.5–7.0), temperature (318–363K) and solid to liquid ratio (5–15 wt. %.) over a period of 60 minutes which is a crucial step in wet (FGD). Characterization of the sorbent was done using X–ray fluorescence (XRF), X–ray diffraction (XRD), Furrier transform infrared (FTIR), scanning electron microscope (SEM) and Branauer-Emmett-Teller (BET) surface area. BET surface area results showed an increase in the specific surface area and SEM observation indicated a porous structure was formed after dissolution. The experimental data was analyzed using the shrinking core model and the diffusion through the product layer was found to be the rate limiting step. The activation energy for the process was calculated to be 10.64kJ/mol.

Key words: flue gas desulphurization, coal fly ash, dissolution, shrinking core model, activation energy.

4.2. Introduction

The increase in the use of coal in thermal power plants has led to an increase in production of waste such as coal fly ash. Coal fly ash is an industrial by-product generated during coal combustion for production of energy. It is collected before flue gas reaches the chimney using either electro-static precipitators, bag filters or cyclones. It is considered hazardous because it contains elements such as boron, vanadium, chromium and arsenic which are harmful to the environment (Mishra et al., 2010; Temuujin et al., 2009). Fly ash is largely used in concrete as cement replacement and making geo-polymers. However, most of the fly ash produced is disposed in ash ponds or landfills (Bakharev, 2005; Swanepoel and Strydom, 2002).

Because fly ash is a waste material, it is economical to be used as a partial substitute or as a reagent in flue gas desulphurization (FGD). It is mainly composed of SiO_2, Al_2O_3, CaO and Fe_2O_3 (Goodarzi, 2006). It can therefore be utilized in FGD processes as a supplement to act as a source of Ca^{2+}, Al^{3+} and Si^{4+} ions which can improve the total SO_2 removal efficiency in both wet and dry flue gas desulphurization systems (Song and Park, 2001). Studies have shown that sorbents prepared from fly ash exhibit improved reactivity towards SO_2 and also improved sorbent utilization. The amorphous silica in fly ash reacts with hydrated lime to form calcium silicate hydrates in the presence of water (pozzolanic reaction). The calcium silicate hydrates attach to each other forming large particles with more porous structure which leads to an increase in sorbent surface area and improved pore volume (Ogenga et al., 2009; Lin and Shih, 2003; Jozewicz and Rochelle, 1986).

Fly ash dissolution is dependent on its chemical composition and the dissolution process variables such as temperature, particle size, acid concentration, pH and solid to liquid ratio. A study by Kashiwakura et al. (2011) on the dissolution of solenoid from coal fly ash particles found out that it is dependent on the pH and acid concentration. Brouwers & Van Eijk, (2002) did a theoretical study on the dissolution of pulverized powder coal fly ash. A shrinking core model was developed for the outer and inner region to explain the behavior of the reaction rate constant as the solid changes. It was reported that the reactivity of fly ash corresponds to the silica content and the outer

region is less reactive than the inner region. Pietersen et al. (1989) observed a significant increase in dissolution rate of fly ash with increase in the reactant pH (NaOH solution) and also increase in the ambient temperature. A study by Tanaka & Fujii (2009) showed that fly ash dissolution is greatly affected by the presence of Si^{4+} and Al^{3+}. The presence of these ions in solution increases with increase in dissolution period and is accelerated with increased stirring speed. Si^{4+} and Al^{3+} are reagents for pozzolanic reaction which takes place in presence of water and leads to formation of products with high surface area.

This study looks into the possibility of using fly ash in wet flue gas desulphurization with a focus on its dissolution kinetics in adipic acid using a pH stat apparatus. It is an improvement to the previous work (Koech et al., 2013) on dissolution of fly ash for wet FDG process. The extent of dissolution of fly ash is determined by analyzing the amount calcium ions leached into solution which is the most active component during sorbent – SO_2 reaction. Using the experimental data to fit into the shrinking model, a semi-empirical model to describe the dissolution of calcium ions from fly ash was developed. The sorbent before and after dissolution was characterized using BET surface area, XRD and SEM.

4.3. Materials and Experimental Method

4.3.1. Materials

Coal fly ash was obtained from a coal-fired thermal power plant. XRF results showed that the chemical composition of the studied fly ash in wt. % consisted of 49.71% SiO_2, 32.12% Al_2O_3, 10.52% CaO, 3.89% Fe_2O_3, 1.89% TiO_2, 0.15% H_2O and 1.92% loss on ignition. Coal fly ash was crushed using a ball mill and sieved to different particle sizes using shaking screen sieves. Adipic acid and Calcium ion standards for the AAS were supplied by CJ Labs.

4.3.2. Experimental

A given amount of coal fly ash was added to the reactor vessel containing a solution. The temperature, solid to liquid ratio, particle size and acid concentration were varied at constant stirring speed of 200 rpm. This was done using a temperature controlled

magnetic stirrer. The pH of the reaction mixture was determined using pH electrode dipped into the solution and connected to a pH controller. When the pH exceeds the set value, the pump is activated to add acid to the reaction vessel and lowers the pH value to the set point.

A sample was then be removed, filtered and prepared for analysis of calcium ions using Atomic Absorption Spectrophotometer (AAS). Three calcium standard solutions (1, 5 and 10 ppm) were first prepared from the calcium ion standards for the AAS (1000 ppm). The standard solution was used to calibrate the AAS machine before analyzing the samples. The AAS machine atomizes the samples in the flame, through which radiation of a chosen wavelength (using a hollow cathode lamp) is sent. The amount of absorbed radiation is a quantitative measure for the concentration of the element to be analyzed. The gas mixture of acetylene and nitrous-oxide was used in the AAS instrument.

The dissolution fraction was calculated as:

$$X = \frac{Calcium\ ions\ in\ solution}{Total\ amount\ of\ calciuim\ ions\ in\ the\ original\ sample}$$

4.3.3. Characterization techniques

Qualitative and quantitative analysis of the studied fly ash before and after dissolution was done using XRD. A back loading preparation method was used for XRD analysis. Two samples were scanned after addition of 20% Si for qualitative determination of amorphous content. It was analyzed with a PANalytical Empyrean diffractometer with PIXcel detector and fixed with Fe filtered Co-Kα radiation. X'pert Highscore Plus software was used to identify the phases present in the samples.

The functional groups present in the samples were determined using FTIR analysis. The analysis determined using a Perkin Elmer spectrum (400FT-IR/FT-NIR) machine equipped with a universal attenuated total reflectance (ATR) accessory. There was no sample preparation required for the instrument. The samples were scanned at a range of 4000 to 650 cm^{-1}

The surface area analysis was conducted using Micrometrics 2020 Porosity Analyser. The samples were degassed at 150 °C under vacuum condition for 24 hours using

nitrogen gas. The specific surface area was determined using the Brunauer-Emmett-Teller (BET) method. The micro porous volume and area were obtained using the Barrett-Joyner-Halenda (BJH) procedure.

The morphological structure of the samples at different dissolution periods was studied using scanning electron microscope (SEM). The samples were sprinkled on an adhesive carbon tape and were metallized using gold before the analysis. The images of the samples were recorded at various magnifications.

4.4. Results and Discussion

4.4.1. Mechanism for dissolution of fly ash in adipic acid

Coal fly ash mainly consists of SiO_2, Al_2O_3, CaO Fe_2O_3 and TiO_2. These are chemical components that will be affected as dissolution takes place. The mechanism for dissolution of SiO_2, Al_2O_3, CaO Fe_2O_3 and TiO_2 in adipic acid is therefore shown in eq. 2-6.

Adipic acid dissociates into solution to form adipate ions:

$$C_6H_{10}O_{4(aq)} \rightarrow C_6H_8O_{4(aq)}^{2-} + 2H_{(aq)}^{+} \quad (4.1)$$

The dissolution of SiO_2, Al_2O_3, CaO, Fe_2O_3 and TiO_2 is by adipate complexation to form their respective adipate complexes (Kashiwakura et al., 2011):

$$SiO_{2(s)} + 2C_6H_8O_{4(aq)}^{2-} + 4H_{(aq)}^{+} \rightarrow Si(C_6H_8O_4)_{2(aq)} + 2H_2O_{(l)} \quad (4.2)$$

$$Al_2O_{3(s)} + 3C_6H_8O_{4(aq)}^{2-} + 6H_{(aq)}^{+} \rightarrow Al_2(C_6H_8O_4)_{3(aq)} + 3H_2O_{(l)} \quad (4.3)$$

$$TiO_{2(s)} + 2C_6H_8O_{4(aq)}^{2-} + 4H_{(aq)}^{+} \rightarrow Ti(C_6H_8O_4)_{2(aq)} + 2H_2O_{(l)} \quad (4.4)$$

$$CaO_{(s)} + C_6H_8O_{4(aq)}^{2-} + H_2O_{(l)} \rightarrow Ca(C_6H_8O_4)_{(aq)} + 2OH_{(aq)}^{-} \quad (4.5)$$

$$Fe_2O_{3(s)} + 3C_6H_8O_{4(aq)}^{2-} + 3H_2O_{(l)} \rightarrow Fe_2(C_6H_8O_4)_{3(aq)} + 6OH_{(aq)}^{-} \quad (4.6)$$

Dissociation of silicon, aluminium, titanium, iron and calcium adipate in the bulk will occur due to super saturation (Rocha et al., 2004). This leads to formation of silicon,

aluminium, titanium, iron and calcium ions in solution with adipate ions (Kashiwakura et al., 2011).

$$Si(C_6H_8O_4)_{2(aq)} \leftrightarrow Si^{4+}_{(aq)} + 2C_6H_8O^{2-}_{4(aq)} \quad (4.7)$$

$$Al_2(C_6H_8O_4)_{3(aq)} \leftrightarrow 2Al^{3+}_{(aq)} + 3C_6H_8O^{2-}_{4(aq)} \quad (4.8)$$

$$Ti(C_6H_8O_4)_{2(aq)} \leftrightarrow Ti^{4+}_{(aq)} + 2C_6H_8O^{2-}_{4(aq)} \quad (4.9)$$

$$CaC_6H_8O_{4(aq)} \leftrightarrow Ca^{2+}_{(aq)} + C_6H_8O^{2-}_{4(aq)} \quad (4.10)$$

$$Fe_2(C_6H_8O_4)_{3(aq)} \leftrightarrow 2Fe^{3+}_{(aq)} + 3C_6H_8O^{2-}_{4(aq)} \quad (4.11)$$

The presence of CaO in the coal fly ash is important because Ca^{2+} is the most reactive ion during chemo-sorption reaction in flue gas desulphurization. Apart from dissolution by adipate complexation (eq. 5), hydrogen complexation can also cause CaO dissolution releasing calcium ions into solution (Dube et al., 2014).

CaO dissolution by hydrogen complexation:

$$CaO_{(s)} + H^{+}_{(aq)} \rightarrow Ca^{2+}_{(aq)} + OH^{-}_{(aq)} \quad (4.12)$$

Calcium ions from super saturation (eq. 10) can be utilised more in pozzolanic reaction with fly ash being the source of silica and alumina to form alumino-silicate complex compounds (Karatepe et al., 1998).

Pozzolanic reaction:

$$Ca^{2+}_{(aq)} + 2SiO_{2(s)} + Al_2O_{3(s)} + OH^{-}_{(aq)} \rightarrow CaAl_2Si_2O_8.H_2O_{(s)} \quad (4.13)$$

Calcium alumino-silicate hydrate is formed from the pozzolanic reaction which increases the surface area of the sorbent and hence improves the rate of SO_2 absorption in flue gas desulphurization.

4.4.2. XRD analysis

XRD analysis was used to determine the structural changes on the crystalline phases of coal fly ash after dissolution has taken place. The results are represented in Figure 4.1.

The diffraction peaks shows that it is mainly composed of quartz (SiO_2)-Q, mullite ($Al_6Si_2O_{13}$)-M and silicon (Si)-S. The silicon and quartz peaks diminish after 30 minutes and more after 60 minutes dissolution period. This shows that dissolution had an effect on these compounds and they were leached into solution.

New diffraction peak appears at 2θ=33 in the sorbents after dissolution. This was identified as anorthite ($CaAl_2Si_2O_8$). Dissolution of fly ash leads to Si^{4+} and Al^{3+} being leached out of the amorphous alumino-silicate of fly ash. Leaching of these ions (Si^{4+} and Al^{3+}) increases with prolonged dissolution. A pozzolanic reaction occurs and anorthite is formed in the sorbents after dissolution (Lee et al., 2005). Pozzolanic reaction leads to the formation of sorbents with high surface area which can eventually improve SO_2 absorption capacity during flue gas desulphurization.

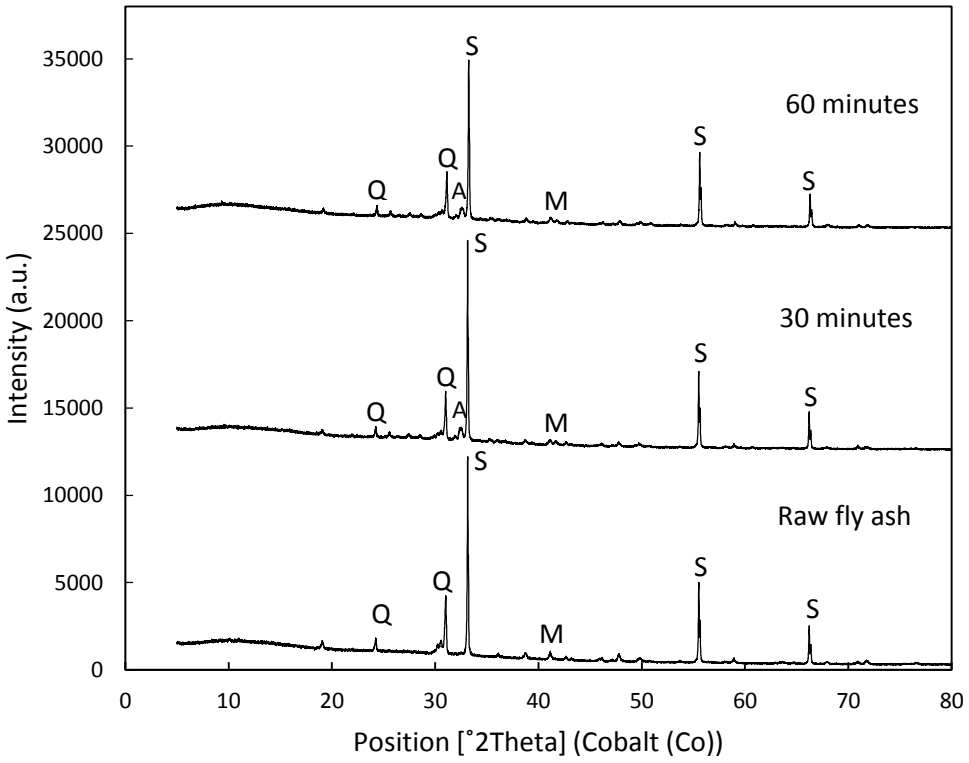

Figure 4. 1: XRD patterns for raw fly ash and sorbents after 30 minutes and 60 minutes dissolution period. (S-silicon, Q-quartz, M-mullite, A-anorthite)

4.4.3. BET specific surface area

The nitrogen adsorption desorption isotherm plot for fly ash before and after dissolution is illustrated in Figure 4.2(a). The figure clearly shows that the sorbents have an adsorption isotherm of type II according the IUPAC (International Union of Pure and Applied Chemistry) classification (Hadjar et al., 2008). This indicates that porosity of fly ash sorbent after dissolution was in the mesopore range. The mesopore range is an effective zone for sulphation reaction between calcium ions and SO_2 during flue gas desulphurization (Ogenga et al., 2009).

The specific surface area increases significantly with prolonged dissolution period (from 0.3669 to 6.9501m^2/g). The increase in surface area is attributed to the products of pozzolanic reaction which yields complex alumino-silicate compounds which are responsible for increased specific surface area in the sorbent (Adamiec et al., 2008). The increase in the specific surface area shows that the formation of calcium alumino-silicate complex continued to change the structure of the particles into a more porous form (Lin and Shih, 2003).

4.4.4. FTIR analysis

The chemical heterogeneity of fly ash at different dissolution periods is shown in Figure 4.2(b). From the diagram, the samples exhibited overlapping absorption bands between 1200 and 900 cm^{-1}. These overlapping bands indicate the presence of quartz and mullite in the samples (Criado et al., 2007) and it is also due to the asymmetrical stretching of amorphous alumino-silicate formed by the reaction of extracted Si^{4+} and Al^{3+} ions. The series of bands representing quartz appear at 1084 and 796 cm^{-1}.

The bands appearing at 1410, 1440 and 1582 cm^{-1} are assigned to the asymmetrical stretching vibration of CaO band (Thiruppathi et al., 2009). The depleted peaks of CaO band is due to the effect of dissolution after which CaO goes into solution. This is excellent agreement with the results from XRD analysis.

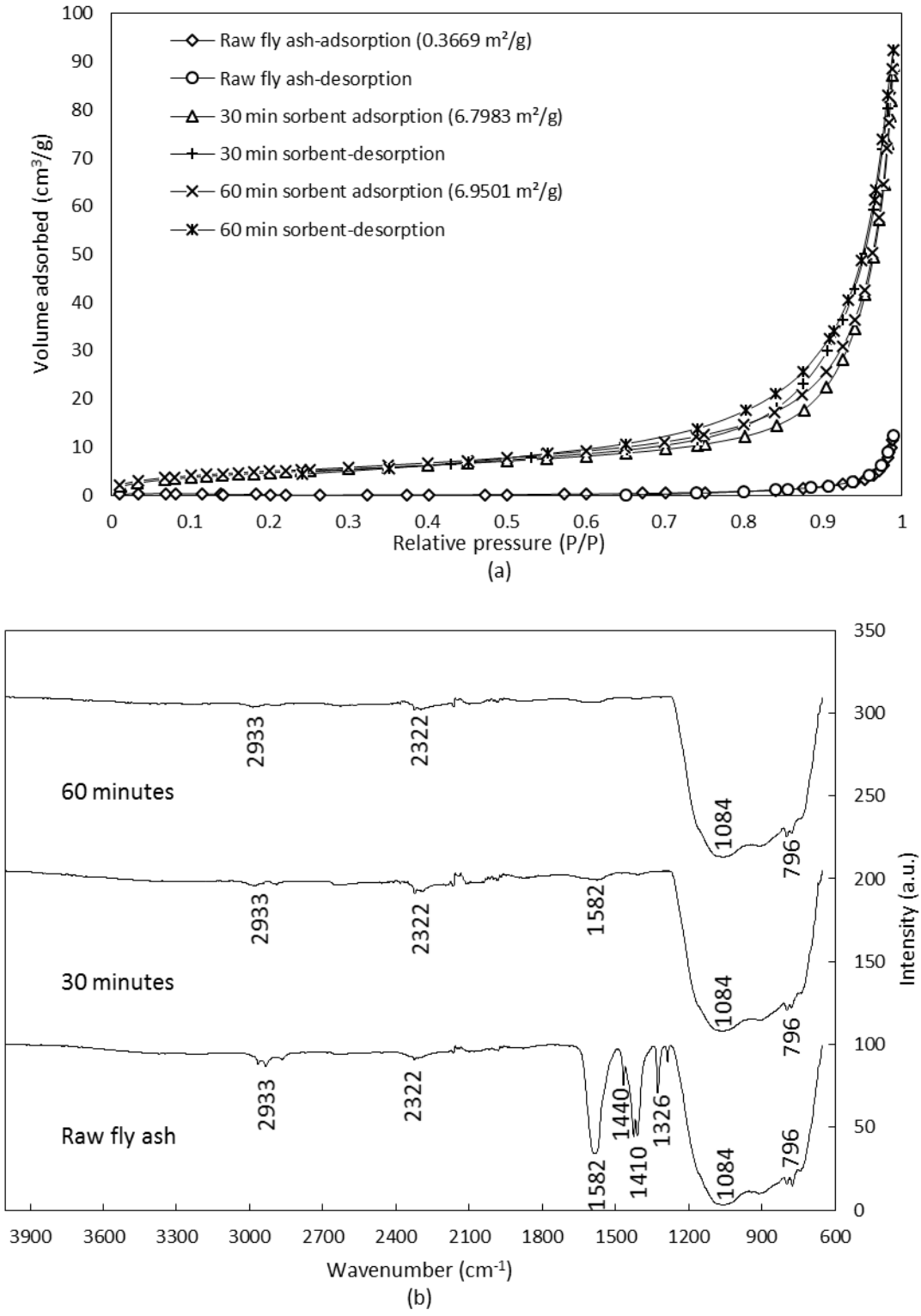

Figure 4. 2: Adsorption-desorption isotherm plot (a) and FTIR spectra (b) for fly ash at different dissolution periods.

4.4.5. Surface morphology

Figure 4.3 shows the surface morphology of fly ash samples at different dissolution periods. Raw fly ash mainly consists of particles that are rounded and spherical in shape with smooth surfaces. The smooth surface in the fly ash is due to alumino-silicate particles that are formed as a result of transformation of mineral particles during coal combustion (Nyale et al., 2013).

The sorbents after exposure to dissolution had their surfaces relatively rough and porous compared to raw fly ash. The sorbent also exhibited deformation of the smooth surfaces after dissolution; this was observed in the sorbent after 60 minutes dissolution period. This indicates that the alumino-silicate compounds in particles of fly ash were extracted into solution (Sarbak and Kramer-Wachowiak, 2002). The agglomerated particles in the sorbent after dissolution are attributed to the formation of calcium alumino-silicate compounds. This is a product of pozzolanic reaction during dissolution as shown in eq. 13. The porous structure combined with agglomerated particles results in an increase in the specific surface area of the sorbents which can improve the SO_2 absorption capacity in flue gas desulphurization (van der Merwe and Strydom, 2006).

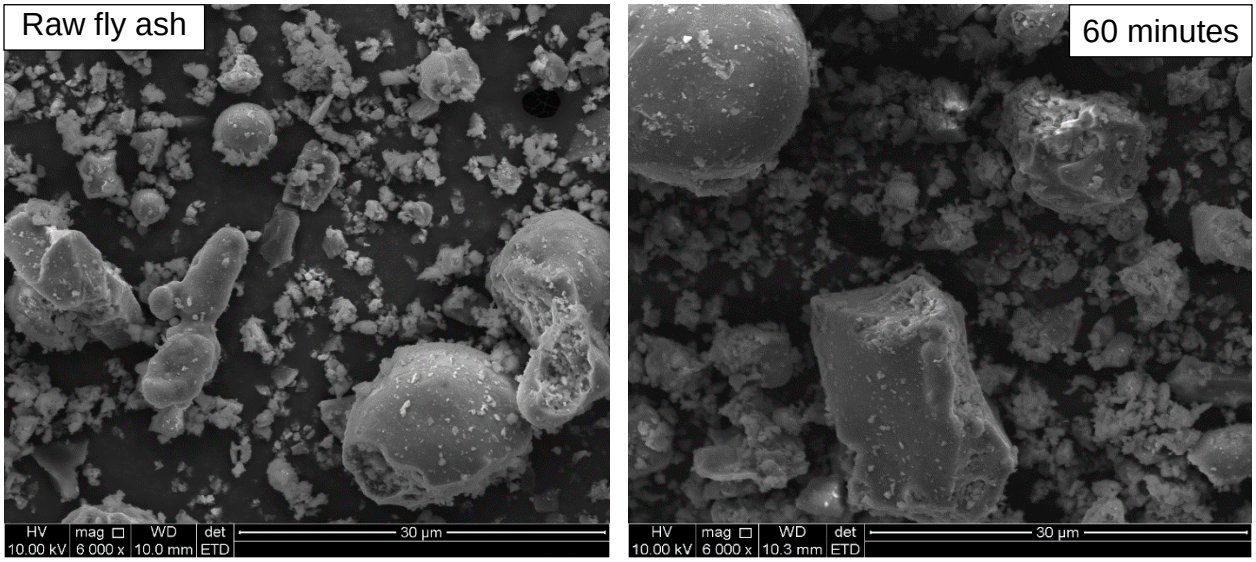

Figure 4. 3: SEM micrographs for raw fly ash and sorbent after 60 minutes dissolution period.

4.4.6. Effect of reaction variables

4.4.6.1. Effect of solid to liquid ratio

The effect of solid to liquid ratio on dissolution of fly ash in adipic acid was done in the range of 5-15 wt. %. The temperature, pH, particle size and acid concentration were kept constant at 60°C, 5.5, -45 µm and 0.1M respectively. The experimental results are represented in Figure 4.4(a). It is evident that the conversion of calcium ions into solution is higher at lower solid to liquid ratio compared to higher solid to liquid ratio within the same dissolution period. This is attributed to the decrease in the fluid reactant per unit weight of the solid as solid to liquid ratio increases.

4.4.6.2. Effect of acid concentration

To investigate the effect of acid concentration on dissolution of fly ash, different experiments were performed at a range of 0.05-0.15M adipic acid. The temperature, pH, particle size and solid to liquid ratio were kept constant at 60°C, 5.5, -45 µm and 10 wt. % respectively. Figure 4.4(b) shows the experimental results and it is clear that the conversion of fly ash increases with increase in acid concentration. Increase in acid concentration leads to an increase in H^+ ion activity in the liquid film therefore enhancing reaction on the solid surface.

4.4.6.3. Effect of particle size

Four different size fractions were used to investigate the effect of particle size on the dissolution rate of coal fly ash. The average size fractions used were from -45 to -150 µm. The temperature, pH, solid to liquid ratio and acid concentration were kept constant at 60°C, 5.5, 10 wt. % and 0.1M respectively. The experimental results are represented in Figure 4.4(c) which shows that by reducing the particle size of fly ash, it significantly improved the conversion of calcium ions into solution as compared to larger particle size over the same dissolution period. This is because finer particles have higher surface area, thus enhancing dissolution.

4.4.6.4. Effect of pH

The effect of pH on dissolution of fly ash was studied in the range of 5.5-7.0. The temperature, solid to liquid ratio, particle size and acid concentration were kept constant at 60°C, 10 wt. %, -45 µm and 0.1M respectively. Figure 4.4(d) represents the experimental results for this experiment. It is evident that dissolution rate increases with decrease in pH. This is because the increase in pH causes an increase in the apparent mass transfer coefficient.

4.4.6.5. Effect of temperature

The effect of temperature on the dissolution rate of fly ash was performed in the range of 318-363K. The solid to liquid ratio, pH, particle size and acid concentration were kept constant at 10 wt. %, 5.5, -45 µm and 0.1M respectively. The experimental results are depicted in Figure 4.4(e) and it can be seen that the conversion of calcium ions is enhanced at higher temperatures than at lower temperatures. High temperatures accelerate the reaction rate because there is an increase in energy which results to more collision between reacting molecules which speeds the reaction.

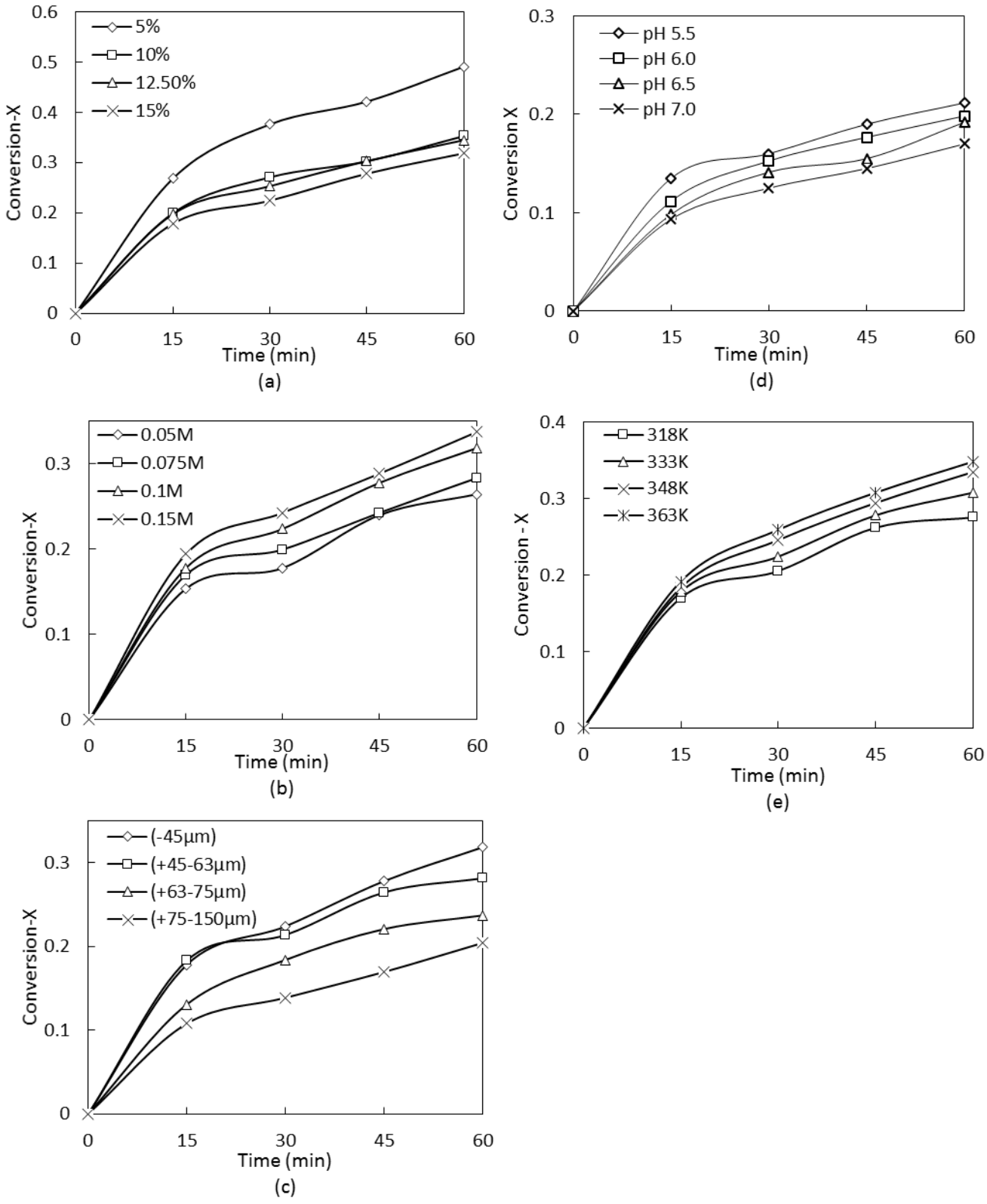

Figure 4. 4: Effect of solid to liquid ratio (a), acid concentration (b), particle size (c), pH (d), and temperature (e) on the dissolution of fly ash

4.4.7. Dissolution kinetics

The dissolution kinetics of fly ash in adipic acid was studied using the shrinking core model for solid-liquid system. The model considers the reaction of the reactants at the surface of the solid particles which results in both aqueous and solid particles (Hsu et al., 2009). The unreacted core of the particle reduces in size as the reaction proceeds, with more solids and aqueous products being formed (Demirkıran, 2008). This model considers the following steps in series:

1. Diffusion of the fluid reactant through the film surrounding the particle to the surface of the solid

2. Penetration and reaction of the fluid reactant through the layer of ash to the surface of the unreacted core

3. Fluid-solid surface chemical reaction at the reaction surface.

It is considered that the slowest step is the rate controlling step. From the above reaction steps, a heterogeneous system is considered to be controlled by: film diffusion, product layer diffusion or chemical reaction at the surface of the core of the unreacted particle. (Levenspiel, 1972). These steps can be integrated and written as follows:

$$X = \frac{3bk_l C_A}{\rho_B R_o} t = kt \qquad \text{Film diffusion equation} \qquad (4.14)$$

$$1-(1-X)^{\frac{1}{3}} = \frac{bk_s C_A}{\rho_B R_o} t = k_r t \qquad \text{Chemical reaction control} \qquad (4.15)$$

$$1+2(1-X)-3(1-X)^{\frac{2}{3}} = \frac{6bD_e C_A}{\rho_B R_o} t = k_d t \qquad \text{Product layer diffusion} \qquad (4.16)$$

The experimental data was fitted into the shrinking core model using eq. 4.15 and 4.16. The fluid media used for this study is liquid in nature and it is therefore considered that mass transfer across the fluid film will have least effect on the system. Therefore the fluid film diffusion step will not be controlling for this case (Maina and Mbarawa, 2011).The apparent rate constants for chemical reaction and product layer diffusion models were obtained by plotting the left side of eq. 4.15 and 4.16 with the reaction

time. The apparent rate constants from the plots and their correlation coefficients are represented in Table 4.1.

Table 4. 1: Dissolution rate constants and their correlations coefficients

Process variables	Surface chemical reaction $1-(1-X)^{\frac{1}{3}}=k_r t$		Product layer diffusion: $1+2(1-X)-3(1-X)^{\frac{2}{3}}=k_d t$	
	$K_r(min)^{-1}$	R^2	$K_d(min)^{-1}$	R^2
Temperature, (K)				
318	0.0016	0.8640	0.00049	0.9729
333	0.0019	0.9100	0.00061	0.9961
348	0.0020	0.9096	0.00073	0.9993
363	0.0021	0.9070	0.00080	0.9989
Solid to liquid ratio (wt.%)				
5	0.0031	0.9129	0.00168	0.9934
10	0.0021	0.8908	0.00080	0.9910
12.5	0.0020	0.8984	0.00077	0.9971
15	0.0019	0.9100	0.00065	0.9961
Concentration (M)				
0.05	0.0015	0.8973	0.00040	0.9804
0.075	0.0016	0.8839	0.00050	0.9837
0.1	0.0019	0.9100	0.00065	0.9961
0.15	0.0020	0.8975	0.00072	0.9935
Particle size				
45µm	0.0019	0.9100	0.00065	0.9961
63µm	0.0016	0.8400	0.00050	0.9685
75µm	0.0014	0.8874	0.00036	0.9861
150µm	0.0011	0.9175	0.00025	0.9914
pH				
5.5	0.0019	0.8060	0.00065	0.9556
6	0.0018	0.8242	0.00059	0.9698
6.5	0.0017	0.8091	0.00054	0.9519
7	0.0016	0.8342	0.00049	0.9744

According to Table 4.1, the product layer diffusion model had the highest regression coefficients. The linear relationship between $1+2(1-X)-3(1-X)^{\frac{2}{3}}$ and the reaction time

is shown in Figure 4.5(a-e) for solid to liquid ratio (a), acid concentration (b), particle size (c), temperature (d) and pH (e). This therefore shows that the equation for the dissolution kinetics for this process follows the product layer diffusion model and therefore can be written as follows:

$$k_d t = 1 + 2(1 - X) - 3(1 - X)^{\frac{2}{3}} \tag{4.17}$$

To include all the reaction parameters, a semi-empirical model can be written as:

$$k_d = K_o C^a \left(\frac{S}{L}\right)^b D^c P^d e^{\left(\frac{-E_a}{RT}\right)} \tag{4.18}$$

Combining eq. 4.17 and 4.18 yields eq. (4.19)

$$1 + 2(1 - X) - 3(1 - X)^{\frac{2}{3}} = K_o C^a \left(\frac{S}{L}\right)^b D^c P^d e^{\left(\frac{-E_a}{RT}\right)} t \tag{4.19}$$

where C is acid concentration, S/L is solid to liquid ratio, D is particle size and P is pH.

The values of the constants *a, b, c* and *d* are the reaction orders with respect to each parameter. Their values were obtained by plotting the natural logarithm of the reaction rate constants against natural logarithm of their respective parameter values. Their plots are represented in Fig 4.6(a-d) for solid to liquid ratio, acid concentration, particle size and pH respectively.

The Arrhenius plot was used to evaluate the activation energy for the dissolution process. According to the Arrhenius plot (illustrated in Figure 4.6(e)), the intercept was found to be 3.5745 and the activation energy evaluated from the slope is 10.64kJ/mol. The value of the activation energy shows that the dissolution of coal fly ash in adipic acid is a product layer diffusion controlled process. When the activation energy is below 20kJ/mol, product layer diffusion is usually the rate controlling step (Levenspiel, 1972; Zafar, 2008; Zhao et al., 2013; Limo and Enweremadu, 2011).

A semi-empirical model for this process can therefore be written as follows:

$$1 + 2(1 - X) - 3(1 - X)^{\frac{2}{3}} = 3.5745 C^{0.5592} \left(\frac{S}{L}\right)^{-0.8621} D^{-0.8055} P^{-1.196} e^{\left(\frac{-E_a}{RT}\right)} t \tag{4.20}$$

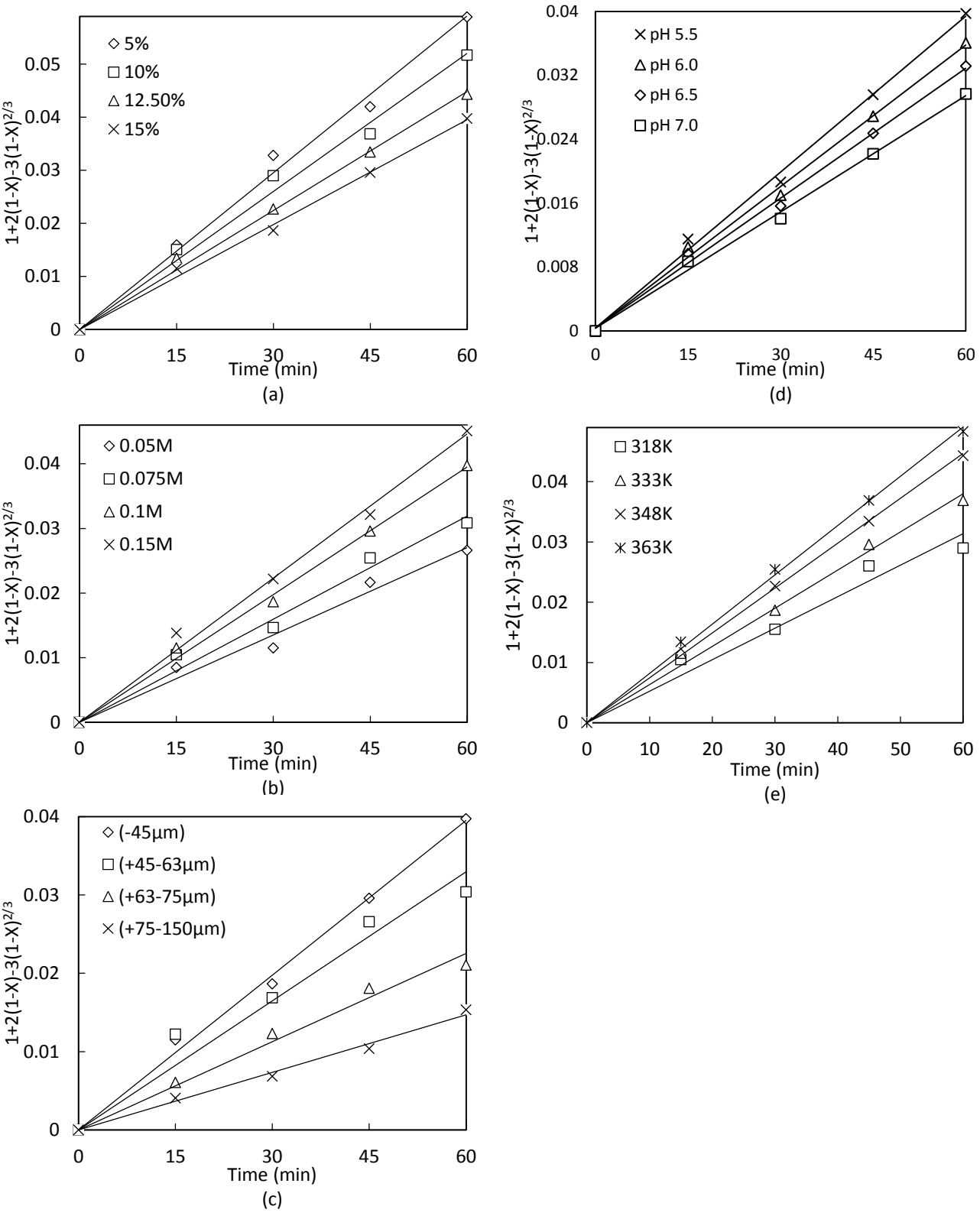

Figure 4. 5: Linear relationship showing variation of $1+2(1-X)-3(1-X)^{\frac{2}{3}}$ with the reaction time for different solid to liquid ratio (a), acid concentration (b), particle size (c), pH (d) and temperature (e).

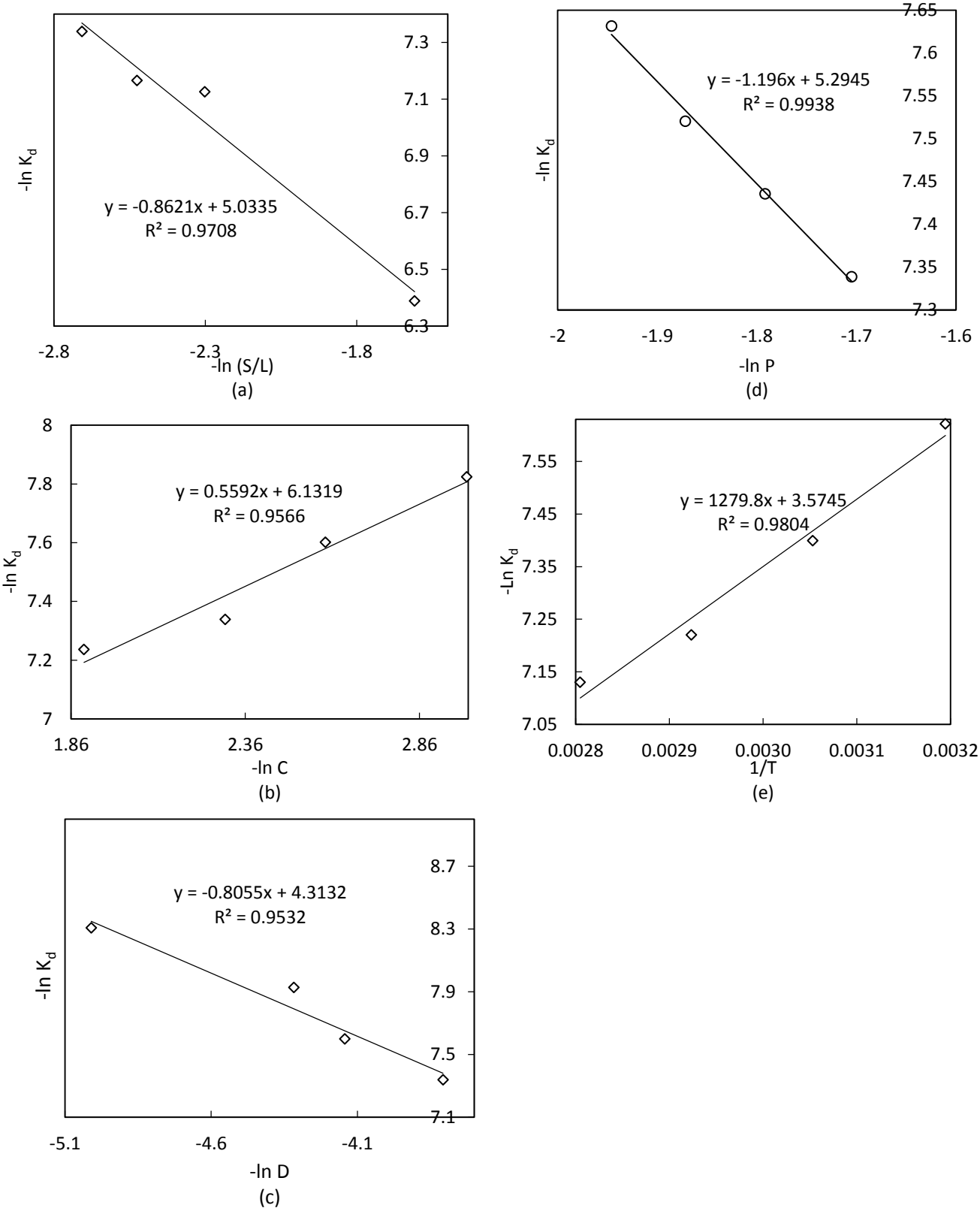

Figure 4. 6: Variation of -ln K_d with -ln S/L (a), -ln C (b), -ln D (c), -ln P (d) and 1/T (e) (Arrhenius plot)

Conclusion

The findings of this study show significant effects of the process variables on the dissolution of fly ash in adipic acid. It was found out that dissolution rate increases with increase in temperature, and acid concentration but decreases with increase in particle size, pH and solid to liquid ratio. Pozzolanic reaction resulted in the formation of anorthite as seen in XRD analysis. This also contributed to a significant increase in the specific surface area of sorbent (0.3669 to 6.9501m^2/g) as observed in the BET surface area analysis. The formation of aggregates and rough surfaces was observed on the surface of the sorbent after dissolution using SEM. The dissolution of fly ash was found to follow the shrinking core model with product layer diffusion model being the rate limiting step. The product layer being reaction products such as anorthite and other compounds. The semi-empirical model describing the dissolution of coal fly ash can be represented as follows:

$$1+2(1-X)-3(1-X)^{\frac{2}{3}} = 3.5745C^{0.5592}\left(\frac{S}{L}\right)^{-0.8621} D^{-0.8055}P^{-1.196}e^{\left(\frac{-E_a}{RT}\right)}t$$

The activation energy for the process was determined to be 10.64 kJ/mol.

4.5. References

Adamiec, P., Benezet, J. and Benhassaine, A. 2008. Pozzolanic reactivity of silico-aluminous fly ash. Particuology, vol. 6, no. 2, pp. 93-98.

Bakharev, T. 2005. Geopolymeric materials prepared using Class F fly ash and elevated temperature curing. Cement and Concrete Research, vol. 35, no. 6, pp. 1224-1232.

Brouwers, H. and Van Eijk, R. 2002. Fly ash reactivity: extension and application of a shrinking core model and thermodynamic approach. Journal of Materials Science, vol. 37, no. 10, pp. 2129-2141.

Criado, M., Fernández-Jiménez, A. and Palomo, A. 2007. Alkali activation of fly ash: Effect of the SiO_2/Na_2O ratio: Part I: FTIR study. Microporous and Mesoporous Materials, vol. 106, no. 1–3, pp. 180-191.

Demirkıran, N. 2008. A study on dissolution of ulexite in ammonium acetate solutions. Chemical Engineering Journal, vol. 141, no. 1, pp. 180-186.

Dube, G., Osifo, P. and Rutto, H. 2014. Preparation of bagasse ash/CaO/ammonium acetate sorbent and modeling their desulphurization reaction. Clean Technologies and Environmental Policy, vol. 16, no. 5, pp. 891-900.

Goodarzi, F. 2006. Characteristics and composition of fly ash from Canadian coal-fired power plants. Fuel, vol. 85, no. 10–11, pp. 1418-1427.

Hadjar, H., Hamdi, B., Jaber, M., Brendlé, J., Kessaissia, Z., Balard, H. and Donnet, J. 2008. Elaboration and characterization of new mesoporous materials from diatomite and charcoal. Microporous and Mesoporous Materials, vol. 107, no. 3, pp. 219-226.

Hsu, W., Lin, M. and Hsu, J. 2009. Dissolution of solid particles in liquids: a shrinking core model. World Acad Sci Eng Technol Chem Mater Eng, vol. 2, pp. 4-8.

Jozewicz, W. and Rochelle, G.T. 1986. Fly ash recycle in dry scrubbing. Environmental Progress, vol. 5, no. 4, pp. 219-224.

Karatepe, N., Mericboyu, A. and Kucukbayrak, S. 1998. Effect of Hydration Conditions on the Physical Properties of Fly Ash-$Ca(OH)_2$ Sorbents. Energy Sources, vol. 20, no. 6, pp. 505-511.

Kashiwakura, S., Ohno, H., Kumagai, Y., Kubo, H., Matsubae, K. and Nagasaka, T. 2011. Dissolution behavior of selenium from coal fly ash particles for the

development of an acid-washing process. Chemosphere, vol. 85, no. 4, pp. 598-602.

Koech, L., Everson, R., Neomagus, H. and Rutto, H. 2013. Dissolution Study of Bottom Ash in Wet Flue Gas Desulphurization, Int'l Conference on Industrial, Manufacturing, Automation and Mechanical Engineering Johannesburg, South Africa, November 27 - 28.

Lee, K.T., Bhatia, S. and Mohamed, A.R. 2005. Preparation and characterization of sorbents prepared from ash (waste material) for sulfur dioxide (SO_2) removal. Journal of Material Cycles and Waste Management, vol. 7, no. 1, pp. 16-23.

Levenspiel, O. 1972, Chemical Reaction Engineering, 2nd edn, John Wiley and Sons., New York.

Limo, R.H. and Enweremadu, C. 2011. The dissolution study of a South African magnesium-based material from different sources using a pH-stat. Chemical Industry and Chemical Engineering Quarterly, vol. 17, no. 4, pp. 459-468.

Lin, R. and Shih, S. 2003. Characterization of Ca $(OH)_2$/fly ash sorbents for flue gas desulfurization. Powder Technology, vol. 131, no. 2, pp. 212-222.

Maina, P. and Mbarawa, M. 2011. Investigating effects of zeolites as an agent to improve limestone reactivity toward flue gas desulfurization. Energy & Fuels, vol. 25, no. 5, pp. 2028-2038.

Mishra, S., Langwenya, S., Mamba, B. and Balakrishnan, M. 2010. Study on surface morphology and physicochemical properties of raw and activated South African coal and coal fly ash. Physics and Chemistry of the Earth, Parts A/B/C, vol. 35, no. 13, pp. 811-814.

Nyale, S.M., Babajide, O.O., Birch, G.D., Böke, N. and Petrik, L.F. 2013. Synthesis and Characterization of Coal Fly Ash-based Foamed Geopolymer. Procedia Environmental Sciences, vol. 18, no. 0, pp. 722-730.

Ogenga, D., Siagi, Z., Onyango, M. and Mbarawa, M. 2009. Influence of hydration variables on the properties of South African calcium/siliceous-based material. Frontiers of Chemical Engineering in China, vol. 3, no. 1, pp. 46-51.

Pietersen, H.S., Fraay, A.L. and Bijen, J.M. 1989. Reactivity of fly ash at high pH, MRS Proceedings Cambridge Univ Press, , pp. 139.

Rocha, S.D., Mansur, M.B. and Ciminelli, V.S. 2004. Kinetics and mechanistic analysis of caustic magnesia hydration. Journal of Chemical Technology and Biotechnology, vol. 79, no. 8, pp. 816-821.

Sarbak, Z. and Kramer-Wachowiak, M. 2002. Porous structure of waste fly ashes and their chemical modifications. Powder Technology, vol. 123, no. 1, pp. 53-58.

Song, H. and Park, J. 2001. Improvement of SO_2 removal by the solubility change of $Ca(OH)_2$ in the spray dryer system. Environmental technology, vol. 22, no. 9, pp. 1001-1006.

Swanepoel, J. and Strydom, C. 2002. Utilisation of fly ash in a geopolymeric material. Applied Geochemistry, vol. 17, no. 8, pp. 1143-1148.

Tanaka, H. and Fujii, A. 2009. Effect of stirring on the dissolution of coal fly ash and synthesis of pure-form Na-A and-X zeolites by two-step process. Advanced Powder Technology, vol. 20, no. 5, pp. 473-479.

Temuujin, J., Williams, R. and Van Riessen, A. 2009. Effect of mechanical activation of fly ash on the properties of geopolymer cured at ambient temperature. Journal of Materials Processing Technology, vol. 209, no. 12, pp. 5276-5280.

Thiruppathi, K., Barathan, S., Anandhan, N. and Sivakumar, G. 2009. Effect of Fly Ash and Water in Hydrated Srpc-A Ftir Study. Applied Physics Research, vol. 1, no. 2, pp. P59.

van der Merwe, E. and Strydom, C. 2006. Hydration of medium reactive magnesium oxide using hydration agents. Journal of Thermal Analysis and Calorimetry, vol. 84, no. 2, pp. 467-471.

Zafar, Z.I. 2008. Determination of semi empirical kinetic model for dissolution of bauxite ore with sulfuric acid: Parametric cumulative effect on the Arrhenius parameters. Chemical Engineering Journal, vol. 141, no. 1, pp. 233-241.

Zhao, J., Li, Y., Han, K., Niu, S. and Lu, C. 2013. Dissolution Characteristics of Calcium-Based Alkaline Industrial Wastes. Journal of Chemical Engineering of Japan, vol. 46, no. 12, pp. 827-832.

5. Leaching kinetics of bottom ash waste as a source of calcium ions

5.1. Abstract

Bottom ash is a waste material from coal-fired power plants and it is known to contain elements which are potentially toxic at high concentration levels when disposed in landfills. This study investigates the use of bottom as a partial substitute sorbent for wet FGD processes by focusing on its leaching kinetics in adipic acid. This was studied basing on the shrinking core model which was applied the experimental data obtained by Koech et al. (2013) on dissolution of bottom ash. The leaching rate constant was obtained from different reaction variables: temperature, pH, acid concentration and solid to liquid ratio which could affect the leaching process. The solid sample of bottom ash was characterized at different leaching periods using X-ray diffraction (XRD) and scanning electron microscope (SEM). It was found out that solid to liquid ratio had a significant effect on the leaching rate constant when compared to other variables. The leaching kinetics showed that diffusion through the product layer was the rate controlling step during leaching and the activation energy for the process was found to be 18.92kJ/mol.

Key words: Bottom ash, leaching kinetics, shrinking core model, rate constant.

5.2. Introduction

Bottom ash is a combustion residue generated during the burning of coal in a power plant. It is entrained in flue gas and falls to the bottom of the furnace where it is collected as a waste. It contains potentially toxic elements which can be harmful to the environment at high concentrations (Kaakinen et al., 1975; Linak and Wendt, 1994; Vassilev et al., 2005). Due to increased use of coal for power in South Africa, there is a continued increase in the amount of bottom ash generated. It has led to large amount of bottom ash being disposed as landfills which has raised a lot of environmental concerns. Power plants are hard pressed to meet the existing environmental laws and regulations and are therefore constantly looking for ways to utilize bottom ash.

Several studies have demonstrated ways of utilizing waste such as bottom ash (Chindaprasirt et al., 2009; Kayabal and Buluş, 2000; Kurama and Kaya, 2008; Park et al., 2009). A study on the leaching behaviour of bottom ash and fly ash done by Wang et al. (1999) indicated that that different element have different leaching behaviours because of their different properties. It was also found out that leaching behaviour of bottom ash is greatly dependent on the pH of the solution and the leaching time. Yan and Neretnieks (1995) studied the dissolution behaviour of bottom ash where it was observed that its dissolution behaviour varies due to the difference in dissolution mechanisms and rates of chemical species that exist in bottom ash. Dincer et al. (2007) studied the use of a locally available bottom ash as an adsorbent for removal of dyes from synthetic textile wastewater. Maximum adsorption was achieved at a pH of 7 and was also noted that bottom ash could be used in treatment of acidic industrial wastewater.

In a wet FGD process, SO_2 is removed from flue gas by contacting it with a sorbent slurry which is prepared by dissolution. Dissolution plays a significant role in a wet FGD process because it affects the overall performance on the process. Bottom ash can be used as a source of calcium and magnesium ions which can react with sulphur dioxide to form calcium sulphite or Calcium sulphate (gypsum). This is environmentally friendly and can be utilized in building and agricultural sectors. Because of this, it can be used as a partial substitute for raw material in wet flue gas desulphurization process because

of its pozzolanic properties. Bottom ash is mainly composed of SiO_2 and Al_2O_3 compounds which are essential ingredients for pozzolanic reaction. Most researchers have studied the properties of pozzolanic materials such as bottom ash (Cheriaf et al., 1999; Jaturapitakkul and Cheerarot, 2003; Karatepe et al., 1998; Kopsick and Angino, 1981) and it has been proven that due to its pozzolanic activity, it leads to formation of products with increased surface area. Increased sorbent surface area leads to improved SO_2 removal capacity because more calcium ions will be exposed for chemo-sorption reaction between SO_2 and the sorbent (Rutto and Enweremadu, 2012)..

Wet FGD systems can be enhanced by use of additives which improves sorbent utilization as well as SO_2 removal efficiency. These additives include organic acids like adipic acid which has been widely accepted because of its buffering effect in wet FGD process. Its buffering effect limits the drop in the pH in the gas-liquid interface thereby accelerating liquid-phase mass transfer (Wang and Burbank, 1982). The use of adipic acid has been proven to improve the utilization of limestone to 80% from 65-70% without adipic acid (Wang and Burbank, 1982). This leads to reduced solid-waste generated from the process.

In the previous work (Koech et al., 2013), it was revealed that the conversion of calcium ions into solution from bottom ash was favoured by low pH and low solid to liquid ratio. It was also favoured with increased slurry temperature and adipic acid concentration. The main purpose of this study is to investigate the leaching kinetics of bottom ash using the experimental data obtained in the previous work (Koech et al., 2013). Attention is given to the leaching rate constant obtained using different variables like pH, acid concentration, temperature and solid to liquid ratio which affects the leaching process. XRD and SEM analysis was done to examine the effect of leaching on solid samples of bottom ash at different leaching periods.

5.3. Method and materials

5.3.1. Materials

The experiments performed by Koech et al. (2013) used bottom ash obtained from a coal-fired thermal power plant in South Africa. Before the experiment bottom ash was

dried, crushed using a ball mill and then sieved to obtain an average size of -45µm size particles using shaking screen sieves. The chemicals used for the study were adipic acid, calcium ions standards (1000ppm) for the AAS and de-ionized laboratory water. The XRF analysis of the bottom ash showed that its chemical composition consisted of the following in wt %: 51.81 % SiO_2, 30.49 % AI_2O_3, 4.67 % Fe_2O_3, 6.82 % CaO, 0.26 % MgO, 0.97 % K_2O, 0.37 % P_2O_5, 0.61 % SO_3 and loss on ignition of 3.97%.

5.3.2. Method

The dissolution experiments by Koech et al. (2013) were done using a pH stat apparatus. The pH was controlled automatically by titrating with a given concentration of adipic acid as shown in Figure 5.1. The variables used in the experiment were temperature, solid to liquid ratio, acid concentration and pH.The slurry pH was controlled automatically by titrating with a known concentration of adipic acid at constant flow rate. Every batch experiment was allowed to run for 60 minutes with sample being removed every 15 minutes, filtered and analyzed for calcium ions using Solaar S4 Atomic Absorption Spectrophotometer (AAS) from Themo Electron Corporation, South Africa. The cumulative leaching fraction was evaluated as:

$$X = \left(\frac{Calcium\ ions\ in\ solution}{Total\ amount\ of\ calcium\ ions\ in\ the\ original\ sample}\right)$$

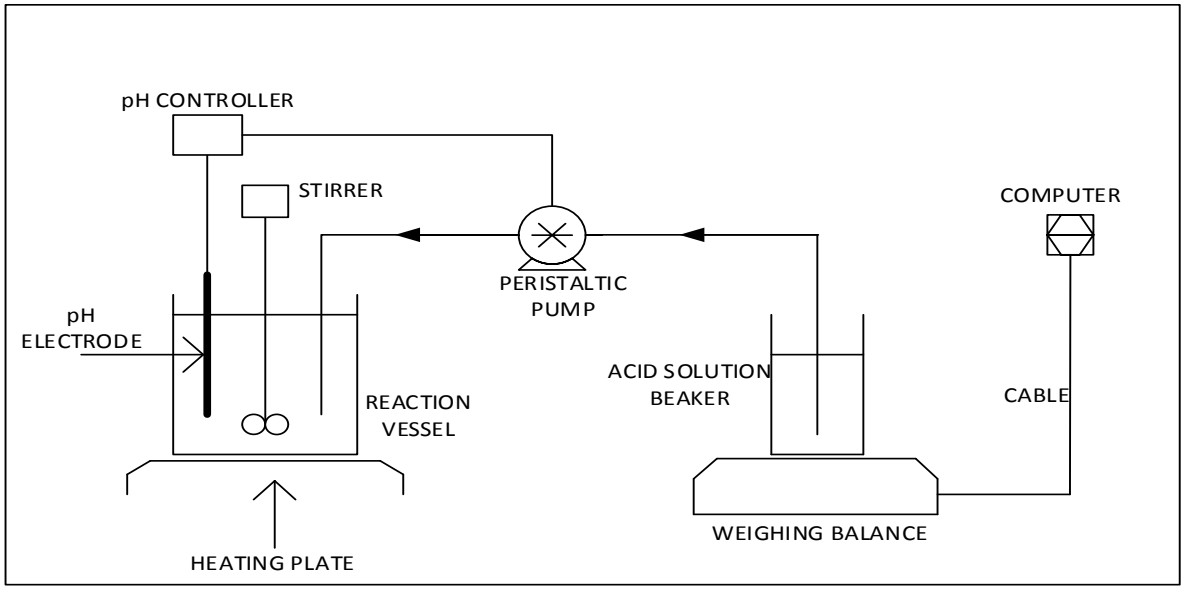

Figure 5. 1: Experimental set up for dissolution of bottom ash in adipic acid

5.3.3. Characterization techniques used

A qualitative analysis of bottom ash was done before and after leaching using XRD. The material was prepared for XRD analysis using a back loading preparation method. Two samples were scanned after addition of 20% Si for qualitative determination of amorphous content. It was analyzed with a PANalytical Empyrean diffractometer with PIXcel detector and fixed with Fe filtered Co-Kα radiation. The phases were identified using X'pert Highscore Plus software.

A Philips XL-30Sscanning electron microscope (SEM) was used to observe the morphological structures of the samples at different leaching periods. The samples were sprinkled on an adhesive carbon tape and were metallized using gold before the analysis. The images of the samples were recorded at various magnifications.

5.3.4. Leaching kinetics theory

The leaching of bottom ash in adipic acid is a heterogeneous reaction system consisting of solid particles and fluid reactant. For a system like this, leaching rate may be generally controlled by one of the following steps: diffusion through the fluid film, diffusion through the ash or chemical reaction at the surface of unreacted core (Levenspiel, 1972; Zafar, 2008).

The experimental data was analyzed on the basis of shrinking core model in order to determine the rate controlling step. The shrinking core model considers that a reaction first occurs at the surface of the particle and moves towards the centre. As the reaction proceeds, the unreacted core of the particle is reduced in size while more products are formed. For a reaction of this kind, the following steps are considered to occur in series:

1. Diffusion of the fluid reactants from the bulk liquid phase through the liquid film to the solid surface.
2. Reaction between the fluid reactants and the solid particle.
3. Diffusion of the reaction products from the solid surface back into the bulk liquid phase.

It is considered that the slowest of the above steps is rate controlling step. The above steps can be integrated and written as follows (Levenspiel, 1972):

$$X = \frac{3bk_gC_A}{\rho_B R_0} t = k_r t \quad \text{Film diffusion control} \quad (5.1)$$

$$1 - (1 - X)^{\frac{1}{3}} = \frac{bk_sC_A}{\rho_B R_0} t = k_r t \quad \text{Chemical reaction control} \quad (5.2)$$

$$1 + 2(1 - X) - 3(1 - X)^{\frac{2}{3}} = \frac{6bD_eC_A}{\rho_B R_0} t = k_d t \quad \text{Product layer diffusion} \quad (5.3)$$

The film diffusion control is not considered as a rate limiting step for this case because the fluid reactant is liquid and therefore offers minimal resistance for transport of reactants to the surface of the particle. The experimental data from different reaction variables were analyzed using eqn. 5.2 and 5.3. Multiple regression coefficients and apparent rate constants (dissolution rate constants) were obtained from the integral rate expressions. This was done by plotting the left side of eqn. 5.2 and 5.3 with the reaction time. Their values are shown in Table 1.

5.4. Results and discussion

5.4.1. Mechanism for leaching of bottom ash

From XRF analysis, bottom ash consists mainly of SiO_2, Al_2O_3, CaO and Fe_2O_3. It is considered that all these components are affected by dissolution. Therefore their dissolution mechanism in adipic acid is shown in eqn. 5.5 - 5.8.

Adipic acid dissociates into solution to form adipate ions:

$$C_6H_{10}O_{4(aq)} \rightarrow C_6H_8O_{4(aq)}^{2-} + 2H_{(aq)}^{+} \quad (5.4)$$

The dissolution of SiO_2, Al_2O_3, CaO, and Fe_2O_3 is by adipate complexation to form their respective adipate complexes:

$$SiO_{2_{(s)}} + 2C_6H_8O_{4(aq)}^{2-} + 4H_{(aq)}^{+} \rightarrow Si(C_6H_8O_4)_{2(aq)} + 2H_2O_{(l)} \quad (5.5)$$

$$Al_2O_{3_{(s)}} + 3C_6H_8O_{4(aq)}^{2-} + 6H_{(aq)}^{+} \rightarrow Al_2(C_6H_8O_4)_{3(aq)} + 3H_2O_{(l)} \quad (5.6)$$

$$CaO_{(s)} + C_6H_8O_{4(aq)}^{2-} + H_2O_{(l)} \rightarrow CaC_6H_8O_{4(aq)} + 2OH_{(aq)}^{-} \quad (5.7)$$

$$Fe_2O_{3_{(s)}} + 3C_6H_8O_{4(aq)}^{2-} + 3H_2O_{(l)} \rightarrow Fe_2(C_6H_8O_4)_{3(aq)} + 6OH_{(aq)}^{-} \quad (5.8)$$

Silica and aluminium oxide consume hydroxides while earth alkali (CaO) and iron oxide produce them (Brouwers and Van Eijk, 2002).The adipate complexes formed in eqn. 5.5-5.8 will undergo dissociation due to super saturation (Rocha et al., 2004). This will lead to formation of silicon, aluminium, titanium, iron and calcium ions in solution with adipate ions.

$$Si(C_6H_8O_4)_{2(aq)} \leftrightarrow Si_{(aq)}^{4+} + 2C_6H_8O_{4(aq)}^{2-} \quad (5.9)$$

$$Al_2(C_6H_8O_4)_{3(aq)} \leftrightarrow 2Al_{(aq)}^{3+} + 3C_6H_8O_{4(aq)}^{2-} \quad (5.10)$$

$$CaC_6H_8O_{4(aq)} \leftrightarrow Ca_{(aq)}^{2+} + C_6H_8O_{4(aq)}^{2-} \quad (5.11)$$

$$Fe_2(C_6H_8O_4)_{3(aq)} \leftrightarrow 2Fe_{(aq)}^{3+} + 3C_6H_8O_{4(aq)}^{2-} \quad (5.12)$$

The presence of CaO in the coal fly ash is important because Ca^{2+} is the most active part during chemo-sorption reaction in flue gas desulphurization. Apart from dissolution by adipate complexation, CaO can also undergo hydrogen complexation releasing calcium ions into solution (Dube et al., 2014).

CaO dissolution by hydrogen complexation:

$$CaO_{(s)} + H_{(aq)}^{+} \rightarrow Ca_{(aq)}^{2+} + OH_{(aq)}^{-} \quad (5.13)$$

Calcium ions from super saturation (eqn. 11) can be utilised more in pozzolanic reaction to form alumina-silicate complex compounds (Karatepe et al., 1998).

Pozzolanic reaction:

$$Ca_{(aq)}^{2+} + 2SiO_{2(s)} + Al_2O_{3(s)} + 2OH_{(aq)}^{-} \rightarrow CaAl_2Si_2O_8.H_2O_{(s)} \quad (5.14)$$

The product formed (calcium alumino-silicate hydrate) from the pozzolanic reaction leads to an increase in the surface area of the sorbent which thus improves its SO_2 absorption capacity during flue gas desulphurization.

5.4.2. XRD analysis

The phase composition of bottom ash as received and at different dissolution periods is illustrated in Figure 5.2. The XRD patterns show that it is a siliceous material because it is mainly composed of quarts and silicon. The diffraction peaks appearing at 2θ=24.4,

31.1 and 33.4 represents quarts while the peaks appearing at 2θ=55.7 and 66.4 represent silicon. The analyzed samples also contained mullite appearing at 2θ=30.4 and 41.6 while anorthite appeared at 2θ=33.3.

The effect of dissolution on the samples is observed mainly on quarts and silicon. There is a reduction of the quarts and silicon peaks in the samples after dissolution. Dissolution had least effect on quartz peak appearing at 2θ=31.1 and also on anorthite at 2θ=33.3. The sample after 60 minutes dissolution period had the lowest diffraction peaks for silicon at 2θ=66.4. This indicates that Si^{4+} ions were extracted into solution which may react with Al^{3+} and Ca^{2+} ions to form products with increased surface area. This can improve SO_2 capture during flue gas desulphurization (Karatepe et al., 1998).

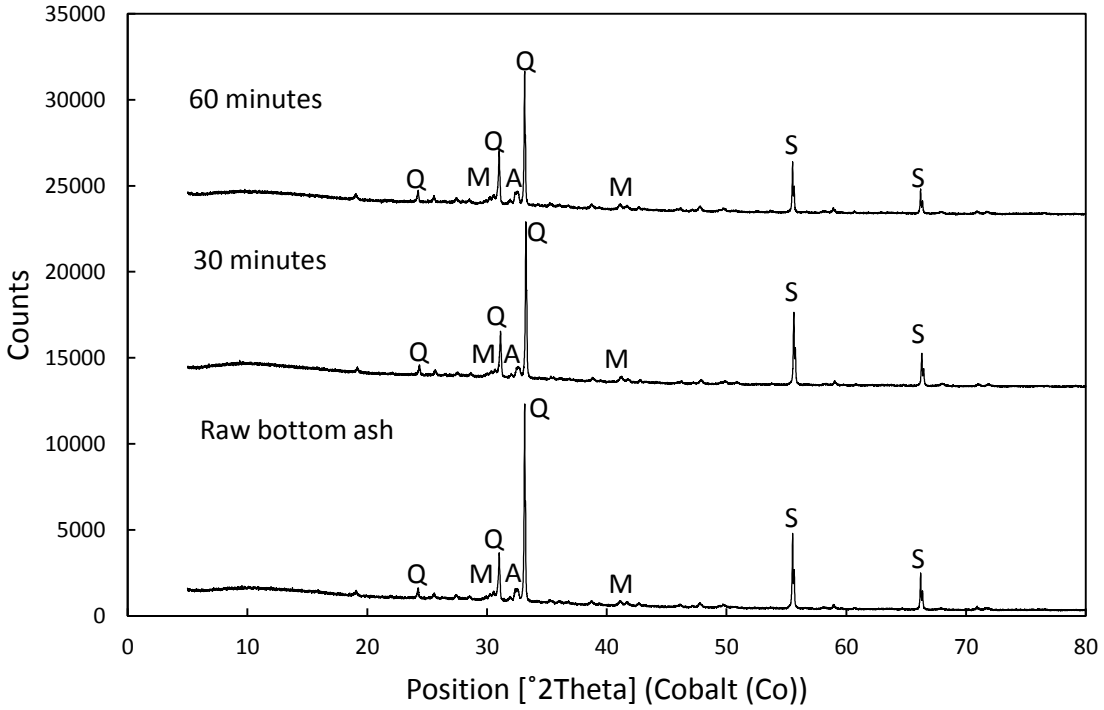

Figure 5. 2: XRD diffraction patterns for raw bottom ash, after 30 minutes and 60 minutes dissolution periods (Q-Quarts, M-Mullite, S-Silicon and A-Anorthite)

5.4.3. Effects of reaction variables on leaching rate constant

Table 5.1 shows the apparent rate constants both for the surface chemical reaction and the product layer diffusion models with their respective regression coefficients. It is evident from the table that diffusion though the product layer is the rate controlling step

for the process because of the largest regression coefficients. The product layer diffusion models (relationship between $1 + 2(1 - X) - 3(1 - X)^{\frac{2}{3}}$ and the reaction time) are represented in Figure 5.3 for (a) acid concentration, (b) solid to liquid ratio, (c) pH and (d) temperature.

The effect of acid concentration was studied by varying adipic acid concentration from 0.05M, 0.075M, 0.1M and 0.15M. The temperature, solid to liquid ratio and pH were kept constant at 333K, 7.5g/100ml and 5.5 respectively. The values of rate constants at different acid concentrations are shown in Table 5.1. It shows that increasing the concentration of adipic acid causes an increase in the rate constant. This is because of increased H^+ ion activity when acid concentration is increased leading to increased leaching rate. The effect of solid to liquid ratio on the rate constant was found to be significant. This was studied by performing different experiments at 5, 7.5, 12.5 and 15g/100ml solid to liquid ratio. The temperature, acid concentration and pH were maintained at 333K, 0.1M and 5.5 respectively. The rate constant increased appreciably when solid to liquid to liquid ratio is was reduced. This is because an increase in the amount of solid per unit liquid volume decreases the dissolution rate (Maina and Mbarawa, 2011). Figure 5.3(b) also shows that diffusion through the product layer was strongly dependent on the solid to liquid ratio giving a rate constant of 0.000861 min^{-1} at 5 wt.% and 0.000151 min^{-1} at 15 wt.%. The variation shows that it had the most significant effect on the rate constant compared to other leaching variables.

The effect of pH was studied by carrying out different batch experiments at pH of 5.5, 6.0, 6.5 and 7.0. This was done while the temperature, acid concentration and solid to liquid ratio were kept constant at 333K, 0.1M and 7.5g/100ml. The obtained values of the rate constants at different pH values were found to decrease with increase in pH. This shows that leaching rate is influenced mainly by diffusion though the product layer at lower pH. From the product layer diffusion model in Figure 5.3(c), the values of the rate constant obtained ranged from 0.000433 min^{-1} to 0.000305 min^{-1} at a pH of 5.5 and pH of 7.0 respectively. High values of the rate constant were obtained at low pH because there is high concentration of H^+ which increases dissolution reaction between the fluid reactant and the solid particles (Ganor et al., 1995).

To study the effect of temperature, different experiments were performed at 303K, 318K, 333K and 348K while the pH, solid to liquid ratio and acid concentration were maintained at 5.5, 7.5g/100ml and 0.1M respectively. From Table 5.1, the values of rate constant at different temperatures increased with increase in temperature. At a temperature of 303K the rate constant was 0.000261 min $^{-1}$ and then it increased to 0.000742 min $^{-1}$ at a temperature of 348K. There was significantly huge gap between the values obtained at 333K and 348K. This is because high temperatures affect the kinetic characteristics of the leaching process and this leads to high reactivity (Bharadwaj et al., 2013).

Table 5. 1: Regression coefficients and the apparent rate constants

Process variables	Surface chemical reaction: $1-(1-X)^{1/3}=K_r t$		Product layer diffusion: $1-3(1-X)^{2/3}+2(1-X)=K_d t$	
	$K_r(min)^{-1}$	R^2	$K_d(min)^{-1}$	R^2
Temperature (K)				
303	0.000465	0.8972	0.000271	0.9876
318	0.000503	0.8681	0.000312	0.9835
333	0.000593	0.8938	0.000430	0.9893
348	0.000778	0.8887	0.000726	0.9917
Solid to liquid ratio (wt. %)				
5	0.002576	0.8881	0.000861	0.9969
7.5	0.001815	0.8439	0.000433	0.9897
12.5	0.001330	0.8473	0.000236	0.9953
15	0.001048	0.9267	0.000151	0.9783
Concentration (M)				
0.05	0.001483	0.7902	0.000294	0.9627
0.075	0.001664	0.8439	0.000363	0.9733
0.1	0.001815	0.7790	0.000433	0.9897
0.15	0.002231	0.8217	0.000642	0.9850
pH				
5.5	0.001815	0.8439	0.000433	0.9897
6	0.001718	0.8722	0.000391	0.9976
6.5	0.001596	0.8422	0.000335	0.9963
7	0.001517	0.8318	0.000305	0.9919

For a heterogeneous reaction system, the dissolution rate is a function of temperature and it is expressed using the Arrhenius equation:

$$K_d = K_o e^{\frac{E_a}{RT}} \quad (5.17)$$

$$LnK_d = LnK_o + \frac{E_a}{RT} \quad (5.18)$$

The Arrhenius plot was used to obtain the activation energy for the system and the pre-exponential factor K_o. Using the apparent rate constants for temperature from Table 5.1, the Arrhenius plot was drawn. This is illustrated in Figure 5.4. The activation energy was found to be 18.92kJ/mol. The activation energy in a heterogeneous reaction system can also be used to distinguish between transport controlled reactions, surface chemical reactions or mixed reactions. From the value of the activation energy, it is evident that the dissolution of bottom ash in adipic acid is a product layer diffusion controlled process. The activation energy for product layer diffusion controlled process is usually below 20kJ/mol (Cama et al., 1999).

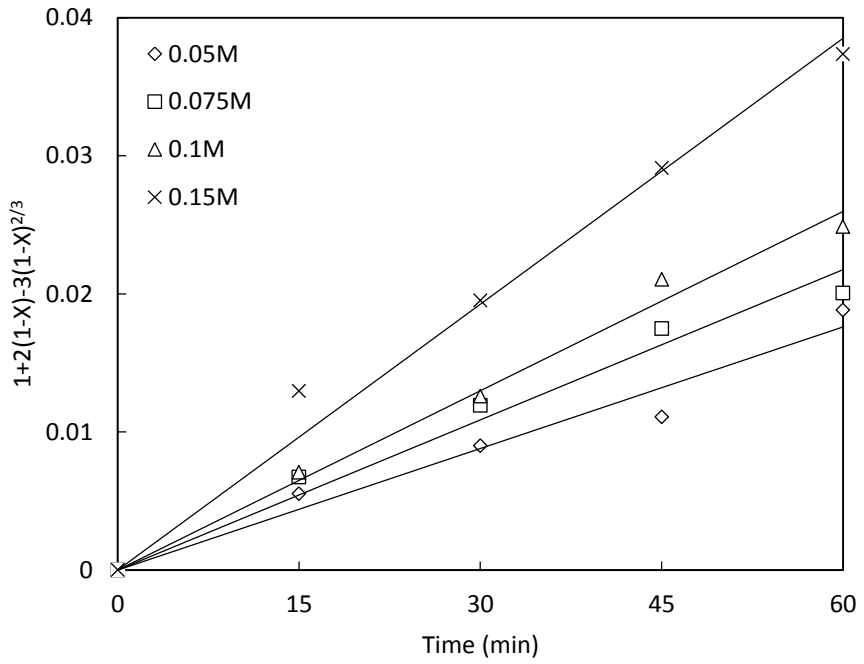

(a)

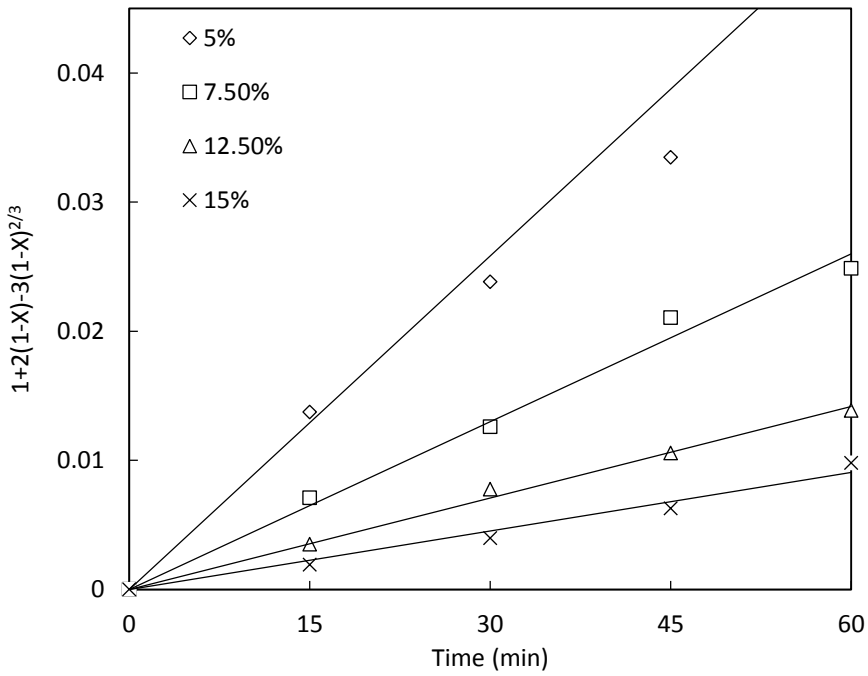
◇ 5%
□ 7.50%
△ 12.50%
× 15%
0.04
0.03
0.02
0.01
0
1+2(1-X)-3(1-X)^2/3
0
15
30
45
60
Time (min)

(b)

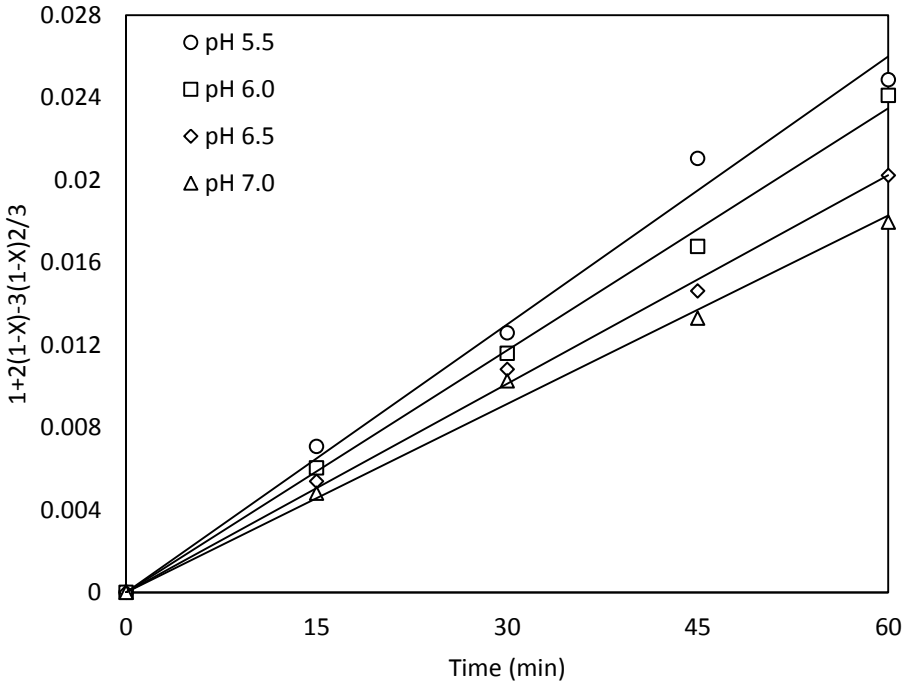
○ pH 5.5
□ pH 6.0
◇ pH 6.5
△ pH 7.0
0.028
0.024
0.02
0.016
0.012
0.008
0.004
0
1+2(1-X)-3(1-X)2/3
0
15
30
45
60
Time (min)

(c)

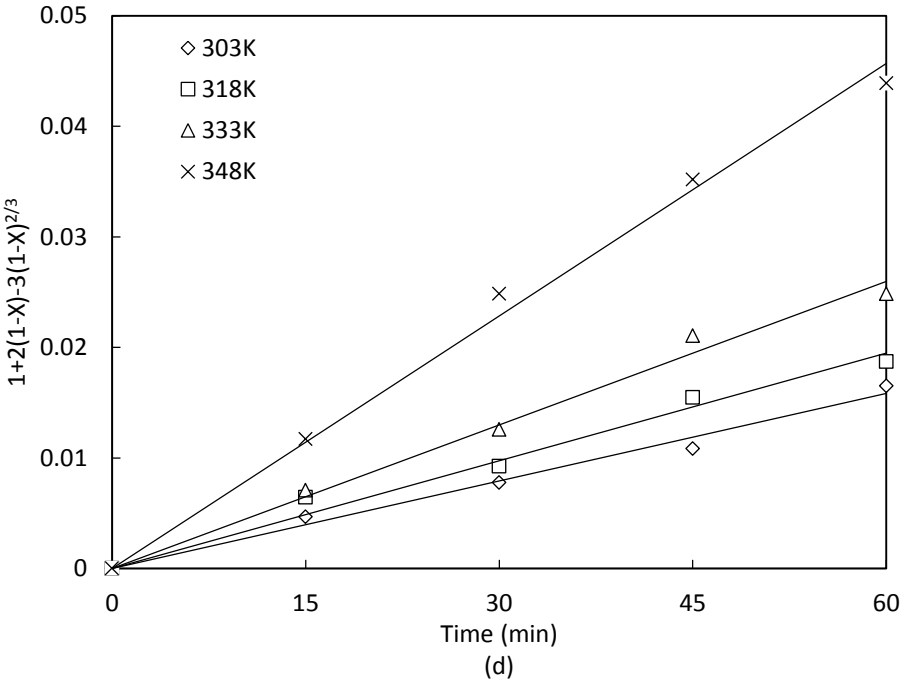

Figure 5. 3: Linear relationship between $\mathbf{1}+\mathbf{2}(\mathbf{1}-\boldsymbol{X})-\mathbf{3}(\mathbf{1}-\boldsymbol{X})^{\frac{\mathbf{2}}{\mathbf{3}}}$ and the reaction for acid concentration (a), solid to liquid ratio (b), pH (c) and temperature (d).

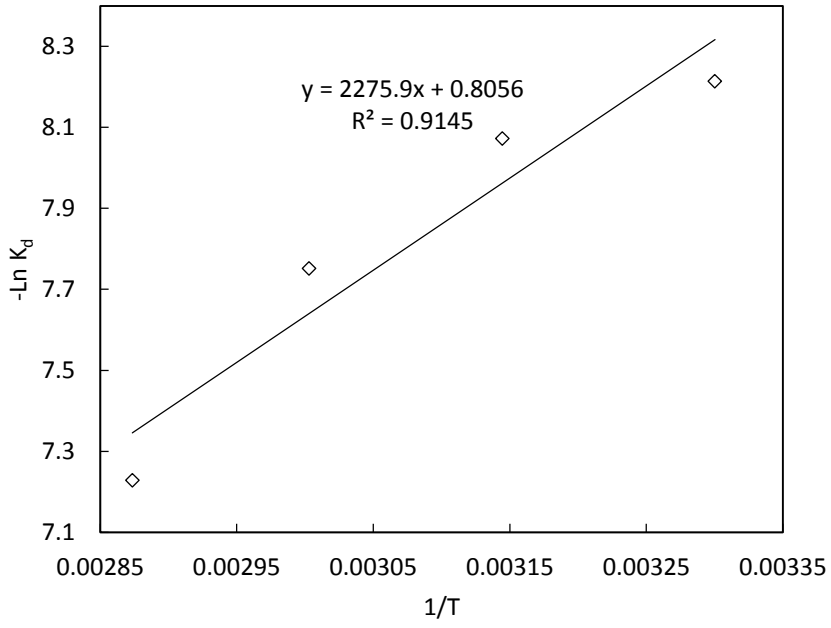

Figure 5. 4: Arrhenius plot for bottom ash dissolution

5.4.4. SEM analysis

The morphological structure of the samples studied at different dissolution periods is represented in Figure 5.5. It is evident that the studied bottom ash is composed of particles of different sizes that are porous with irregular shapes. This is due to the different states of silica that are responsible for irregular shapes of the particles (Sarbak et al., 2004). It is also observed that raw bottom ash has microcrystals on the surface of large particles; this means that the sample may contain mullite, and plerospheres containing Si, Al, Ca and Fe (Shim et al., 2003).

The surface morphology of the samples after dissolution (Figure 5.5(b)) varies significantly. It reveals particles with deformed shapes that are rough and more porous relative to the raw bottom ash. This is attributed to the leaching of silica, alumina and calcite out of the particle surface during dissolution. This was also evident in XRD analysis where quarts and silica peaks diminished with prolonged dissolution periods.

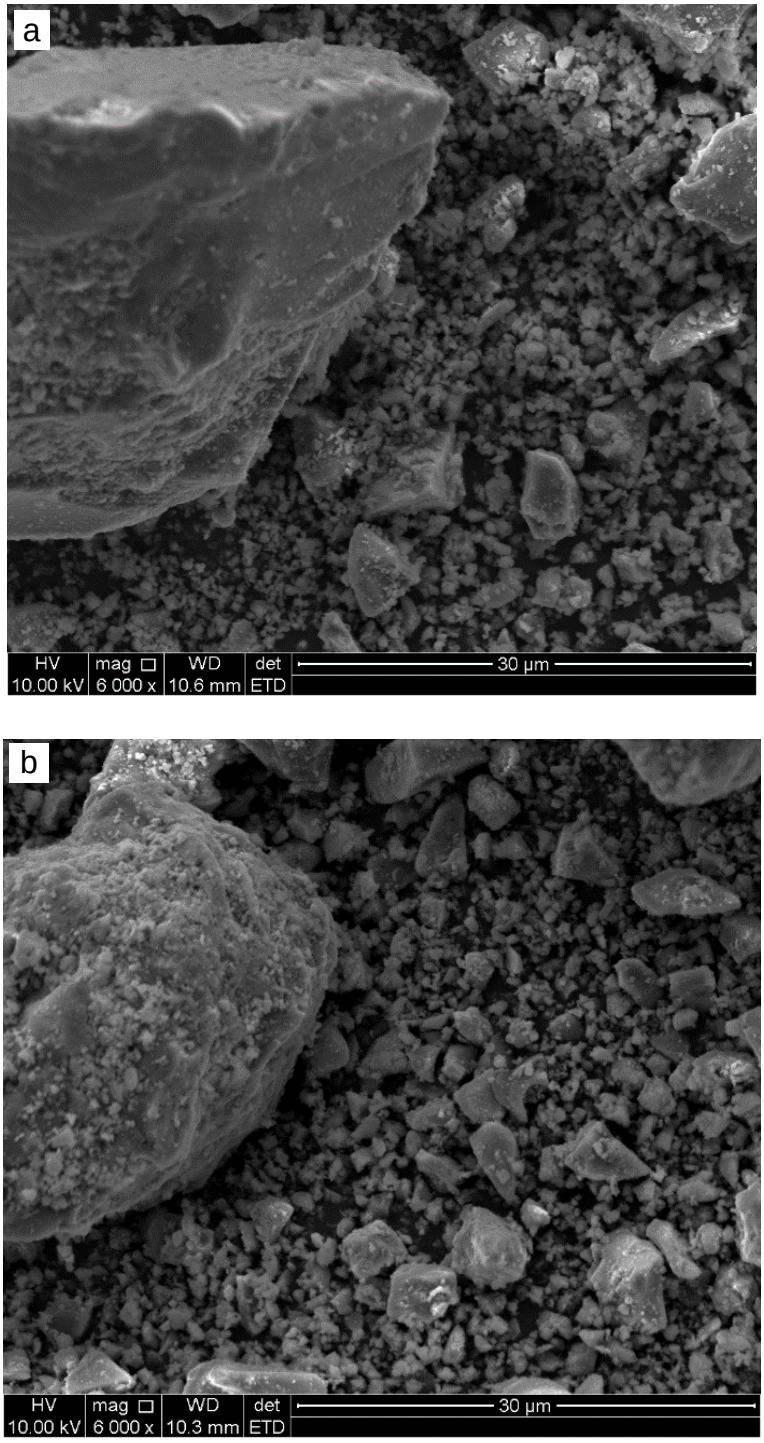

Figure 5. 5: SEM images for raw bottom ash (a) and after 60 minutes dissolution period (b).

Conclusion

The findings of this study show that it is possible to leach out calcium ions from bottom ash waste which can be used in wet FGD and reduce anthropogenic

pollution. The results indicated that the effect of solid to liquid ratio on the leaching rate was more significant giving a leaching rate constant of 0.000861 min^{-1} at 5 wt.% and 0.000151 min^{-1} at 15 wt.%. It was also found that bottom ash leaching follows the shrinking core model with the product layer being the rate limiting step. The activation energy for this step was found to be 18.92kJ/mol.

5.5. References

Bharadwaj, H.K., Lee, J., Li, X., Liu, Z., Keener, T.C., 2013. Dissolution kinetics of magnesium hydroxide for CO_2 separation from coal-fired power plants. J. Hazard. Mater. 250, 292-297.

Brouwers, H., Van Eijk, R., 2002. Fly ash reactivity: extension and application of a shrinking core model and thermodynamic approach. J. Mater. Sci. 37, 2129-2141.

Cama, J., Ayora, C., Lasaga, A.C., 1999. The deviation from equilibrium effect on dissolution rate and on apparent variations in activation energy. Geochim. Cosmochim. Acta 63, 2481-2486.

Cheriaf, M., Rocha, J.C., Pera, J., 1999. Pozzolanic properties of pulverized coal combustion bottom ash. Cem. Concr. Res. 29, 1387-1391.

Chindaprasirt, P., Jaturapitakkul, C., Chalee, W., Rattanasak, U., 2009. Comparative study on the characteristics of fly ash and bottom ash geopolymers. Waste Manage. 29, 539-543.

Dinçer, A.R., Güneş, Y., Karakaya, N., 2007. Coal-based bottom ash (CBBA) waste material as adsorbent for removal of textile dyestuffs from aqueous solution. J. Hazard. Mater. 141, 529-535.

Dube, G., Osifo, P., & Rutto, H. 2014. Preparation of bagasse ash/CaO/ammonium acetate sorbent and modelling their desulphurization reaction. Clean Technologies and Environmental Policy, *16*, 891-900

Ganor, J., Mogollon, J.L., Lasaga, A.C., 1995. The effect of pH on kaolinite dissolution rates and on activation energy. Geochim. Cosmochim. Acta 59, 1037-1052.

Jaturapitakkul, C., Cheerarot, R., 2003. Development of bottom ash as pozzolanic material. J. Mater. Civ. Eng. 15, 48-53.

Kaakinen, J.W., Jorden, R.M., Lawasani, M.H., West, R.E., 1975. Trace element behavior in coal-fired power plant. Environ. Sci. Technol. 9, 862-869.

Karatepe, N., Mericboyu, A., Küçükbayrak, S., 1998. Effect of Hydration Conditions on the Physical Properties of Fly Ash-$Ca(OH)_2$ Sorbents. Energy Sources 20, 505-511.

Kayabal, K., Buluş, G., 2000. The usability of bottom ash as an engineering material when amended with different matrices. Eng. Geol. 56, 293-303.

Koech, L., Everson, R., Neomagus, H., Rutto, H., 2013. Dissolution Study of Bottom Ash in Wet Flue Gas Desulphurization. Int'l Conference on Industrial, Manufacturing, Automation and Mechanical Engineering, Johannesburg, South Africa, November 27-28, 2013

Kopsick, D.A., Angino, E.E., 1981. Effect of leachate solutions from fly and bottom ash on groundwater quality. J. Hydrol. 54, 341-356.

Kurama, H., Kaya, M., 2008. Usage of coal combustion bottom ash in concrete mixture. Constr. Build. Mater. 22, 1922-1928.

Levenspiel, O., 1972. Chemical Reaction Engineering, 2 ed. John Wiley and Sons., New York.

Linak, W.P., Wendt, J.O., 1994. Trace metal transformation mechanisms during coal combustion. Fuel Process Technol 39, 173-198.

Maina, P., Mbarawa, M., 2011. Enhancement of lime reactivity by addition of diatomite. Fuel Process Technol 92, 1910-1919.

Park, S.B., Jang, Y.I., Lee, J., Lee, B.J., 2009. An experimental study on the hazard assessment and mechanical properties of porous concrete utilizing coal bottom ash coarse aggregate in Korea. J. Hazard. Mater. 166, 348-355.

Rocha, S.D., Mansur, M.B., Ciminelli, V.S., 2004. Kinetics and mechanistic analysis of caustic magnesia hydration. J. Chem. Technol. Biotechnol. 79, 816-821.

Rutto, H. and C. Enweremadu. 2012. Dissolution of a South African calcium based material using urea: An optimized process. Korean Journal of Chemical Engineering 29:1-8.

Sarbak, Z., Stańczyk, A., Kramer-Wachowiak, M., 2004. Characterisation of surface properties of various fly ashes. Powder Technol 145, 82-87.

Shim, Y., Kim, Y., Kong, S., Rhee, S., Lee, W., 2003. The adsorption characteristics of heavy metals by various particle sizes of MSWI bottom ash. Waste Manage. 23, 851-857.

Vassilev, S.V., Vassileva, C.G., Karayigit, A.I., Bulut, Y., Alastuey, A., Querol, X., 2005. Phase–mineral and chemical composition of composite samples from feed coals, bottom ashes and fly ashes at the Soma power station, Turkey. Int. J. Coal Geol. 61, 35-63.

Wang, S. and D. Burbank. 1982. Adipic Acid-Enhanced Lime/Limestone Test Results at the EPA Alkali Scrubbing Test Facility. Flue Gas Desulfurization 188.

Wang, Y., Ren, D., Zhao, F., 1999. Comparative leaching experiments for trace elements in raw coal, laboratory ash, fly ash and bottom ash. Int. J. Coal Geol. 40, 103-108.

Yan, J., Neretnieks, I., 1995. Is the glass phase dissolution rate always a limiting factor in the leaching processes of combustion residues? Sci. Total Environ. 172, 95-118.

Zafar, Z.I., 2008. Determination of semi empirical kinetic model for dissolution of bauxite ore with sulfuric acid: Parametric cumulative effect on the Arrhenius parameters. Chem. Eng. J. 141, 233-241.

6. The effect of fly ash addition on limestone dissolution rate constant

6.1. Abstract

Limestone dissolution is a very important factor in flue gas desulphurization system because it determines its reactivity towards SO_2. Fly ash which is siliceous material has been reported to improve sorbent reactivity. This study investigates the effect of adding fly ash to limestone on its dissolution rate constant. The experiments were carried out using a pH stat apparatus where the effects of the reaction variables: limestone to fly ash ratio, slurry pH, reaction temperature and concentration of acid used were investigated. Central Composite Design (CCD) of experiment was used to develop a model which correlates the dissolution rate constant and the reaction variables. It was found that fly ash had a positive effect on the dissolution rate constant of limestone with the pH having the most significant effect. The dissolution rate constant was found to increase with an increase in temperature and acid concentration. XRD analysis showed products of hydration formed which are mainly calcium silicate hydrates on the samples. This led to increase in the specific surface area as observed in the BET analysis.

Key words: limestone dissolution, rate constant, fly ash, response surface and shrinking core model.

6.2. Introduction

Flue gas desulphurization is the most relevant technology used in large scale power utilities such as coal-fired power plants to remove sulphur dioxide from flue gas. In order to improve the SO_2 removal efficiency and sorbent utilization in FGD system, the sorbent reaction with SO_2 can be activated by adding of siliceous materials. Siliceous compounds can be found in fly ash which mainly contains SiO_2, Al_2O_3, Fe_2O_3 and CaO. The use of fly ash in FGD systems has economic advantage and also reduces environmental pollution because they are waste products of coal-fired power plants.

The abundance of SiO_2 and Al_2O_3 in fly ash makes it to be considered a pozzolanic material. SiO_2 and Al_2O_3 reacts with limestone in the presence of water to form calcium silicate hydrates, calcium aluminate hydrates or calcium alumino silicate hydrates (Ogenga et al., 2009; Liu et al., 2002; Karatepe et al., 1998b). The pozzolanic reaction products get deposited on the surface of fly ash and its surface areas increases with increasing hydration time and temperatures (Karatepe et al., 1998a). The surface area is an important parameter because sorbent reactivity with SO_2 strongly depends on it. The pozzolanic products increase sorbent reactivity by making calcium ions more accessible during chemo-sorption reaction (Lee et al., 2005a).

Recent studies on the use of fly ash in FGD systems have indicated an improved sorbent utilization when it is used during sorbent preparation. Ogenga et al. (Ogenga et al., 2009) studied the influence of hydration variables on South African calcium/siliceous-based material. An increase in the specific surface area of the sorbent prepared from fly ash was observed from 8.8 to 23.6 m^2/g. It was also observed that the sorbent had an increased porous structure compared to fly ash or CaO alone. Chiung et al. (Liu et al., 2002) also studied the kinetics of reaction of $Ca(OH)_2$/fly ash sorbent with SO_2. The sorbent prepared from $Ca(OH)_2$ and fly ash showed increased reactivity towards SO_2 as compared to pure $Ca(OH)_2$ with high degree of Ca utilization observed. An increase in the conversion was also observed with an increase in the specific surface area in the prepared sorbent. Shi and Xu (Shi and Xu, 2001) found out that lime reactivity improves significantly when fly ash is added because fly ash increases lime dispersion and it extends its effective surface area.

Lee et al. (Lee et al., 2005a) also developed regression models to correlate the significance of variables to the surface areas in different sorbents. Their results showed that sorbents prepared from fly ash and oil palm exhibited the highest SO_2 removal capacity which was attributed to the difference in microstructural properties of the sorbents. Their XRD analysis indicated the presence of calcium alumino silicate hydrate as a product of hydration which contributed to increased surface area.

The effect of fly ash on the reactivity of limestone is investigated in this study. This is done using a pH stat apparatus and analyzing calcium ions in solution which a direct measure of limestone reactivity. The experimental results were correlated to the shrinking core model during dissolution of limestone in wet FGD process. A central composite design is used to see the effects of the reaction variables (i.e. slurry pH, reaction temperature, limestone to fly ash ratio and acid concentration) on the dissolution rate constant and also develop a quadratic model relating the rate constant and reaction variables.

6.3. Materials and method

The materials used for this experiment were limestone and coal fly ash. Limestone was obtained from a local mine and fly ash was obtained from a coal-fired power plant. The raw materials were dried and milled to an average of 45µm particle size using a ball mill. Their chemical compositions were determined by XRF analysis and it is shown in Table 6.1. Hydrochloric acid used as an acid titrant was supplied by Sigma Aldrich, South Africa. Distilled water was also used in the experiment.

Table 6. 1: XRF analysis for limestone and fly ash used

Components	Limestone (wt.%)	Fly ash (wt.%)
CaO	85.34	10.52
MgO	2.4	1.36
Fe_2O_3	0.36	3.89
SiO_2	0.94	49.71
SO_3	0.05	0.32
Al_2O_3	-	27.53
MnO	-	0.06
TiO_2	-	1.89
Na_2O	-	0.36
K_2O	-	0.85
P_2O_5	-	1.42
Cr_2O_3	-	0.02
H_2O	0.07	0.15
LOI	10.84	1.92
Total	100.00	100.00

6.3.1. Method

A pH stat apparatus was used for this experiment to determine the effect of fly ash on the dissolution rate constant of limestone. A volume of 100 ml of distilled water in the reaction vessel was heated to the required temperature while the stirring speed was kept constant at 100 rpm. A variable speed-temperature controlled magnetic stirrer was used to heat and agitate the reaction mixture in the vessel. When the required temperature is achieved, 5g of limestone is added with a pre-determined amount of fly ash. The reaction pH was determined using a pH electrode dipped which sends a signal to the pH controller. When the pH of the reaction mixture exceeds the set value, the pump gets activated and pumps the acid thereby lowering the pH. The set-up for this experiment is illustrated in Figure 6.1. This was repeated by varying the temperature, pH, acid concentration and the amount of fly ash added according the experimental design shown in Table 3. Each experiment was allowed to proceed for 60 minutes with a sample being taken from the reaction mixture every 15 minutes and analyzed for calcium ions using Metrohm 881 cation compact IC machine. The conversion of calcium ions into solution was expressed as:

$$X = \frac{Calcium\ ions\ in\ solution}{Total\ calcium\ ions\ in\ the\ original\ sample}$$

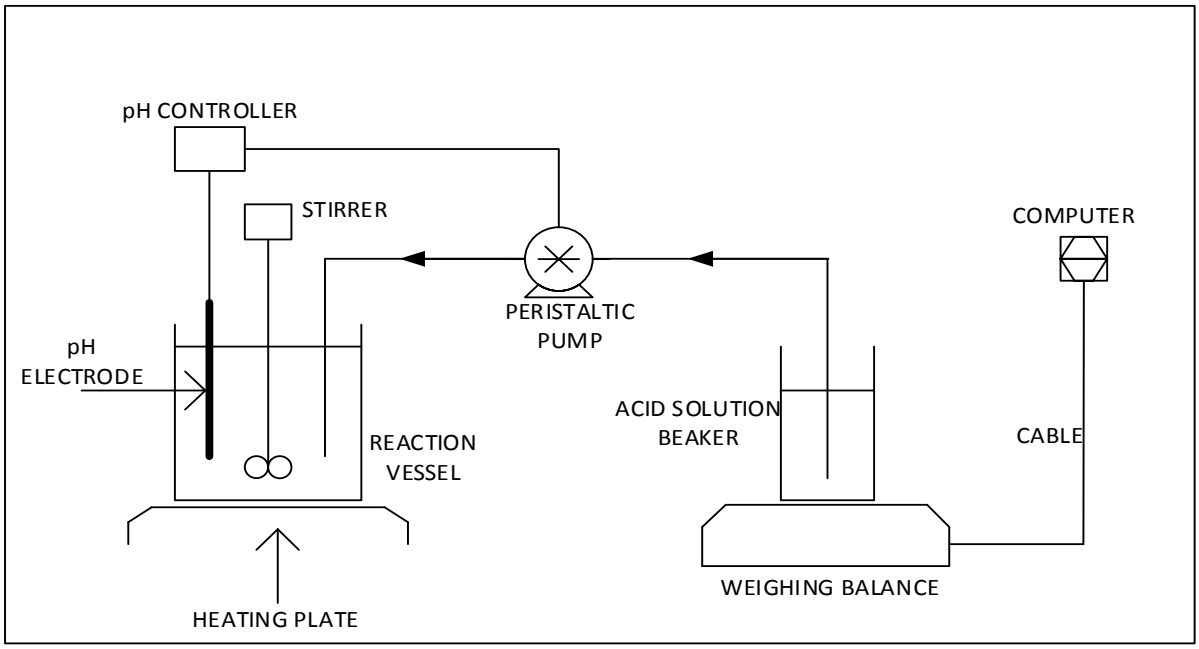

Figure 6. 1: Schematic diagram representing the experimental set up.

6.3.2. Sorbent characterization

The samples at different dissolution periods and conditions were subjected to XRD, SEM and BET surface area analysis methods. X-ray diffraction (XRD) was done to determine the crystalline phases in the samples. This was done using PANalytical Empyrean diffractometer with PIXcel detector and fixed with Fe filtered Co-Kα radiation. The specific surface area of the samples was determined by nitrogen adsorption using the Brunauer-Emmett-Teller (BET) method. The surface morphology was observed using Philips XL-30S scanning electron microscope (SEM). This was done by sprinkling the samples on an adhesive carbon tape and metalized using gold before being taking images.

6.3.3. Kinetic analysis

For a non-catalytic heterogeneous reaction system consisting of solid particles surrounded by fluid reactant, a shrinking core model is considered. The shrinking core model represents reality in variety of situations and it considers that reaction first occurs on the surface of the particle. The unreacted core of the particle shrinks in size as the reaction proceeds (Levenspiel, 1972). The shrinking core model considers three steps occur in series:

- Diffusion of the fluid reactant through the fluid film to the surface of the solid particle

- Reaction between the fluid reactant and solid particle at the surface of the particle
- Diffusion of the fluid reactant through the product layer

The rate of reaction in a heterogeneous system can be controlled by one of the above steps. The rate equations can be integrated and represented as:

$$X = \frac{3bk_gC_A}{\rho_B R_0}t = k_l t \qquad \text{Film diffusion control} \qquad (6.1)$$

$$1-(1-X)^{\frac{1}{3}} = \frac{bk_sC_A}{\rho_B R_0}t = k_r t \qquad \text{Chemical reaction control} \qquad (6.2)$$

$$1+2(1-X)-3(1-X)^{\frac{2}{3}} = \frac{6bD_eC_A}{\rho_B R_0}t = k_d t \qquad \text{Product layer diffusion} \qquad (6.3)$$

The reaction rate constant was evaluated by plotting the left side of equation (6.2) and (5.3) with the reaction time. The film diffusion control was not considered because the fluid reactant is liquid and therefore there is minimum resistance due to mass transfer through the film layer (Maina, 2013).

6.3.4. Design of experiment

A central composite design (CCD) which is a standard Response Surface Methodology (RSM) design in the Design Expert 6.0.6 software was used for design of experiment in this study. The dissolution rate constant was evaluated by varying the reaction variables using the CCD design. The reaction variables used include temperature, acid concentration, pH and the amount of fly added. The range of these variables (minimum and maximum) is shown in Table 6.2. CCD helps to investigate the linear, quadratic, cubic and cross-product effects of the four reaction variables on the dissolution rate constant of limestone. It also optimizes the effective variables and gathers information with the number of experimental runs and also analyzes the interaction between the variables (Maina and Mbarawa, 2011). A two-level full factorial CCD (2^4=16) consisting of 8 axial points and 6 centre points was used. With the value of α being 2, the number of experiments was found to be 30. CCD gives a randomized sequence of experiments in order to minimize the effects of uncontrolled variables. Table 6.3 shows a complete design matrix of the experiments generated from the CCD with the dissolution rate constant.

Each response obtained from the experimental runs was used to develop a mathematical model that correlates the dissolution rate constant to the reaction variables using a third order polynomial equation shown in eqn (6.4).

$$Y = b_o + \sum_{j=1}^{4} b_j x_j + \sum_{i,j=1}^{4} b_{ij} x_i x_j + \sum_{j=1}^{4} b_{jj} x_j^2 + \sum_{k,i,j=1}^{4} b_{kij} x_k x_i x_j + \sum_{j=1}^{4} b_{jjj} x_j^3 \quad (6.4)$$

Where Y is the predicted value of the dissolution rate constant (min^{-1}) b_o is the offset term, b_j is the linear effect, b_{ij} is the first order interaction effect, b_{jj} is the squared effect, b_{kij} is the second order interaction effect and b_{jjj} is the cubic effect.

Table 6. 2: Range of reaction variables used

Parameter	Codes	Minimum	Maximum
Temperature (°C)	X_1	30	75
Acid concentration (M)	X_2	0.5	2
pH	X_3	4	7
Limestone to fly ash ratio	X_4	0	1

Table 6. 3: Full factorial design matrix of experiments with response

Expt No.	Temperature (°C)	Concentration (M)	pH	Limestone to fly ash ratio (wt. %)	Response rate constant	R^2
	X_1	X_2	X_3	X_4	(min^{-1})	
1	41.25	0.88	4.75	0.25	0.0031	0.9880
2	63.75	0.88	4.75	0.25	0.0036	0.9525
3	41.25	1.63	4.75	0.25	0.0043	0.9216
4	63.75	1.63	4.75	0.25	0.0046	0.9236
5	41.25	0.88	6.25	0.25	0.0034	0.9651
6	63.75	0.88	6.25	0.25	0.0036	0.8938
7	41.25	1.63	6.25	0.25	0.0031	0.9687
8	63.75	1.63	6.25	0.25	0.0033	0.9804
9	41.25	0.88	4.75	0.75	0.0041	0.9377
10	63.75	0.88	4.75	0.75	0.0043	0.9383
11	41.25	1.63	4.75	0.75	0.0046	0.7904
12	63.75	1.63	4.75	0.75	0.0051	0.9836
13	41.25	0.88	6.25	0.75	0.0034	0.9583
14	63.75	0.88	6.25	0.75	0.0038	0.9537
15	41.25	1.63	6.25	0.75	0.0034	0.9823
16	63.75	1.63	6.25	0.75	0.0036	0.9588
17	30	1.25	5.5	0.5	0.0031	0.9803
18	75	1.25	5.5	0.5	0.0043	0.9433

19	52.5	0.5	5.5	0.5	0.0029	0.9862
20	52.5	2	5.5	0.5	0.0044	0.9096
21	52.5	1.25	4	0.5	0.0046	0.9332
22	52.5	1.25	7	0.5	0.0023	0.9654
23	52.5	1.25	5.5	0	0.0031	0.9897
24	52.5	1.25	5.5	1	0.0049	0.9755
25	52.5	1.25	5.5	0.5	0.0041	0.9753
26	52.5	1.25	5.5	0.5	0.0042	0.9721
27	52.5	1.25	5.5	0.5	0.0043	0.9841
28	52.5	1.25	5.5	0.5	0.0042	0.9777
29	52.5	1.25	5.5	0.5	0.0042	0.9875
30	52.5	1.25	5.5	0.5	0.0041	0.9546

6.4. Results and discussion

Table 6.3 shows a full factorial design matrix with respective response (dissolution rate constant). The dissolution rate constant obtained was between 0.0023 and 0.0051 per minute. The consistency of the experimental runs was evident on the results obtained from 6 centre points (Experiments 25–30). The response obtained for these experimental runs was close with little variation.

Using multiple regression analysis, the dissolution rate constant was correlated with the reaction variables using the polynomial equation represented in eqn. (6.4). The final predictive second order quadratic model in terms of coded values is represented as:

$$Y = -0.016494 + 1.21 \times 10^{-4}(X_1) + 8.19 \times 10^{-3}(X_2) + 4.23 \times 10^{-3}(X_3) + 4.82 \times 10^{-3}(X_4) - 7.56 \times 10^{-7}\left(X_1{}^2\right) - 7.87 \times 10^{-4}\left(X_2{}^2\right) - 2.68 \times 10^{-4}\left(X_3{}^2\right) - 3.70 \times 10^{-4}\left(X_4{}^2\right) - 2.07 \times 10^{-6}(X_1.X_2) - 4 \times 10^{-6}(X_1.X_3) + 1.33 \times 10^{-6}(X_1.X_4) - 9.64 \times 10^{-4}(X_2.X_3) - 3.6 \times 10^{-4}(X_2.X_4) - 5.27 \times 10^{-4}(X_3.X_4) \quad (6.5)$$

The magnitude of the effect of the reaction variables on the dissolution rate constant was checked using Prob>F value in the ANOVA analysis as shown in Table 6.4. The values of Prob>F less than 0.05 indicate that the model terms have significant effect on the dissolution rate constant. In this case all the reaction variables are significant but pH is the most significant because it has the lowest Prob>F value. This was also supported by the F-value as shown in the Table 6.4. High F-value means the variable has significant effect on the dissolution rate constant. The quadratic effect of the pH was also found to be significant with Prob>F value being 0.0078 and the F-value being 9.40. This was also the case with the quadratic effect of the pH and acid concentration having the F-value of 15.64 and Prob>F value of 0.0013. The least significant effect was observed on the quadratic effect of temperature and the amount of fly ash having F-value of 0.00299 and Prob>F value of 0.9571. The quadratic effect of temperature and concentration was also observed to have low significance on the dissolution rate constant having F-value of 0.016 and Prob>F value of 0.9002.

The quality of model was validated using a plot of the predicted values and the experimental results as shown in Figure 6.2. From the plot, most the data points lie along the line of unit slope. This implies that the model best describes the

relationship between the reaction variables and the dissolution rate constant. The value of R^2 obtained for the quadratic model is 0.9101. This shows that 91.01% of the total variation in the response could be attributed to the empirical model.

Table 6. 4: Analysis of variance (ANOVA) for the empirical model

Source	Sum of Squares	DF	Mean Square	F Value	Prob > F
Model	1.14E-05	14	8.17E-07	10.85	< 0.0001
X_1	9.68E-07	1	9.68E-07	12.86	0.0027
X_2	1.34E-06	1	1.34E-06	17.74	0.0008
X_3	4.66E-06	1	4.66E-06	61.97	< 0.0001
X_4	2.05E-06	1	2.05E-06	27.28	0.0001
X_1^2	2.51E-07	1	2.51E-07	3.33	0.0879
X_2^2	3.36E-07	1	3.36E-07	4.46	0.0519
X_3^2	7.08E-07	1	7.08E-07	9.4	0.0078
X_4^2	1.47E-08	1	1.47E-08	0.19	0.6652
$X_1 X_2$	1.23E-09	1	1.23E-09	0.016	0.9002
$X_1 X_3$	1.82E-08	1	1.82E-08	0.24	0.6298
$X_1 X_4$	2.25E-10	1	2.25E-10	2.99E-03	0.9571
$X_2 X_3$	1.18E-06	1	1.18E-06	15.64	0.0013
$X_2 X_4$	1.82E-08	1	1.82E-08	0.24	0.6298
$X_3 X_4$	1.56E-07	1	1.56E-07	2.07	0.1705
Residual	1.13E-06	15	7.53E-08		

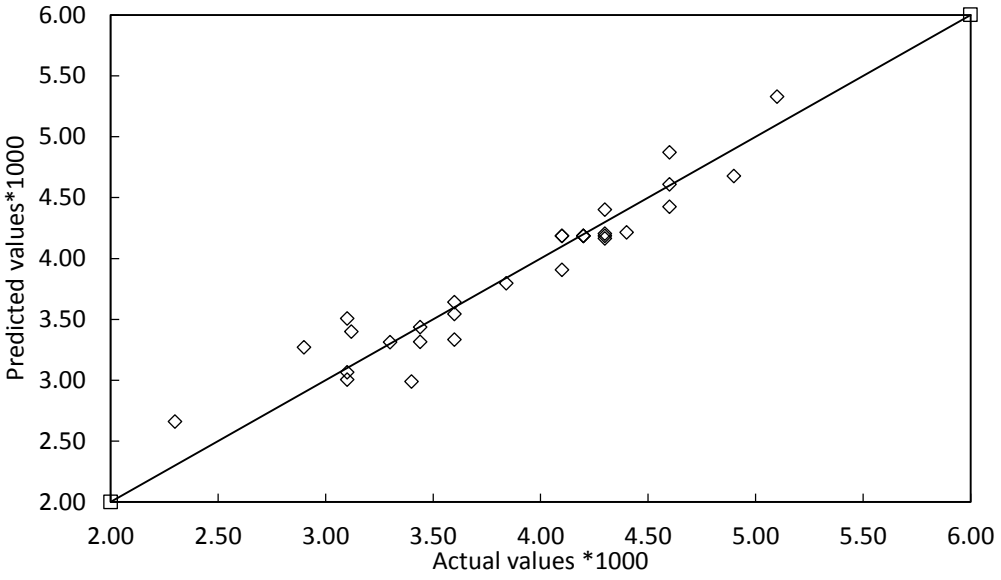

Figure 6. 2: A plot of the predicted values from the model with the actual results

6.4.1. Dissolution rate limiting step

The rate limiting step was determined by fitting the experimental data using equations (2) and (3) for surface chemical reaction and diffusion through the product layer respectively. Figure 6.3 shows the relationship between conversion and time for 4 selected experiments (Experiments number 1, 12, 22 and 25). The corresponding surface chemical reaction and product layer diffusion models are shown in Figure 4 and 5 respectively. A comparison between Figure 6.4 (a) and (b) indicates that chemical reaction at the surface was the rate controlling because of its largest regression coefficients. There was minimal resistance due to diffusion through the product layer which was attributed to the product layer (ash layer) being continuously removed from the particle surface due to agitation (Maina, 2013).

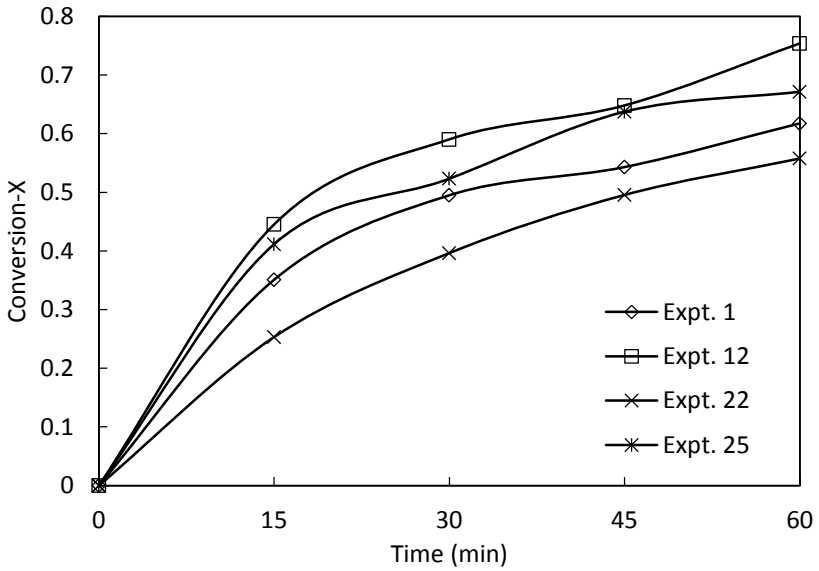

Figure 6. 3: Conversion time graphs for selected experimental runs

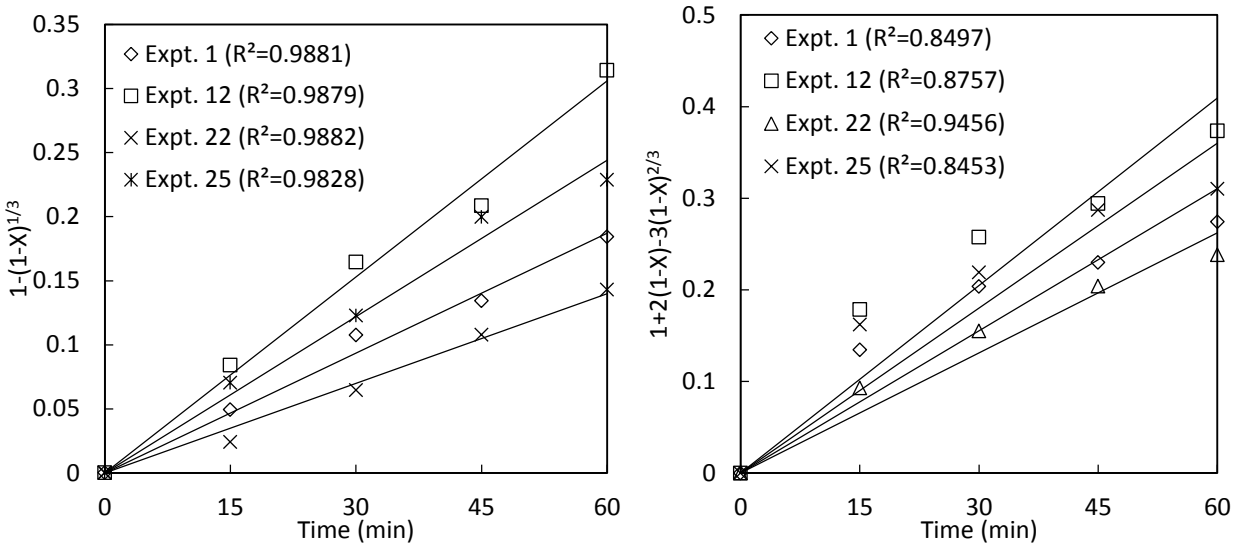

Figure 6. 4: The relationship between (a) $1-(1-X)^{1/3}$ and (b) $1+2(1-X)-3(1-X)^{2/3}$ with the reaction time for the selected experimental runs.

6.4.2. XRD analysis

A qualitative XRD analysis of limestone blended with fly as showed that it mostly contains aluminosilicate compounds with calcite. Limestone is the main source of calcite as this was observed in XRF analysis. From the XRD patterns in Figure 6.5, the occurrence of quartz was observed at 2θ=48.95. High quartz content is due to the abundance of silica in fly ash. The presence of these chemical compounds leads to several reactions involving calcite in limestone with alumina (corundum) and silica in fly ash to form anorthite. This is seen to appear at 2θ=27.10, 31.79, 38.28 and 41.15 in the sample after 60 minutes dissolution period. Anorthite is a product of pozzolanic reaction which occurs in presence of water. The formation of anorthite in the sample leads to an increase in the specific surface area of the sorbent as observed in BET surface area analysis. Increased specific surface area exposes more calcium ions during desulphurization therefore enhancing desulphurization capacity in FGD systems (Lin et al., 2003). Other peaks detected are portlandite which mainly comes from limestone and corundum which is contained in fly ash.

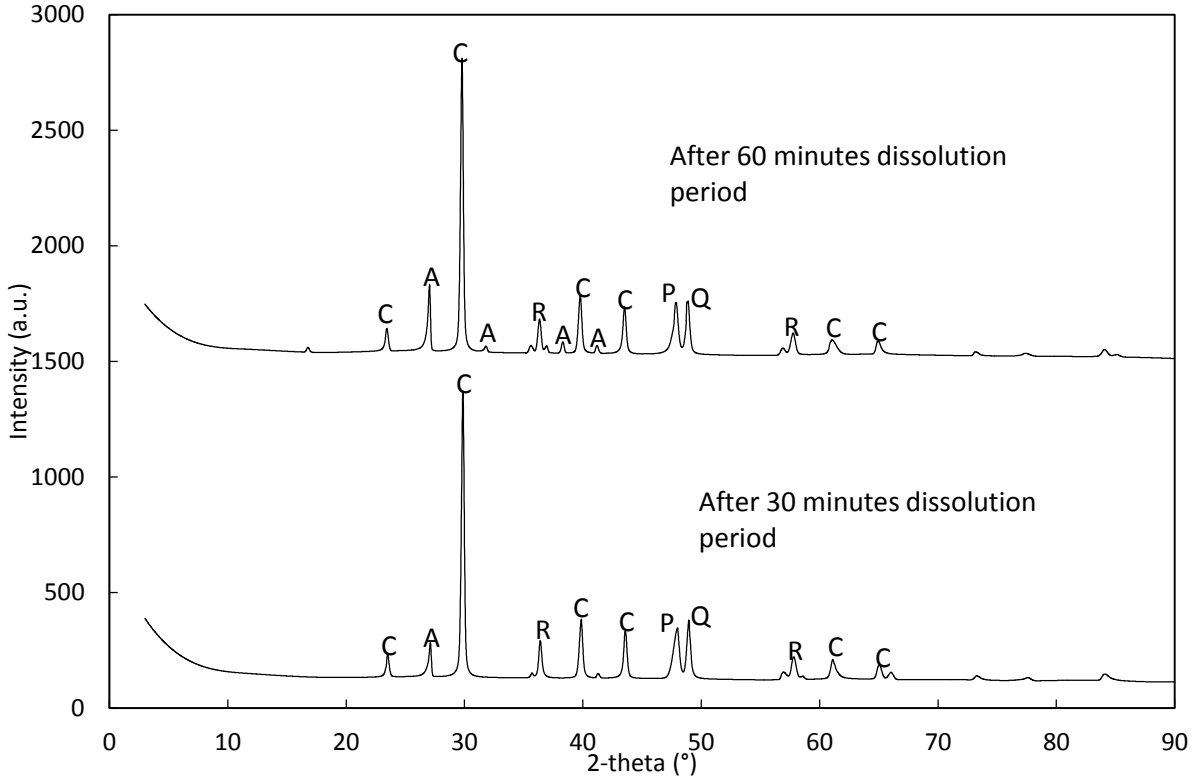

Figure 6. 5: XRD patterns for limestone blended with 1g fly ash after 30 minutes and 60 minutes dissolution periods (A-anorthite, C-calcite, Q-quartz, R-corondum and P-portlandite)

6.4.3. SEM analysis and BET surface area analysis

SEM images of limestone blended with 1g of fly ash at different dissolution periods are shown in Figure 6.6. The presence of particles with smooth surfaces that are spherical in shape is clear in Figure 6.6(a). This is due to unreacted silica contained in fly ash. From Figure 6.6(b) after 60 minutes dissolution period, the presence of agglomerated particles can be seen. This is mostly due to formation of anorthite which is a product of pozzolanic reaction. It is also evident that there is depletion of the spherical particles (silica) which is because of the pozzolanic reaction. The agglomerated particles are seen to be rough in texture which contributes to the increase in the specific surface area.

The BET surface area analysis showed that there was a significant increase in the specific surface area with increase in the amount of fly ash added to limestone. The studied limestone had a specific surface area of 18.5626m^2/g while fly ash had 0.3669m^2/g. Figure 6.7 shows that with 1g of fly ash added, the specific surface area of the blended mixture was found to be 36.2645m^2/g.

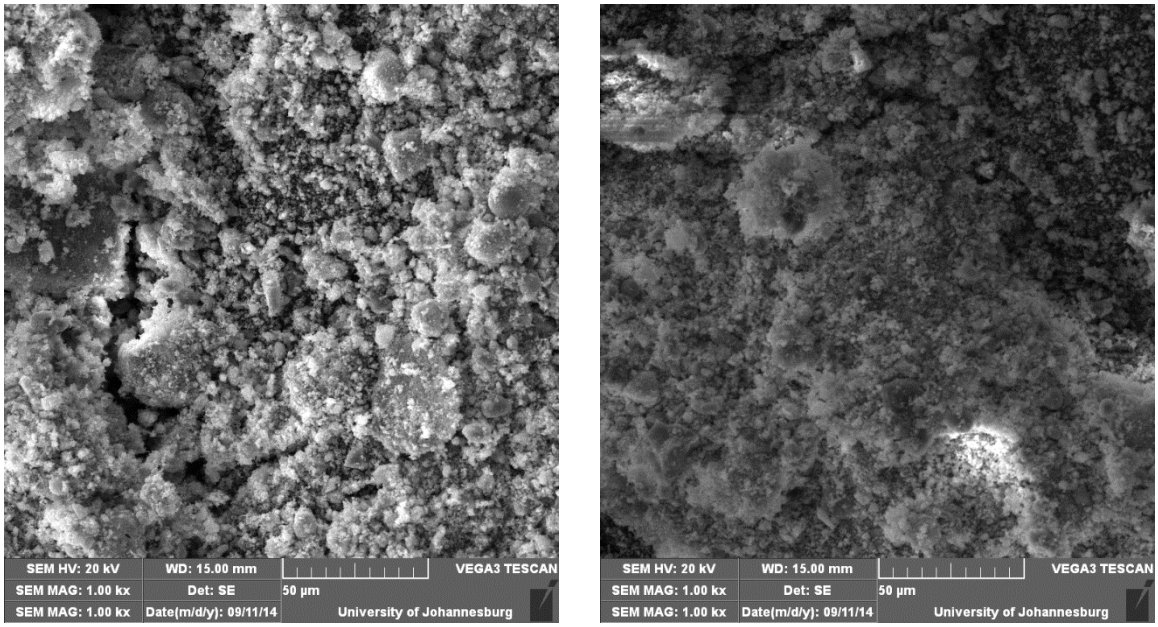

Figure 6. 6: SEM images for limestone blended with 1g fly ash at (a) 30 minutes and (b) 60 minutes dissolution period.

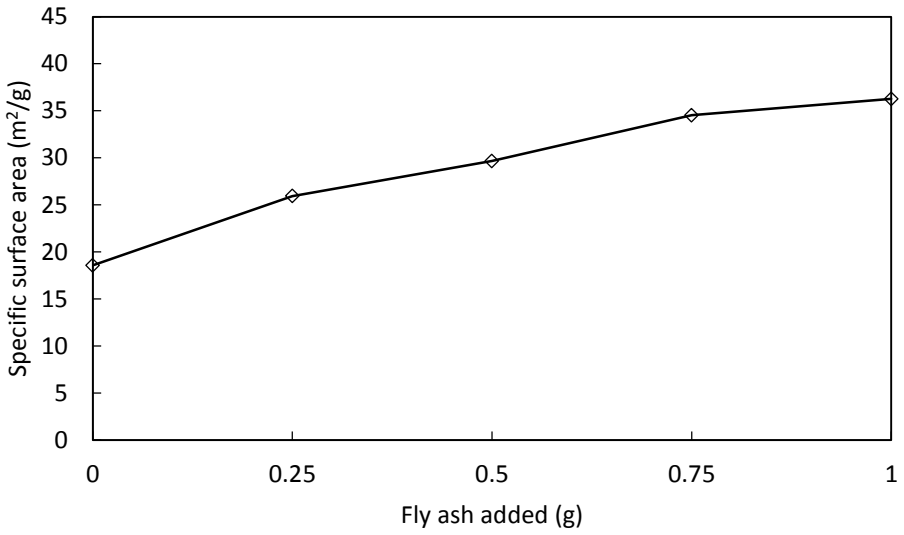

Figure 6. 7: The relationship between the BET surface areas and fly ash added after 60 minutes dissolution period

6.4.4. Effect of reaction variables

6.4.4.1. Effect of pH

Figure 6.8 shows response surface plot and two-dimensional plot for the change in dissolution rate constant with varying pH (X_3) and temperature (X_1). Limestone to fly ash ratio (X_4) and acid concentration (X_2) were kept constant at 0.25 and 1.25M respectively. The pH was found to have the most significant effect on dissolution rate

constant in the experiment as observed from F-value in Table 6.4. It was observed that the dissolution rate constant was high at low pH compared to high pH. Limestone dissolution is dependent on the mass transfer of H^+ ions from the liquid bulk to the surface of the particle. At low pH, there is increased H^+ ion activity in the liquid bulk which means more carbonate ions are attacked leading to an increase in dissolution. Shih et al. (Shih et al., 2000) studied the dissolution of limestone from different sources and found out that the dissolution rate constant is dependent on the mass transfer of hydrogen ions accompanied by chemical reactions in the liquid film surrounding the particle. It was further indicated that the rate of dissolution is enhanced by reaction of H^+ and OH^- in the liquid film. Figure 6.9 also shows the dissolution rate constant with varying pH (X_3) and acid concentration (X_2). The temperature(X_1) and limestone to fly ash ratio (X_4) were kept constant at 52.5°C and 0.5 respectively. The dissolution rate constant is observed to increase at a pH of 4.75 but almost constant at pH of 6.25. This shows that low pH values contributed to high hydrogen activity and dominated over the effect of acid concentration. At higher pH values, there is lower hydrogen ion activity leading to low dissolution rate.

6.4.4.2. Effect of temperature

Temperature plays a significant role during the dissolution process. From Figure 6.8 it is evident that the dissolution rate constant increases with increasing temperature at a pH of 4.75 and 6.25. This was also observed when the temperature (X_1) and limestone to fly ash ratio (X_4) were varied as shown in Figure 6.10. The pH (X_3) and acid concentration (X_2) were kept at 5.5 and 1.25M respectively. The dependence on temperature during dissolution in this experiment is due the rate controlling step being chemical reaction. Chemical reaction controlled processes are dependent on temperature while diffusion controlled processes are slightly dependent on it (Aydogan et al., 2007). An increase in temperature increases chemical reactions between reactants and creates new active sites which in turn enhances the dissolution rate constant. This is important in FGD system because it leads to improved sorbent utilization (Ho and Shih, 1992). Also an increase in temperature decreases the viscosity of the fluid reactants thus increases the rate at which molecules diffuse through boundaries. The reactivity of limestone is affected by the presence of alumina and silica contained in fly ash which reacts to form pozzolanic materials. It has been proven that the solubility of silica and alumina increases when

the temperature is increased (Lee et al., 2005b). This results in more pozzolanic reactions which increases the reactivity of limestone.

6.4.4.3. Effect of limestone to fly ash ratio

Figure 6.10 shows the interaction of dissolution rate constant with varying temperature (X_1) and limestone to fly ash ratio (X_4). The dissolution rate constant at limestone to fly ash ratio of 0.75 is higher than at 0.25 and it is observed to increase with increase in temperature for both cases. This is because fly ash mainly contains silica and alumina which react with limestone to form pozzolanic products. With fly ash being used as an additive in this experiment, increasing its ratio means there is more silica and alumina available to react with limestone in solution and this leads to increase in the reactivity of limestone (Zainudin et al., 2005). At lower limestone to fly ash ratio, there is limited silica and alumina available for reaction with limestone and therefore its reactivity is lowered. A similar trend was observed when the pH (X_3) and limestone to fly ash ratio (X_4) was varied as seen in Figure 6.11 where the dissolution rate constant is higher at limestone to fly ash ratio of 0.75 than at 0.25 but it decreases with increasing pH for both cases.

6.4.4.4. Effect of acid concentration

Figure 6.12 represents the relationship between the dissolution rate constant with varying temperature (X_1) and acid concentration (X_2). The pH (X_3) and limestone to fly ash ratio (X_4) were kept at 5.5 and 0.5 respectively. The dissolution rate constant increases with increasing temperature and also with increasing acid concentration. This was also observed when acid concentration (X_2) and limestone to fly ash ratio (X_4) were varied as seen in Figure 6.13 by keeping the temperature and pH constant at 52.5°C and 5.5 respectively. This is due to the increase in acidity which enhances the transport of hydrogen ions in the liquid film between the solid and liquid (Liu et al., 2006). The transport of hydrogen ions from the liquid bulk to the liquid surrounding the particle promotes dissolution by dissociation of the carbonate ions (Frandsen et al., 2001).

Figure 6.14 shows the perturbation which is the deviation of the dissolution rate constant from the reference point caused by the process variables. The figure shows a significant drop in the dissolution rate constant with increasing pH. This indicates that the pH had the most significant effect on the dissolution rate constant as it was

observed in the ANOVA analysis. The dissolution rate constant increased with increasing temperature, acid concentration and limestone to fly ash ratio. Limestone to fly ash ratio had a slightly higher effect compared to temperature and acid concentration.

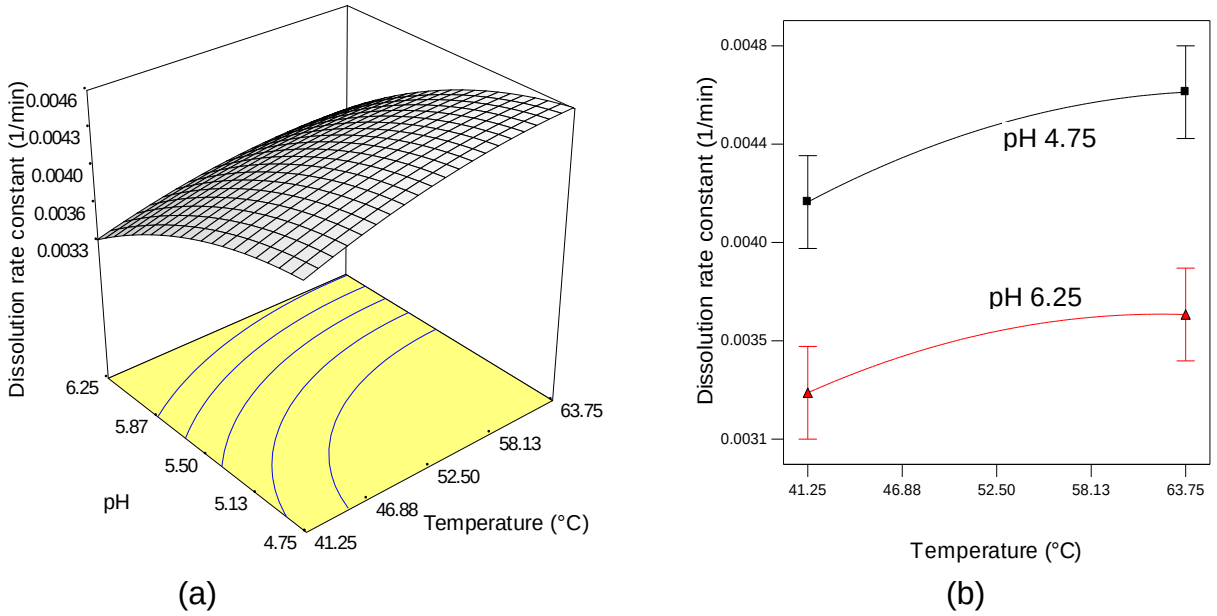

Figure 6. 8: The effect of pH and temperature on the dissolution rate constant (a) response surface method and (b) two-dimensional plot

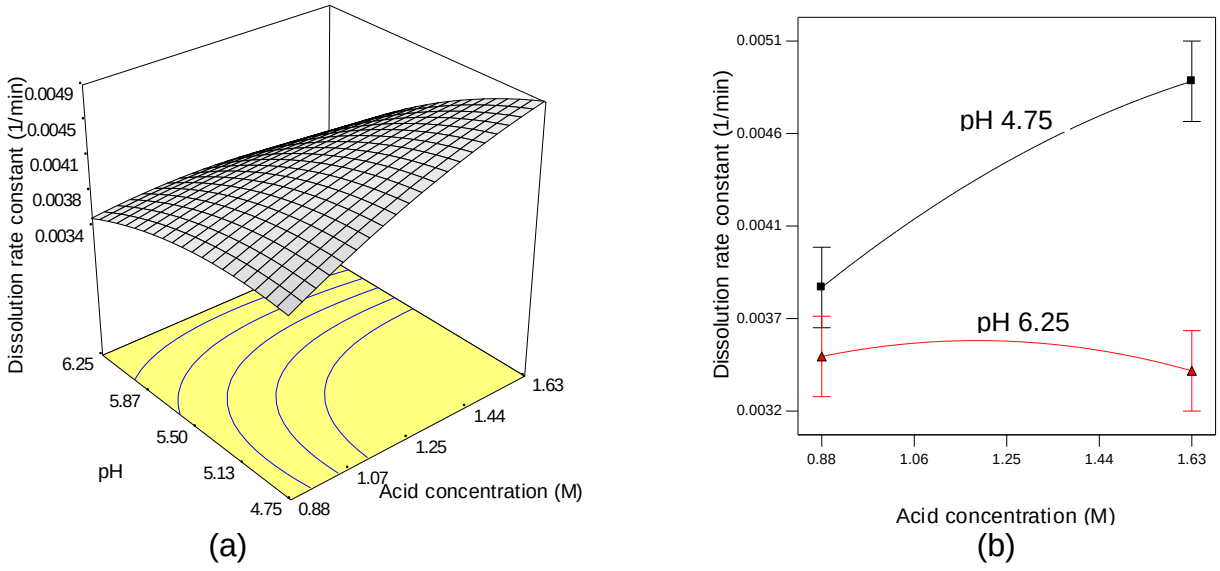

Figure 6. 9: The effect of pH and acid concentration on the dissolution rate constant (a) response surface method and (b) two-dimensional plot

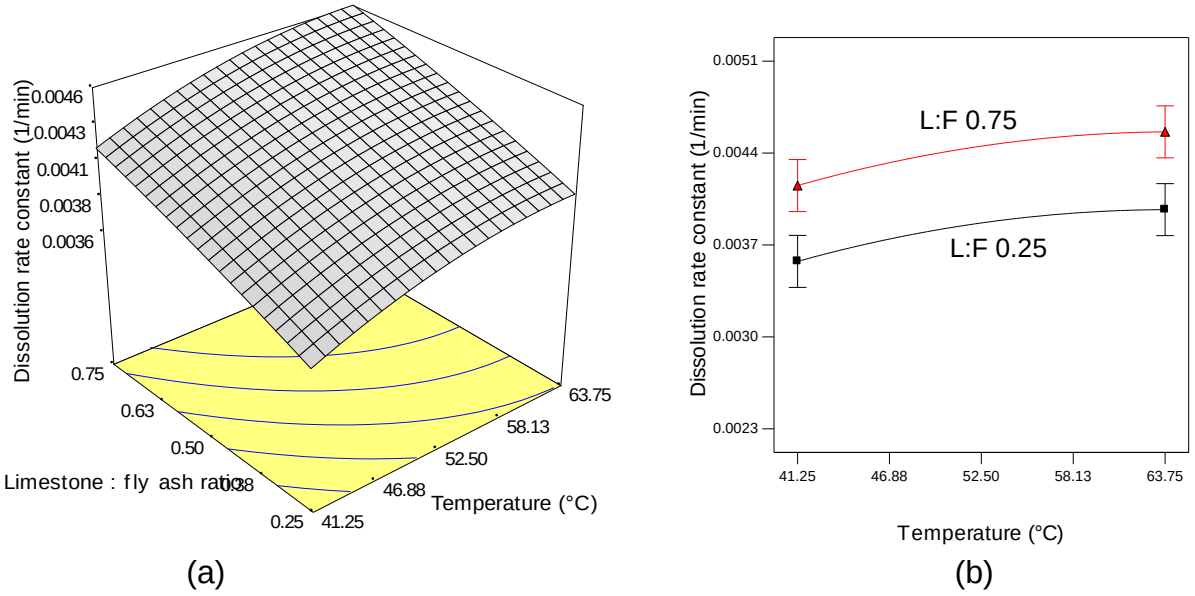

Figure 6. 10: The effect of temperature and limestone to fly ash ratio on the dissolution rate constant (a) response surface method and (b) two-dimensional plot

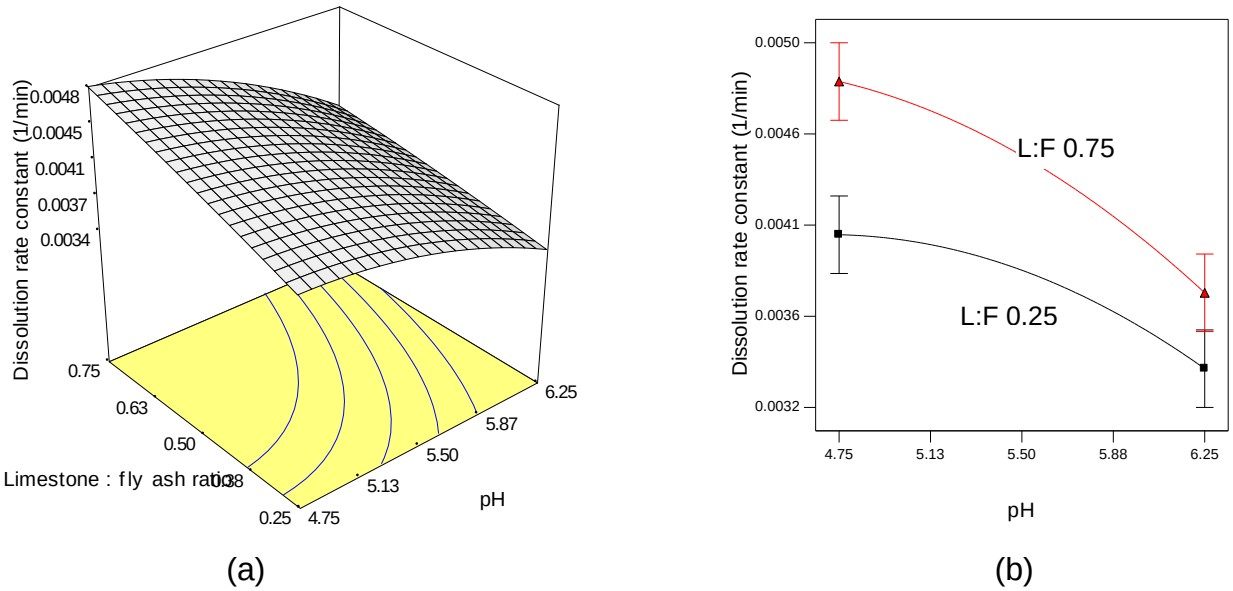

Figure 6. 11: The effect of pH and limestone to fly ash ratio on the dissolution rate constant (a) response surface method and (b) two-dimensional plot

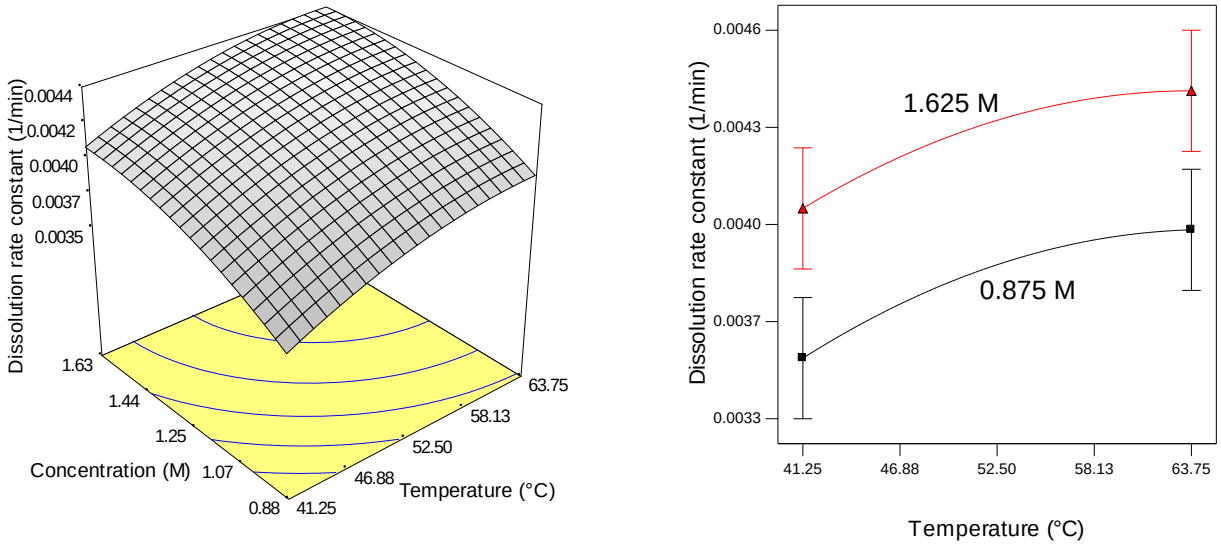

Figure 6. 12: The effect of acid concentration and temperature on the dissolution rate constant (a) response surface method and (b) two-dimensional plot

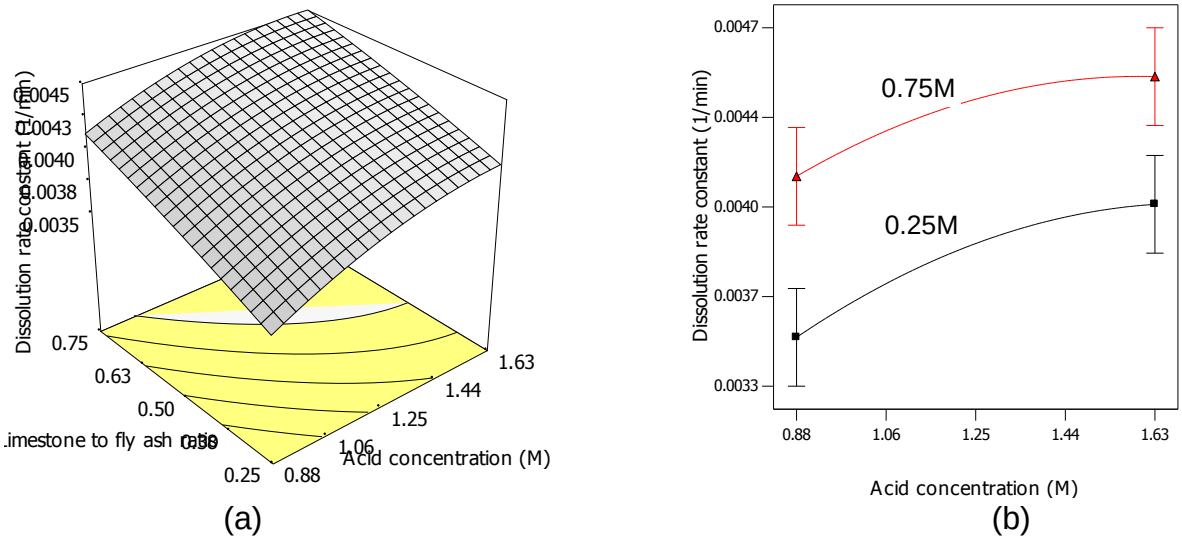

Figure 6. 13: The effect of acid concentration and limestone to fly ash ratio on the dissolution rate constant (a) response surface method and (b) two-dimensional plot

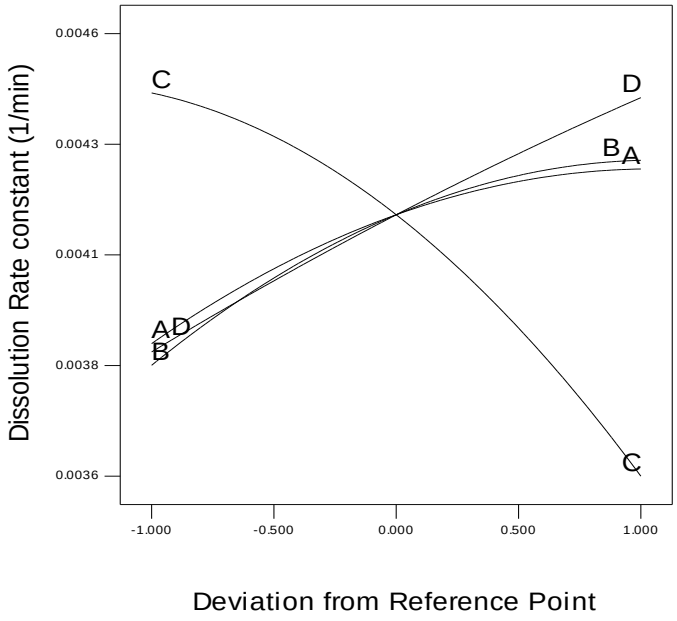

Figure 6. 14: The effect of individual process variable on the dissolution rate constant (A - Temperature, B - Acid concentration, C - pH and D - Limestone to fly ash ratio)

Conclusion

This study presents the findings of the effect of fly ash addition on limestone dissolution rate. Using a central composite design, a predictive model was developed which describes the relationship between the dissolution rate constant and the reaction variables. The model was found to best describe the relationship because of good results when compared to the experimental data. The model results indicated that the pH had the most significant effect on dissolution rate constant which was attributed to increase hydrogen activity at low pH level which enhances limestone dissolution. Addition of fly ash to limestone improved its dissolution rate constant because of its siliceous properties which increases its reactivity. The reaction temperature and the concentration of acid used were found to have positive effects on the dissolution rate constant. Physical properties of the samples indicated an increased specific surface area which is mainly due to products of hydration like anorthite.

6.5. References

Aydogan, S., Erdemoğlu, M., Uçar, G. and Aras, A. 2007. Kinetics of galena dissolution in nitric acid solutions with hydrogen peroxide. Hydrometallurgy, vol. 88, no. 1, pp. 52-57.

Frandsen, J.B., Kiil, S. and Johnsson, J.E. 2001. Optimisation of a wet FGD pilot plant using fine limestone and organic acids. Chemical Engineering Science, vol. 56, no. 10, pp. 3275-3287.

Ho, C.S. and Shih, S.M. 1992. Calcium hydroxide/fly ash sorbents for sulfur dioxide removal. Industrial & Engineering Chemistry Research, vol. 31, no. 4, pp. 1130-1135.

Karatepe, N., Mericboyu, A. and Kucukbayrak, S. 1998a. Effect of Hydration Conditions on the Physical Properties of Fly Ash-Ca(OH)2 Sorbents. Energy Sources, vol. 20, no. 6, pp. 505-511.

Karatepe, N., Ersoy-Mericboyu, A., Demirler, U. and Kucukbayrak, S. 1998b. Determination of the reactivity of Ca (OH)2–fly ash sorbents for SO2 removal from flue gases. Thermochimica acta, vol. 319, no. 1, pp. 171-176.

Lee, K.T., Bhatia, S. and Mohamed, A.R. 2005a. Preparation and characterization of sorbents prepared from ash (waste material) for sulfur dioxide (SO2) removal. Journal of Material Cycles and Waste Management, vol. 7, no. 1, pp. 16-23.

Lee, K.T., Matlina Mohtar, A., Zainudin, N.F., Bhatia, S. and Mohamed, A.R. 2005b. Optimum conditions for preparation of flue gas desulfurization absorbent from rice husk ash. Fuel, vol. 84, no. 2, pp. 143-151.

Levenspiel, O. 1972, Chemical Reaction Engineering, 2nd edn, John Wiley and Sons., New York.

Lin, R., Shih, S. and Liu, C. 2003. Structural properties and reactivities of Ca (OH)2/fly ash sorbents for flue gas desulfurization. Industrial & Engineering Chemistry Research, vol. 42, no. 7, pp. 1350-1356.

Liu, C., Shih, S. and Lin, R. 2002. Kinetics of the reaction of Ca (OH)2/fly ash sorbent with SO2 at low temperatures. Chemical Engineering Science, vol. 57, no. 1, pp. 93-104.

Liu, S., Liu, X. and Xiao, W. 2006. Wet flue gas desulfurization by organic acid-enhanced coarse limestone. Journal of Chemical Industry and Engineering-China, vol. 57, no. 4, pp. 927.

Maina, P. 2013. Improving Lime's Reactivity Towards Flue Gas Desulfurization by using Fly Ash, Bottom Ash and Waste Activated Sludge. ABC Journals, vol. 2, no. 3, pp. 8-19.

Maina, P. and Mbarawa, M. 2011. Enhancement of lime reactivity by addition of diatomite. Fuel Processing Technology, vol. 92, no. 10, pp. 1910-1919.

Ogenga, D., Siagi, Z., Onyango, M. and Mbarawa, M. 2009. Influence of hydration variables on the properties of South African calcium/siliceous-based material. Frontiers of Chemical Engineering in China, vol. 3, no. 1, pp. 46-51.

Shi, L. and Xu, X. 2001. Study of the effect of fly ash on desulfurization by lime. Fuel, vol. 80, no. 13, pp. 1969-1973.

Shih, S., Lin, J. and Shiau, G. 2000. Dissolution rates of limestone from different sources. Journal of hazardous materials, vol. 79, no. 1, pp. 159-171.

Zainudin, N.F., Lee, K.T., Kamaruddin, A.H., Bhatia, S. and Mohamed, A.R. 2005. Study of adsorbent prepared from oil palm ash (OPA) for flue gas desulfurization. Separation and Purification Technology, vol. 45, no. 1, pp. 50-60.

7. Conclusion and recommendations

This study presents the findings of dissolution of a limestone and coal ash for a wet FGD process. Experiments were performed using a pH stat apparatus and adipic acid used as acid titrant. Results showed that the reactivity of limestone increased at low values of pH and solid to liquid ratio and it increased with increase in both temperature and stirring speed. The dissolution of limestone was found to follow the shrinking core model with the chemical reaction at the surface of the particle being the rate controlling step. XRD analysis indicated an increase in portlandite peak with prolonged dissolution period which resulted in increased surface area of the sorbent as observed in BET surface area analysis.

The dissolution of both fly ash and bottom ash is also presented in this study. Both coal fly and bottom ash was found to form an ash layer during dissolution which led to the diffusion through the product layer being the rate controlling step. The ash layer formed is a calcium alumino-silicate compound (anorthite) which is a pozzolanic reaction product and it was observed in XRD analysis. Pozzolanic reaction products were also depicted in SEM analysis where agglomerates and porous structure were formed after dissolution.

Fly ash was found to have a positive effect on the dissolution rate constant of limestone. An increase in the amount of fly ash added to limestone increased the dissolution rate constant of limestone because it contains alumina and silica which increases the reactivity of limestone. The formation of hydration products led to an increase in the specific surface area of limestone from 18.5626 m^2/g to 36.2645m^2/g when fly ash was added. The pH was found to have the most significant effect on the dissolution rate constant compared to other reaction variables because of hydrogen ion activity which is a function of pH.

It is recommended that further studies can be done to test the sulphur dioxide removal capacities of the sorbents obtained from dissolution in this research especially fly ash and limestone blend. It is also recommended to test limestone from different sources having varying calcite composition which can affect the dissolution properties as well as SO_2 removal in wet FGD systems.